Natural Frequency of a Horizontal Soil Layer
Part II: Saturated Sand Bed

S.P.G. Madabhushi

CUED/D-SOILS/TR273 (1994)

Synopsis

The dynamic response of a saturated, horizontal soil layer is investigated by conducting two centrifuge tests. The depth of the sand bed in each of these centrifuge tests was arranged such that the small strain natural frequency of the sand bed was very high compared to the driving frequency of the earthquake. When the correct natural frequency of the sand bed was estimated using the shear modulus corrected for shear strain amplitude induced by the earthquake loading and taking into account the reduced effective stresses within the sand bed following the generation of excess pore pressures, the natural frequencies of the sand beds were much lower and close to the driving frequency of the earthquakes.

In the first centrifuge test a strong earthquake was fired first followed by a smaller second earthquake. All the subsequent earthquakes had increasing intensity. Smaller excess pore pressures were generated during the smaller second earthquake and all other earthquakes resulted in large excess pore pressures. Also during the second earthquake the attenuation of base shaking was small as it travelled towards the sand surface. Calculation of the natural frequency of the sand bed during earthquake 2 has shown that it is indeed close to the driving frequency of the earthquake there by resulting in the smallest attenuation. In all other earthquakes the driving frequency was far from the natural frequency causing significant attenuation of base shaking as it travelled towards the sand surface. Also the data suggested that the rate of excess pore pressure build up is a function of the strength of the earthquake.

In the second centrifuge test all the earthquakes had increasing intensity. Also all the earthquakes resulted in more or less the same magnitude of excess pore pressures within the sand bed. During the second earthquake the attenuation of base shaking was small as it travelled towards the sand surface. Calculation of the natural frequency of the sand bed during earthquake 2 has shown that it is indeed close to the driving frequency of the earthquake there by resulting in the smallest attenuation. In the first earthquake it was shown that the natural frequency is far above the driving frequency and in all other earthquakes the driving frequency was far below the natural frequency causing significant attenuation of base shaking as it travelled towards the sand surface. As in the previous centrifuge test the data suggested that the rate of excess pore pressure build up is a function of the strength of the earthquake.

Natural Frequency of a Horizontal Soil Layer

Part II: Saturated Sand Bed

1.0 Introduction

The present series of centrifuge experiments consider the dynamic response of a horizontal sand bed subjected to earthquake loading. In the first series of experiments we have considered the dynamic behaviour of a dry sand bed and analysed the data in terms of amplification of accelerations within the sand bed at different heights and at different frequencies, Madabhushi (1994).

However some of the major concerns regarding a saturated sand bed during an earthquake are the phenomena associated with liquefaction. During the recent Northridge earthquake in the Los Angeles area there were extensive sand boils observed on the upstream side of the old lower San Fernando dam. This dam is not in service following the 1971 earthquake which inflicted severe damage to this dam, Seed et al (1975). Also sand boils were observed following the Northridge earthquake along the Pacific coast and a severe liquefaction induced failure of quay wall at the Ring Harbour in the Redando beach area of Los Angeles. In this report the dynamic response of saturated sand beds in the presence of excess pore pressures induced by earthquake loading will be studied

The dynamic response of a horizontal sand bed will depend on

i) the stiffness of soil ;
ii) the material damping in the soil.

The stiffness of a soil element depends on the void ratio and confining pressure to which it is subjected. In the case of a saturated sand bed it also depends on the excess pore pressure generated during the earthquake. For a given soil layer we can find the average confining stress at the mid depth of the soil layer and estimate the small strain shear modulus of soil. Based on this we can calculate the shear wave velocity in the

soil and hence the natural frequency of the soil layer. The dynamic response in the case of saturated sand bed depends strongly on the magnitude of the excess pore pressures generated during the earthquake. The material damping in the soil will have two components namely

i) hystertic damping in the soil skeleton ;
ii) viscous damping in the pore fluid.

The effects of material damping on the soil have been discussed elsewhere (Bolton and Wilson, 1992 and Madabhushi, 1994) and will not be considered in this report. The main aim of this report will be to compare dynamic response of the saturated sand bed based on the data from the present series of experiments with the dynamic response of the dry sand bed presented in the earlier report, Madabhushi (1994).

In the present report the data from the centrifuge tests on horizontal sand bed which is completely saturated and subjected to model earthquakes will be presented. In the next two sections the stiffness of the saturated soil bed and the generation of excess pore pressures during the earthquake loading will be explained. Following this the centrifuge modelling technique and model preparation methods will be explained. Finally the data from the centrifuge tests and the analysis of the data will be presented. Conclusions based on the analyses of the present series of centrifuge test data and future research planned will be presented in the end.

2.0 Excess Pore Pressures

On shearing a soil element exhibits two distinct types of behaviour depending upon its initial relative density. A dense soil deposit experiences dilation on shearing while a loose soil deposit undergoes densifrcation. In Fig.1 these two distinct behaviours are presented schematically under drained conditions.

During an earthquake loading the soil element is subjected to cyclic shear stresses as the stress waves propagate from the bed rock towards the surface of the soil layer. In the case of a loose saturated sand bed these cyclic shear stresses will induce a tendency

of 'densification' as shown in Fig.1. However unlike the static loading, during a dynamic loading event like an earthquake there is no time for drainage of the pore fluid from the soil layer. Hence the tendency for densification is manifested as a rise in the pore pressure. We term this as an excess pore pressure which is over and above the

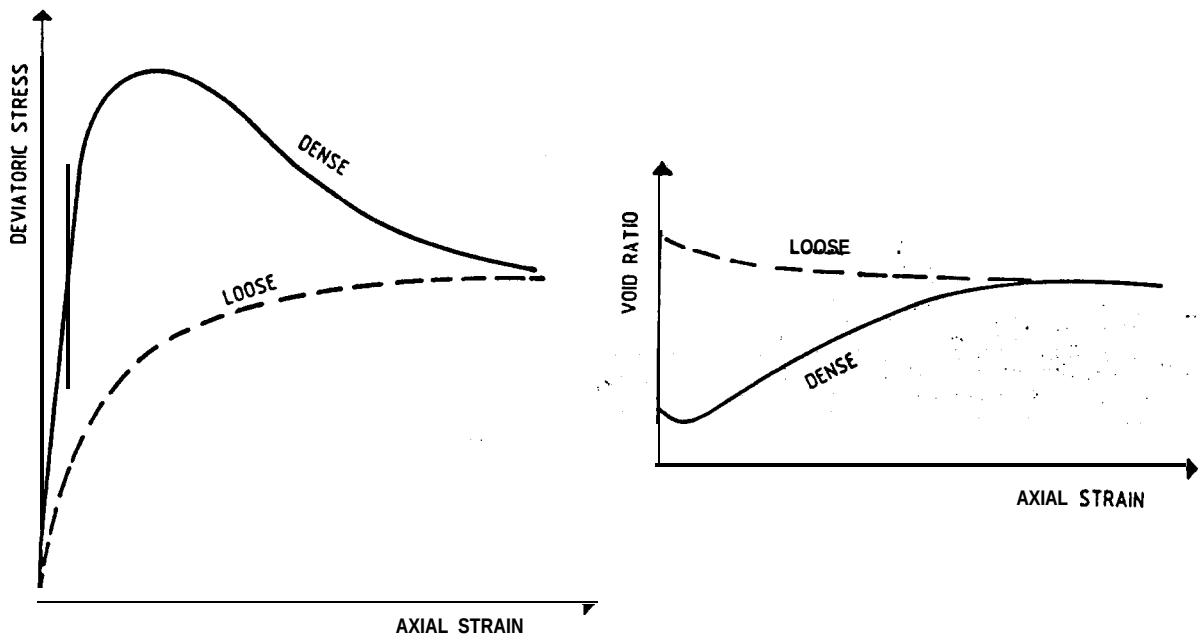

Fig. 1 Loose and dense sand behaviour under drained conditions

normal hydrostatic pore pressure. The effective stress within the soil layer under these conditions may be expressed as

$$\sigma' = \sigma - (u_{hydrostatic} + u_{excess}) \text{ .....(1)}$$

With the generation of excess pore pressures the effective stress is reduced. This in turn will cause a degradation in the soil stiffness. The dynamic response of the sand layer will reflect the degradation in soil stiffness.

3.0 Stiffness of the soil layer

Consider a horizontal saturated sand bed as shown in Fig.2. Let the depth of the soil layer be 'z'. The effective vertical stress at any depth of this saturated soil layer may be obtained as

4.0 Natural frequency

The natural frequency of the dry soil bed may be obtained in terms of the shear wave velocity in the soil. If 'V_S' is the shear wave velocity in soil then the natural frequency may be obtained as

$$\varpi_n = \frac{(n + \frac{1}{2})\pi V_s}{h} \quad \ldots\ldots (6)$$

where ϖ_n is the natural frequency in the n^{th} mode. In the case of a saturated sand bed the shear wave velocity V_S depends on the shear modulus and the saturated density of soil (γ). In general we can write

$$V_s = \sqrt{\frac{G}{\gamma}} \quad \ldots\ldots (7)$$

Using Eqs. 2 to 7 the small strain natural frequency of a soil layer can be estimated. However this calculation will change when the earthquake loading induces significant shear strains in the soil.

5.0 Shear strains

The shear strain amplitude may be large in a strong earthquake. The shear modulus in such a case will be only a fraction of the small strain shear modulus. **Hardin** and Drnevich (1972) suggested a hyperbolic variation of shear modulus with shear strain. Using this variation the tangent modulus (G_t) at any shear strain amplitude (γ) is obtained as

$$G_t = G_{max} \frac{1}{1 + \frac{\gamma}{\gamma_r}} \quad \ldots\ldots\ldots (8)$$

where γ_r is the reference shear strain given by

$$\gamma_r = \frac{\tau \, max}{G \, max} \quad \ldots\ldots\ldots (9)$$

The maximum shear stress can be obtained from the Mohr circle of stresses as

$$\tau_{max} = \sqrt{\{0.5(1+K_o)\sigma_v' \sin\varphi\}^2 - \{0.5(1-K_o)\sigma_v'\}^2} \quad \ldots\ldots(10)$$

where ϕ is the angle of internal friction. The shear stress τ induced in a soil element at any depth 'z' due to the earthquake loading is calculated as

$$\tau = K_h \gamma z \quad \ldots\ldots\ldots(11)$$

where K_h is the horizontal acceleration due to earthquake loading. The shear strain γ is obtained as

$$\gamma = \frac{\tau}{G_{max} - \frac{\tau}{\gamma_r}} \quad \ldots\ldots\ldots(12)$$

Knowing γ and γ_r and using Eq.8 the tangent modulus of soil is calculated. Using Eq.6 the natural frequency of the soil is obtained.

6.0 Sand beds in centrifuge tests

As explained in earlier section a centrifuge model with a horizontal sand bed is constructed to have its natural frequency close to one of the driving frequencies of the earthquake. Centrifuge tests MG-4 and MG-5 were carried out on two such horizontal sand beds. In this section the calculation of the sand bed depths which have a resonant frequency at one of the driving frequencies observed in earlier section will be explained.

In the first centrifuge test MG-4 the sand bed was to have a depth of 155.0 mm. The dry density of the sand bed was 1208.21 kg/m3 and the void ratio was 1.19. The saturated density of the soil layer is calculated to be 1752.31 kg/m^3. Using Eqs.l to 6 the small strain natural frequency of this soil layer was estimated as 233.7 Hz. Assuming a 21 % earthquake and using Eqs. 7 to 11 the natural frequency of the soil layer during this earthquake is estimated as 105.3 Hz. In this calculation no excess pore pressures were taken into consideration. As explained earlier the generation of

excess pore pressures will lead to a degradation in soil stiffness and the natural frequency calculated above will be even lower in such an event.

In the second centrifuge test MG-5 the sand bed was to have a depth of 100.0 mm. The dry density of the sand bed was 1315.3 kg/m^3 and the void ratio was 1.015. The saturated density of the soil layer was calculated to be 1818.9 kg/m^3. Using Eqs.2 to 7 the small strain natural frequency of this soil layer was estimated as 43 1.5 Hz. Assuming a 22 % earthquake and using Eqs. 8 to 12 the natural frequency of the soil layer during this earthquake is estimated as 278.0 Hz. Again in this calculation no excess pore pressures were taken into consideration. As explained in the previous sections the generation of excess pore pressure will lead to a degradation in the soil stiffness and the natural frequency will be even lower in such an event.

7.0 Sand

For the centrifuge tests reported here Leighton Buzzard 100/170 sand was used. This type of sand has been extensively used in the triaxial and centrifuge tests and is available commercially. The maximum and minimum void ratio's of this soil are 1.318 and 0.475 respectively.

8.0 Instrumentation

8.1 Accelerometers

In the centrifuge tests reported here miniature piezoelectric accelerometers manufactured by D.J. Birchall were used to measure acceleration in the soil, on the model container during earthquakes. The device has a resonant frequency of about 50 kHz and a maximum error of 5%. The weight of the transducer is about 5 grams. Fig. 3. shows the dimensions of the transducer. For tests on saturated soil accelerometers were sealed with silicone rubber.

8.2 Pore Pressure Transducers

Pore pressures in the saturated soil were monitored by Druck PDCR 81 pore pressure transducers. This type of pore pressure transducers have a linear range up to 300 kPa and weigh about 10 grams. The corner frequency of the dynamic response of the transducer is 15 kHz. The maximum error is 0.2 %. In the centrifuge tests reported here, the active diaphragm of the PPT is covered with a porous brass stone. The dimensions of the PPT are presented in Fig.4.

All the pore pressure transducers were calibrated by applying standard water pressures on the active diaphragm. The output generated by the device was measured using a digital voltmeter and calibration constant was obtained in the units of 'kPa/mV'.

9.0 Model Preparation

The sand in the model was poured into the package through a hopper system in the model preparation room at the Cambridge Geotechnical Centrifuge Centre. The void ratio of the sand in the model was controlled by the height and the flow rate of sand pouring, of which trial tests were performed in advance. At the appropriate places the transducers were put into the sand. After the required height of sand layer had been achieved the surface of sand was levelled by a modified vacuum cleaner. The void ratio and density of the model were estimated and the natural frequency of the soil layer was calculated using Eqs.2 to 12.

After the final profile of the horizontal sand bed was achieved the model was vacuum levelled. The strong box is then covered with a lid and is subjected to a vacuum pressure of -30 cm of Mercury. After evacuating the model under this pressure for about 1 hour the blended silicone oil with a viscosity of 50 centiStokes is admitted at the base of the embankment and the saturation is carried out very slowly until the level of silicone oil coincided with the crest of the embankment. Care was exercised to see that the silicone oil level on both the slopes of the embankment are the same through

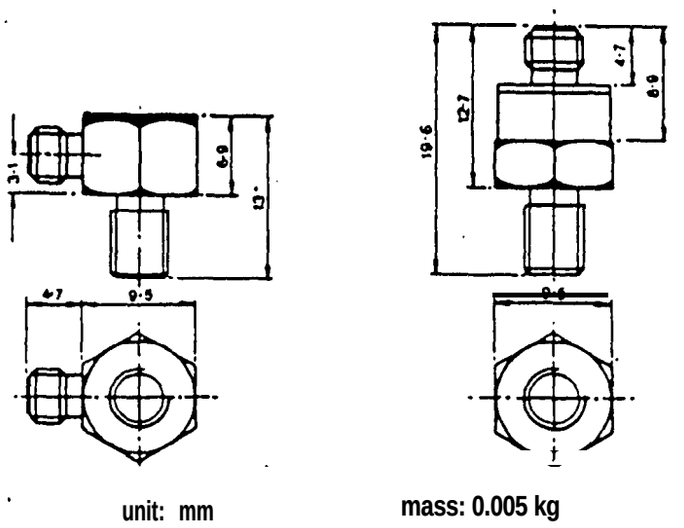

Fig 3 Typical dimensions of an accelerometer

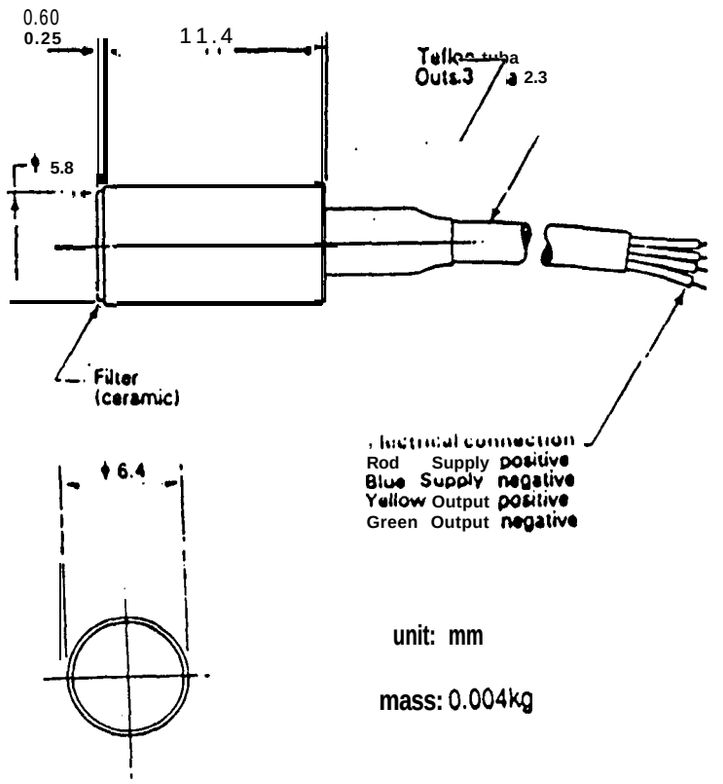

Fig.4 Typical dimensions of a pore pressure transducer

$$\sigma'_v = \gamma' z \ldots\ldots (2)$$

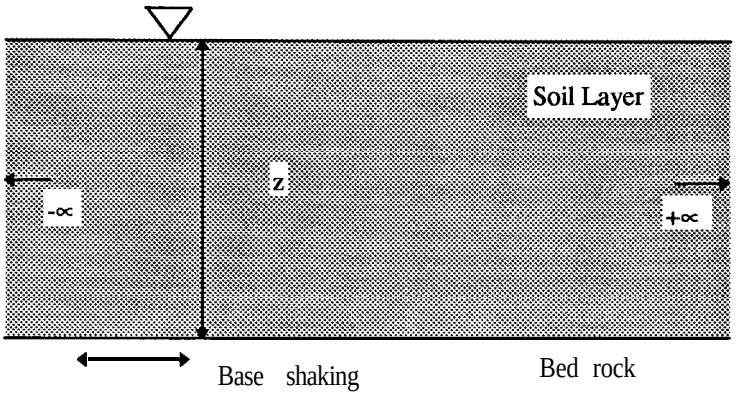

Fig.2. Saturated sand bed of depth 'z'

In the centrifuge model of this soil layer the depth of the soil bed is reduced by the gravity scale factor (n) but the stresses and strains at homologous points will be the same. Let us assume the height of the soil layer in the centrifuge model be 'h' such that h = Z/n. The effective vertical stress at any depth in the centrifuge model is calculated as

$$\sigma'_v = \gamma' hng \ldots\ldots (3)$$

The confining pressure (σ'_m) at any depth is obtained as

$$\sigma'_m = \frac{(1+ 2Ko)}{3}\sigma'_v \ldots\ldots\ldots (4)$$

where K_o is the coefficient of the earth pressure at rest. Assuming a value for K_o we can calculate the confining pressure in terms of the effective stress. The small strain shear modulus G_{max} may be calculated following Hardin and Drnevich (1972) as

$$G_{max} = 100\frac{[3-e]^2}{[1+e]}\{\sigma'_m\}^{0.5} \ldots\ldots\ldots (5)$$

where σ'_m and G_{max} are in MPa and 'e' is the void ratio of the soil.

out the saturation process. The whole process of saturation took about 10 hours for each model.

10.0 Test Procedure

After the saturation was completed the centrifuge model was transported very carefully on to the centrifuge arm. Immediately after the loading procedure was complete the strong box was fixed using wooden wedges to make the centrifuge model level. Pre flight checks were completed at this stage. Just before starting up the centrifuge motor, the strong box was released to hang freely at the end of the arm.

The centrifuge acceleration was increased in steps of 20g, 40g and 50g. At each stage the pore pressures within the model were monitored using a DVM. After the testing acceleration of 50g was achieved at the centroid of the model the steady acceleration was maintained for 20 minutes before any earthquake was fired. The pore pressures were monitored again after the 20 minutes. An earthquake was fired and the data was plotted. The strength of the subsequent earthquakes was gradually increased. When the test was finished the centrifuge was showed down and stopped. The model was recovered from the pit carefully and the post test profile of the horizontal sand bed was measured.

11.0 Data Acquisition

Data from the instruments in the centrifuge model was acquired using two systems. A 14 Channel Racal tape recorder was used to record data by running the tape recorder at high speed. Subsequent digitisation was carried out by playing back the tape at a slower speed. This enables to capture more than 1000 data points per channel during the 100 ms earthquake event. Also a direct data acquisition system which uses high speed A/D converter card working under Global Lab data acquisition system was used to acquire 16 channels of data directly on to the PC in real time. Data are plotted out

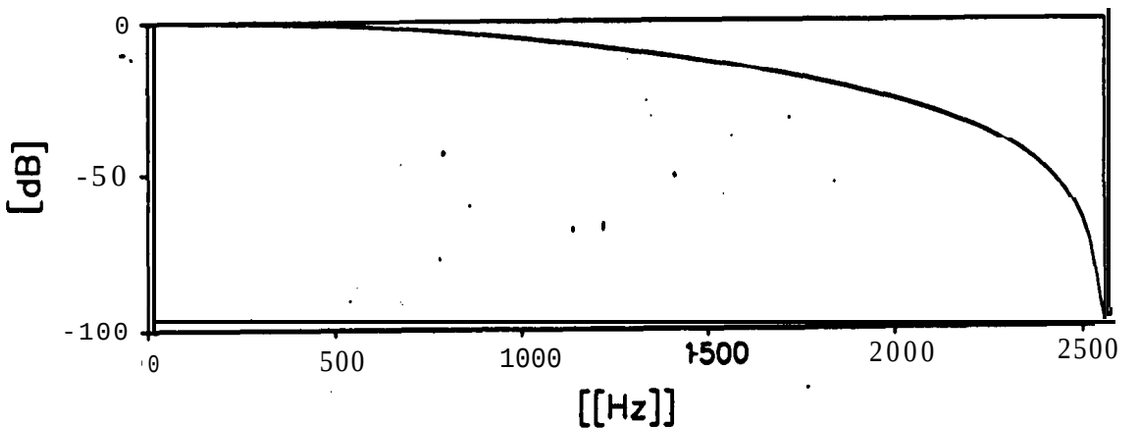

Fig.5 Filter **Characteristics**

channel by channel and also recorded in the accompanying diskettes. Photographs were taken during the model preparation, before and after each centrifuge test. A standard low pass Bessel filter was used to smooth the data and reduce the high frequency electrical noise. The filter characteristics are presented in Fig.5

All the acceleration time histories recorded during the present series of centrifuge tests are expressed as a percentage of the centrifuge acceleration. For example, the peak acceleration of 25 % means that the magnitude of the peak acceleration is $25/100 \times 50 \times 9.81 = 122.6$ m/s^2 in a '50g' centrifuge test.

12.0 Centrifuge test MG-4

As explained in Sec.6 the depth of the sand bed for this centrifuge test was 155.0 mm. The construction of the centrifuge model was in three stages and at the end each stage the void ratio and dry density of sand bed were estimated. The natural frequency of the soil was computed using Eqs.1 to 12. The final depth of sand bed required so that its natural frequency is close to the driving frequency of the model earthquake was determined after each stage. The schematic diagram showing the section of the model and placement of the instruments during this centrifuge test is presented in Fig.6. In table 1 the exact location of each transducer during this experiment is presented. A total of five earthquakes were fired on this centrifuge model at 50g. The data from these earthquakes is presented in Figs.7 to 26. The salient features of the data are presented here while a detailed analysis of the data is presented in next section.

As explained in Sec. 11 two data acquisition systems were used during this centrifuge test. Important transducers were logged on both these systems so that reliable measurements can be made. Earthquake 1 had a strength of about 25 %. In Figs.7 and 8 the data from all the instruments acquired using the Racal tape recorder are presented, In Figs.9 and 10 the data obtained directly using Global Lab data acquisition system are presented. Considering the three accelerometers 1926, 3477 and 3441 (see

Fig.6) which are placed along the vertical column in the middle of the sand bed we can see that there is significant attenuation of peak acceleration from 21.8 % at the base of the sand column to about 9 % at the surface of the sand bed. Note that ACC 1926 was not recorded on the Racal tape recorder due to a fault on this channel but was recorded by the Global Lab acquisition system (see Figs.6 and 9). Traces recorded by ACC 3477 and 3441 in Fig.6 show a clear attenuation of peak accelerations after first few cycles. This event coincides with the rise of excess pore pressures indicated by PPT's 6260 and 6270 as seen in Figs.7 and 8. The vertical accelerometers 1572, 1925 and 5756 in Fig.9 are clearly picking up the horizontal accelerations suggesting that they have changed their orientation following the rise of excess pore pressures. ACC 3492 did not function during this test. In general both the accelerometers and pore pressure transducers placed along the same horizontal plane recorded very similar accelerations and excess pore pressures confirming the uniformity of the centrifuge model.

A small earthquake which produced a peak acceleration of 9.1 % was fired next. The data from this earthquake are presented in Figs. 11 to 14. The magnitude of the excess pore pressures generated during this earthquake was much smaller compared to earthquake 1. This can be observed by comparing PPT's 6514, 6260 and 6270 in Figs.1 1 and 12 with corresponding traces obtained during earthquake 1. The accelerometers 1926, 3477 and 3441 along the vertical column in the middle of the sand bed show only a small attenuation of peak acceleration. In particular ACC 3441 near the surface of the sand bed registers all the cycles of base motion unlike in earthquake 1. This is consistent with the smaller excess pore pressures generated during this earthquake. There was a fault on the amplifier circuit connected to accelerometer 3477. Also the Racal tape recorder channel connected to PPT 6270 was faulty after earthquake 2. The correct excess pore pressures experienced by this transducer was recorded by the Global Lab acquisition system as seen in Fig.14 This was the case during all of the subsequent earthquakes.

Earthquake 3 had a strength of 14.7 %. The data from this earthquake are presented in Figs. 15 to 18. It is interesting to note that the magnitude of excess pore pressures generated during this earthquake are almost equal to those generated during earthquake 1. However the accelerometer 3441 near the sand surface registers all the cycles of base motion (see Fig. 15). Again accelerometer 3477 was faulty and remained so during the rest of the earthquakes.

Earthquake 4 had a strength of 22.9 %. The data from this earthquake are presented in Figs. 19 to 22. The excess pore pressures during this earthquake were almost the same as in the previous earthquake as seen in Figs. 19 and 20. It is interesting to see the acceleration time history recorded by ACC 3441 near the soil surface in **Fig.19.** After four cycles the accelerometer registers very small accelerations suggesting that the sand in this region has liquefied

A much stronger earthquake which produced a peak acceleration of about 30 % was fired next. The data from this earthquake are presented in Figs.23 to 26. The magnitude of excess pore pressures generated during this earthquake was **almost** the same as in the previous two earthquakes. However accelerometer 3441 shows signs of liquefaction after first $1^1/_2$ cycles. It does recover partially towards the end of the earthquake when the base shaking has a lower intensity.

In the next section a more detailed analysis of the data from this centrifuge test is presented.

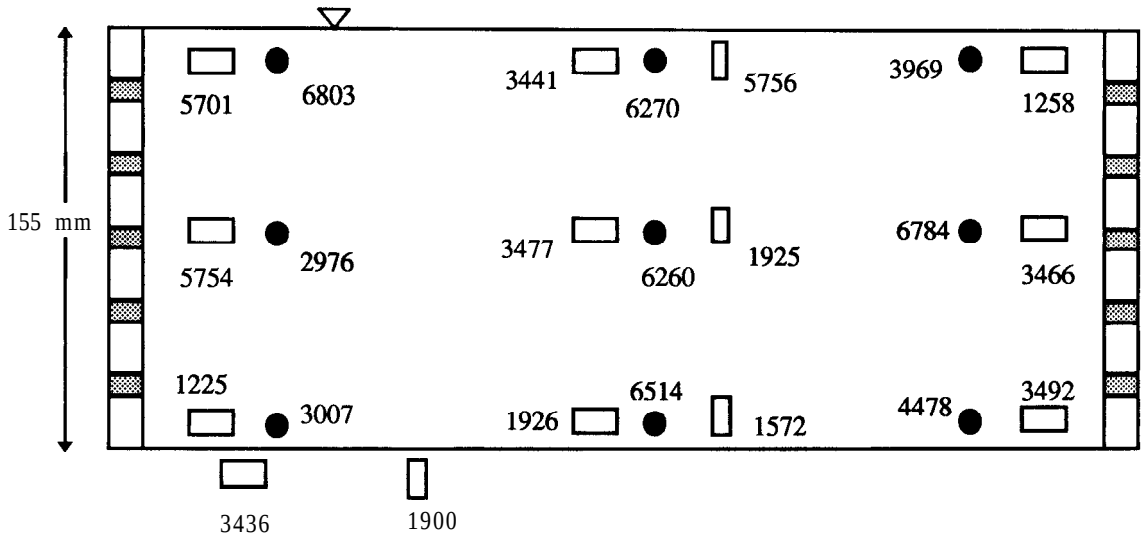

Fig. 6: Schematic diagram showing the placement of transducers in Centrifuge Test MG-4

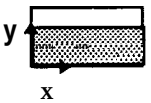

Table 1 Placement of transducers in centrifuge test MG-4

Transducer	x (mm)	Y (mm)
ACC 1225	55	5
ACC 1926	282	5
ACC 1572	360	5
ACC 3492	470	5
ACC 5754	50	80
ACC 3477	263	82
ACC 3466	460	79
ACC 1925	345	80
ACC 5701	56	135
ACC 3441	275	137
ACC 1258	465	133
ACC 5756	355	131
ACC 3436	fixed to the container	
ACC 1900	fixed to the container	
PPT 3007	120	3
PPT 6514	281	3
PPT 4478	475	3
PPT 2926	58	78
PPT 6260	265	80
PPT 6784	458	76
PPT 6803	75	136
PPT 6270	320	135
PPT 3969	440	133

Table 2 Hydrostatic pore pressures in centrifuge test MG-4

PPT NO.	10G	20G	40G	50G
PPT6514	11.95	25.75	53.71	68.18
PPT6260	7.73	16.45	34.19	43.30
PPT6270	6.68	14.72	31.13	39.64
PPT3007	12.40	26.51	54.84	69.55
PPT2976	0.81	1.70	149.66	4.44
PPT6803	4.20	9.31	19.75	25.19
PPT4478	12.51	27.21	56.02	70.80
PPT6784	7.89	17.32	35.85	45.28
PPT3969	5.28	11.67	24.28	30.73

Table 3 Normalised accelerations in the sand column in centrifuge test MG-4

Location	Normalised Acceleration
EQ: 1	
At base of the sand column	1
At the mid depth	0.5
Near the surface of sand bed	0.4128
EQ: 2	
At base of the sand column	1
At the mid depth	1.0106
Near the surface of sand bed	**0.8404**
EQ: 3	
At base of the sand column	1
At the mid depth	--
Near the surface of sand bed	**0.752**
EQ: 4	
At base of the sand column	1
At the mid depth	**--**
Near the surface of sand bed	**0.3247**
EQ: 5	
At base of the sand column	1
At the mid depth	--
Near the surface of sand bed	**0.2895**

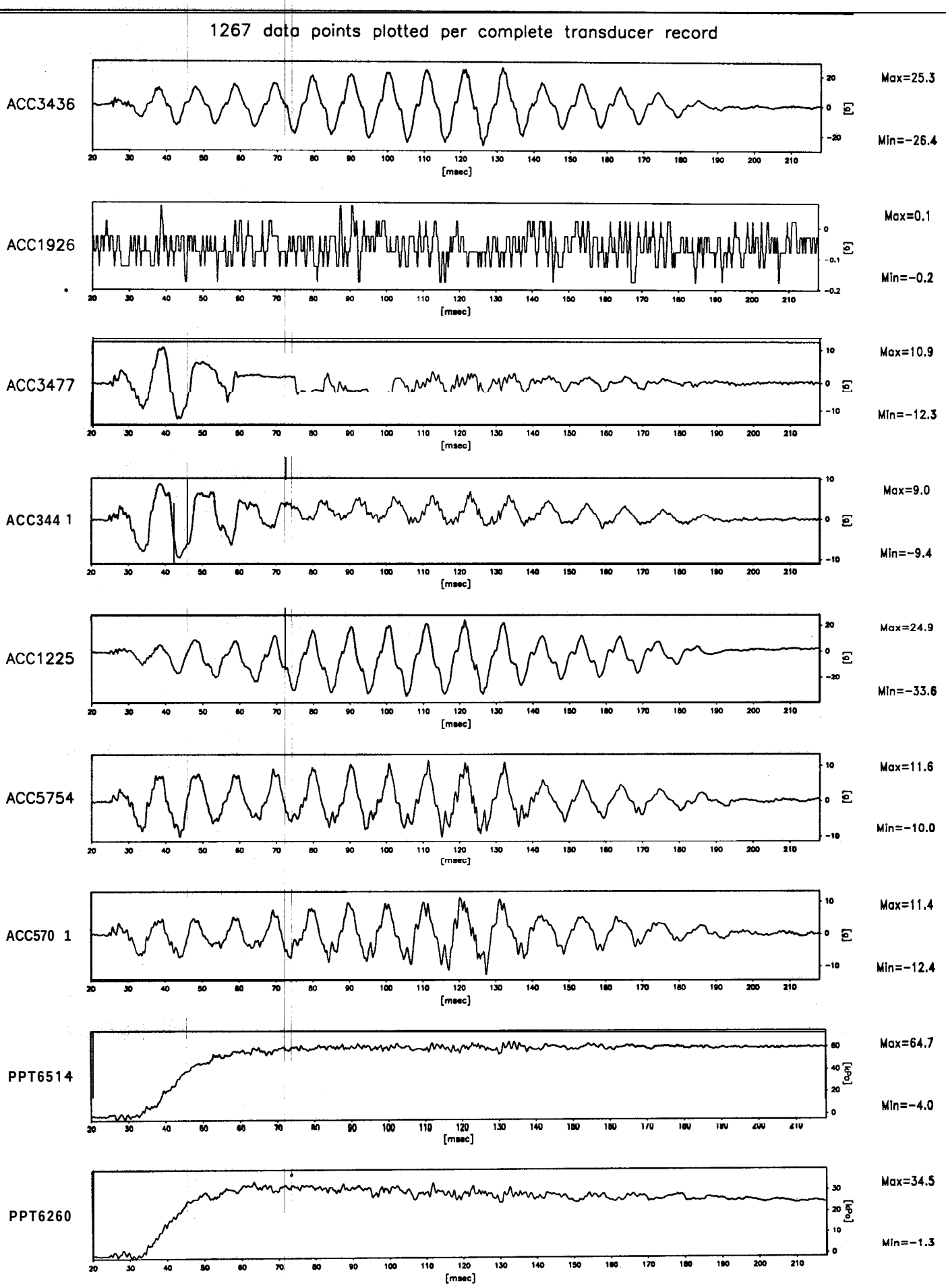

Scales : Model

TEST MG-4 MODEL SAT FLIGHT -1	EQ-1	SHORT TERM TIME RECORDS	G Level 50	FIG.NO. 7

1267 data points plotted per complete transducer record

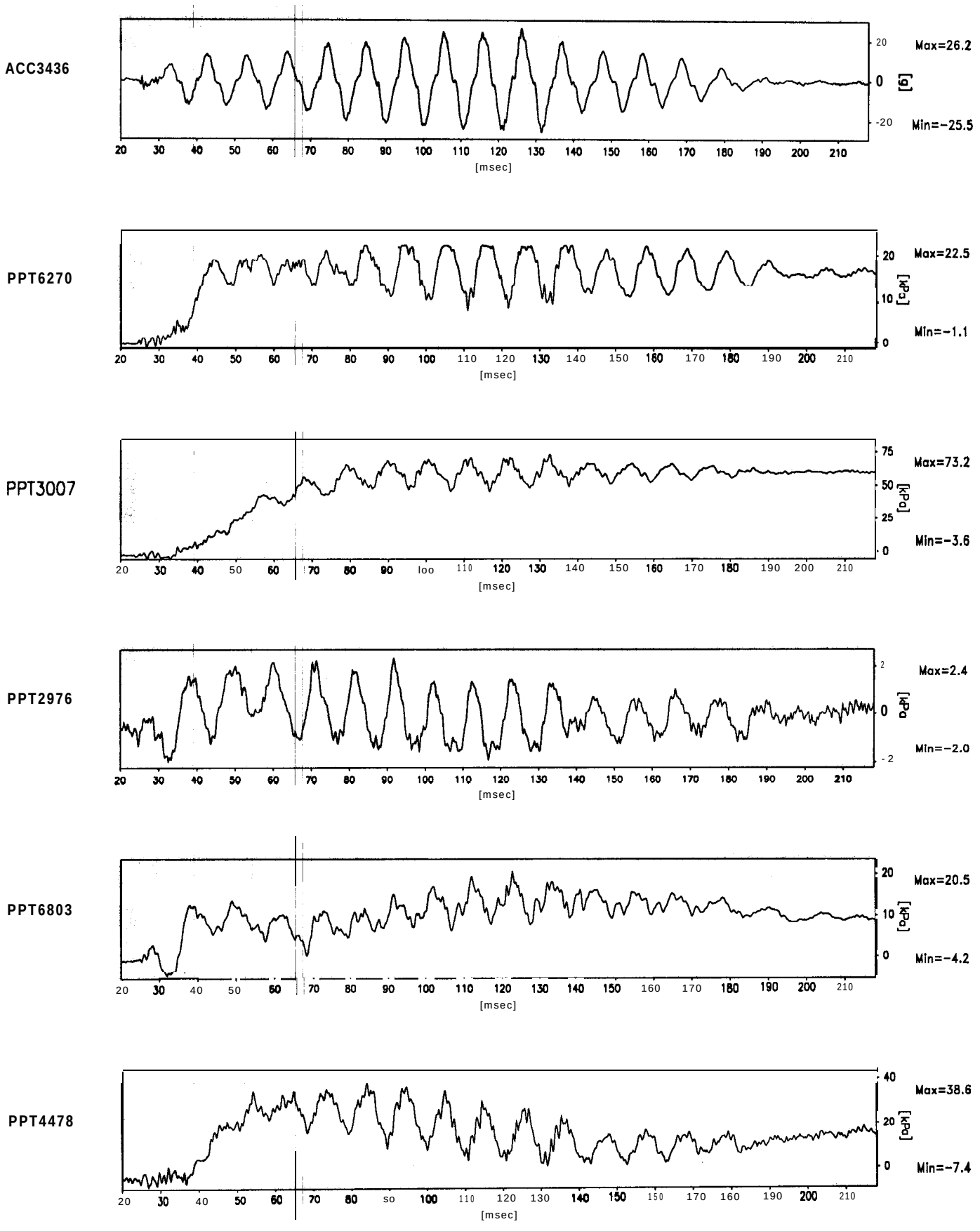

Scales : Model

TEST MG-4 MODEL SAT FLIGHT -1	EQ-1	SHORT TERM TIME RECORDS	G Level 50	FIG.NO. 8

901 data poirits plotted per complete transducer record

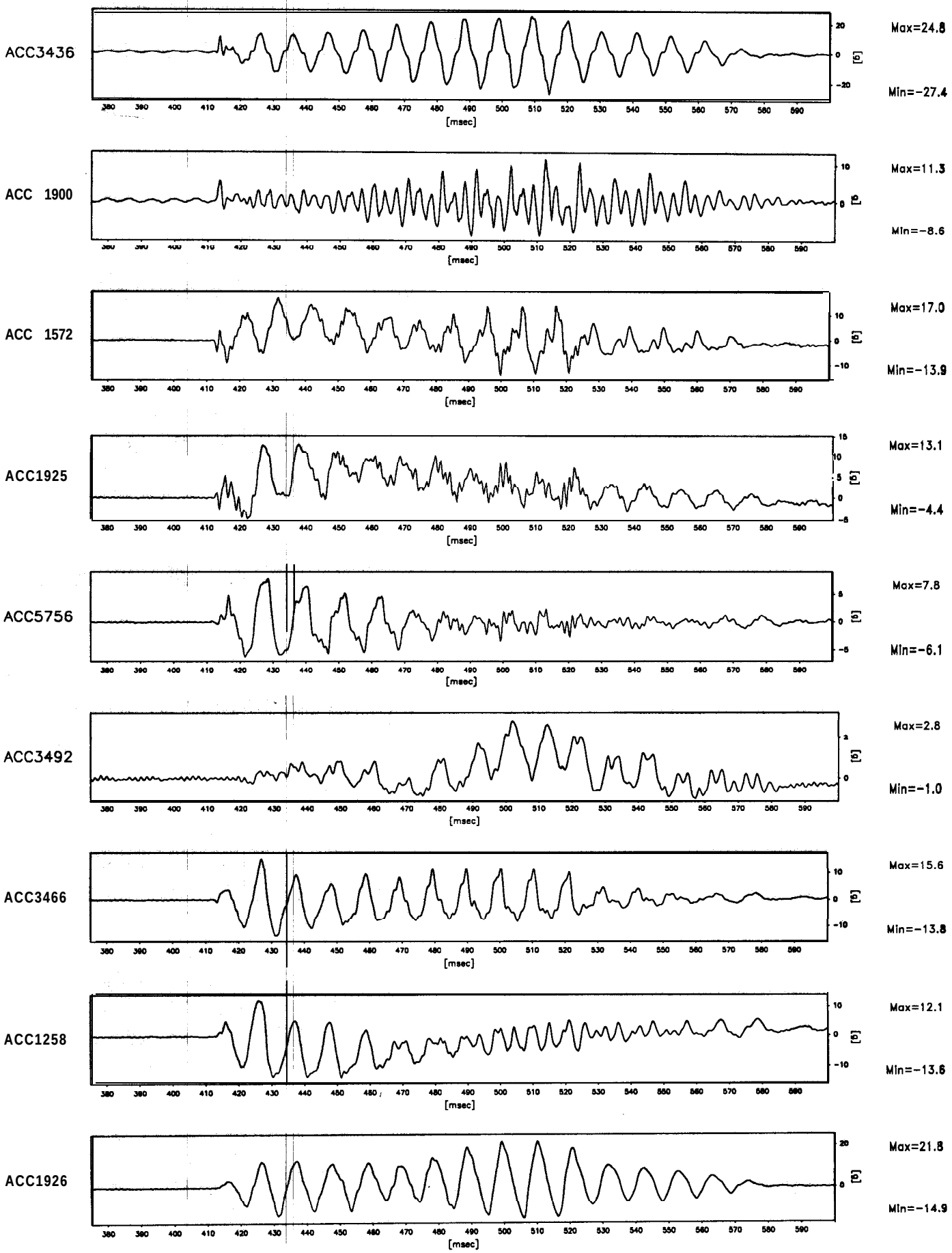

Scales : Model

TEST MG-4 MODEL SAT FLIGHT -1	EQ-1	SHORT TERM TIME RECORDS	G Level 50	FIG.NO. 9

901 data points plotted per complete transducer record

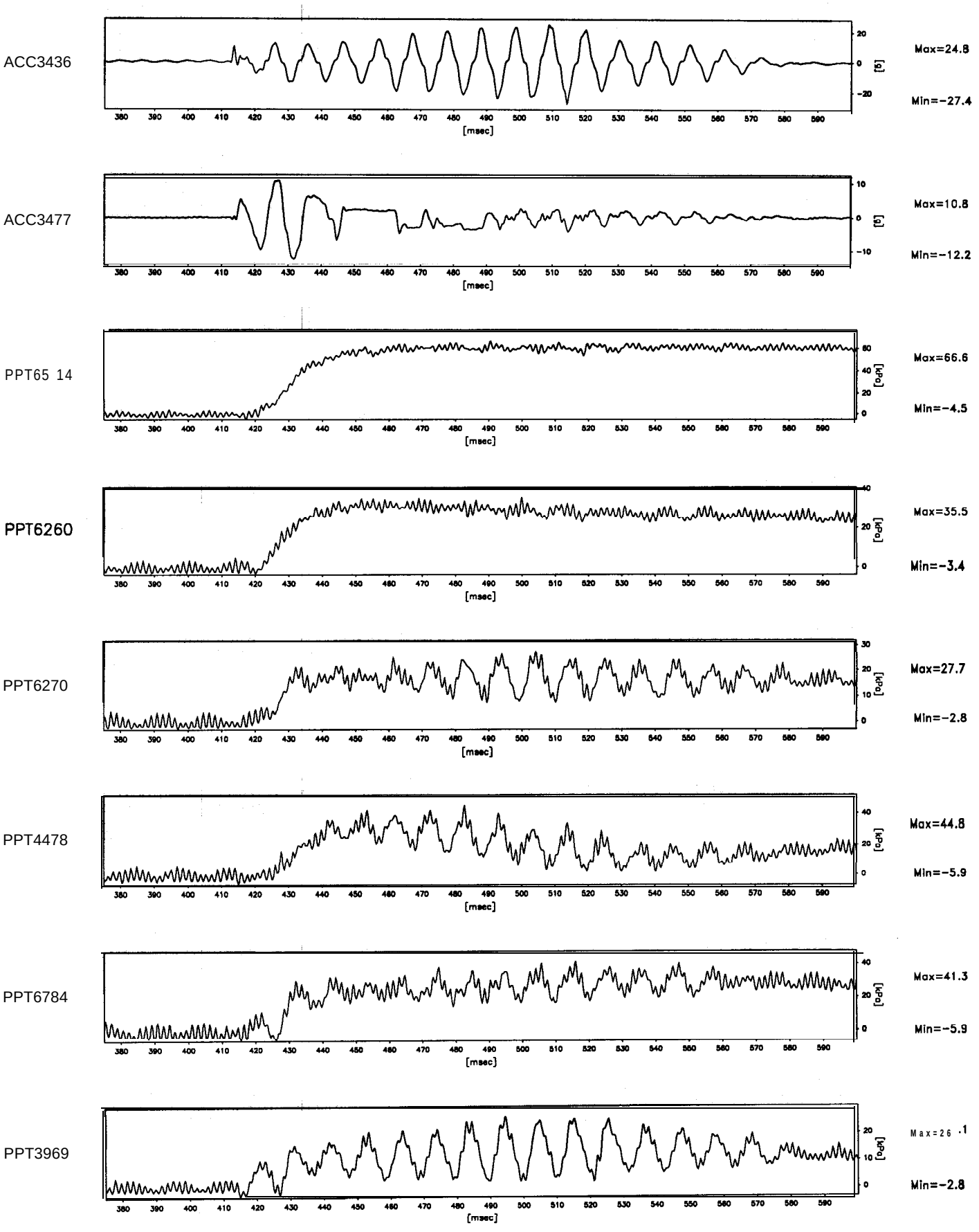

Scales : Model

TEST MG-4 MODEL SAT FLIGHT -1	EQ-1	SHORT TERM TIME RECORDS	G Level 50	FIG.NO. 10

1267 data points plotted per complete transducer record

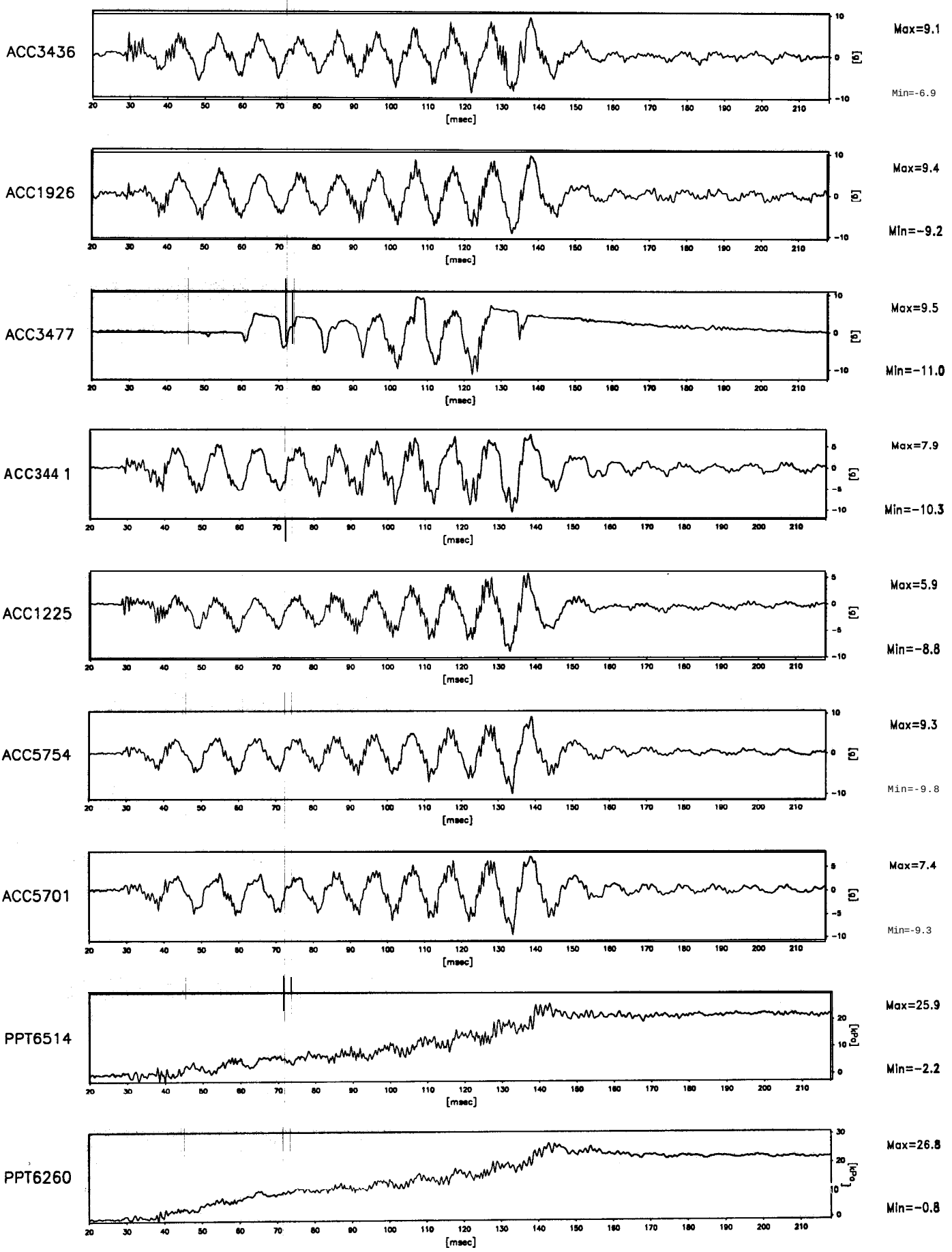

Scales : Model

TEST MG-4 MODEL SAT FLIGHT -1	EQ-2	SHORT TERM TIME RECORDS	G Level 50	FIG.NO. 11

1267 data points plotted per complete transducer record

ACC3436

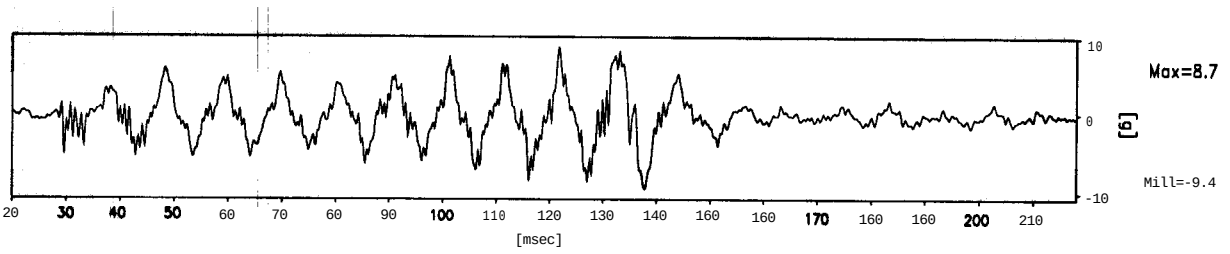

PPT6270

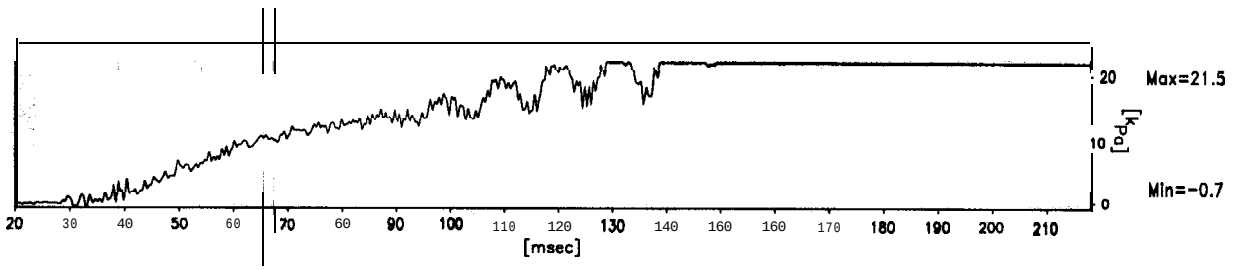

PPT3007

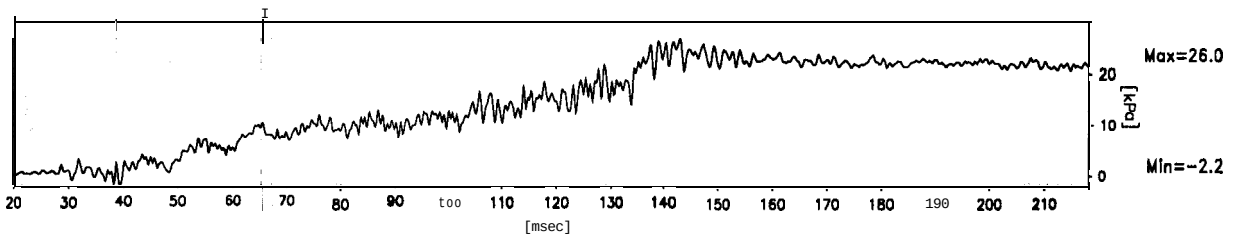

PPT2976

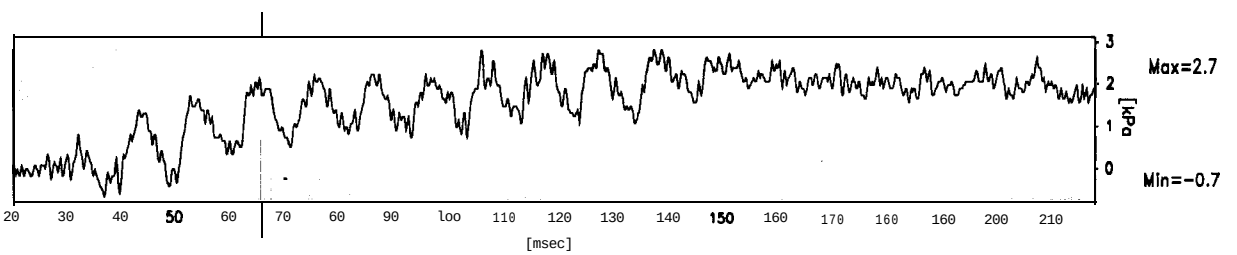

PPT6803

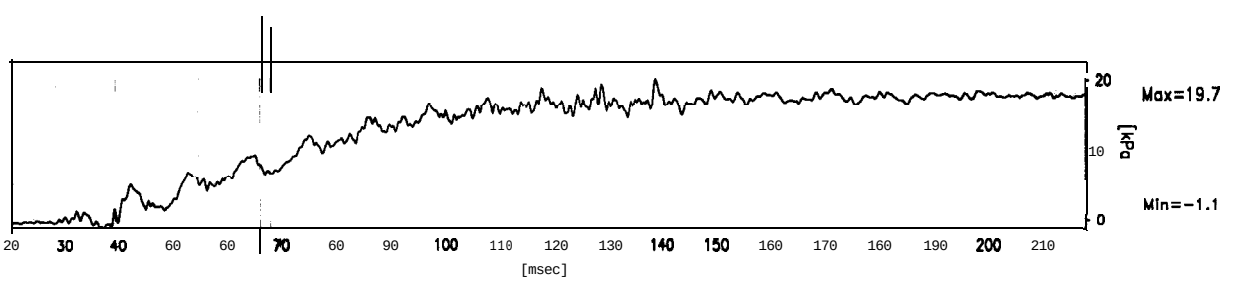

PPT4478

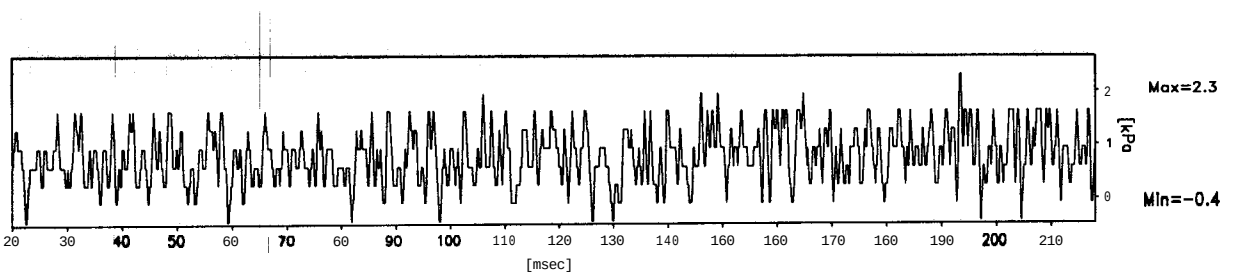

Scales : Model

TEST M G - 4 MODEL SAT FLIGHT -1	EQ–2	SHORT TERM TIME RECORDS	G Level 50	FIG.NO. 12

901 data points plotted per complete transducer record

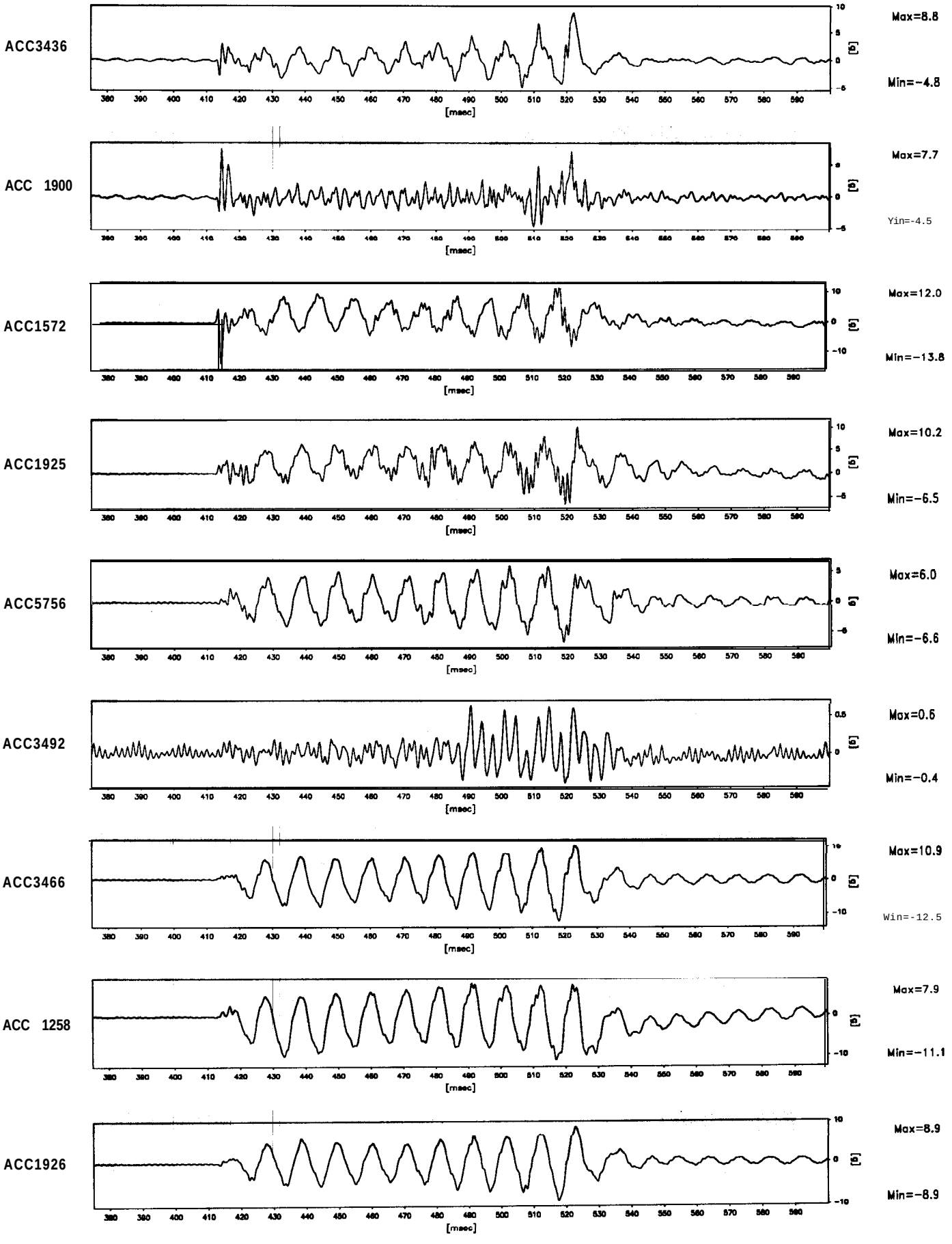

Scales : Prototype

TEST MG-4 MODEL SAT FLIGHT -1	EQ-2	SHORT TERM TIME RECORDS	G Level 50	FIG.NO. 13

901 data points plotted per complete transducer record

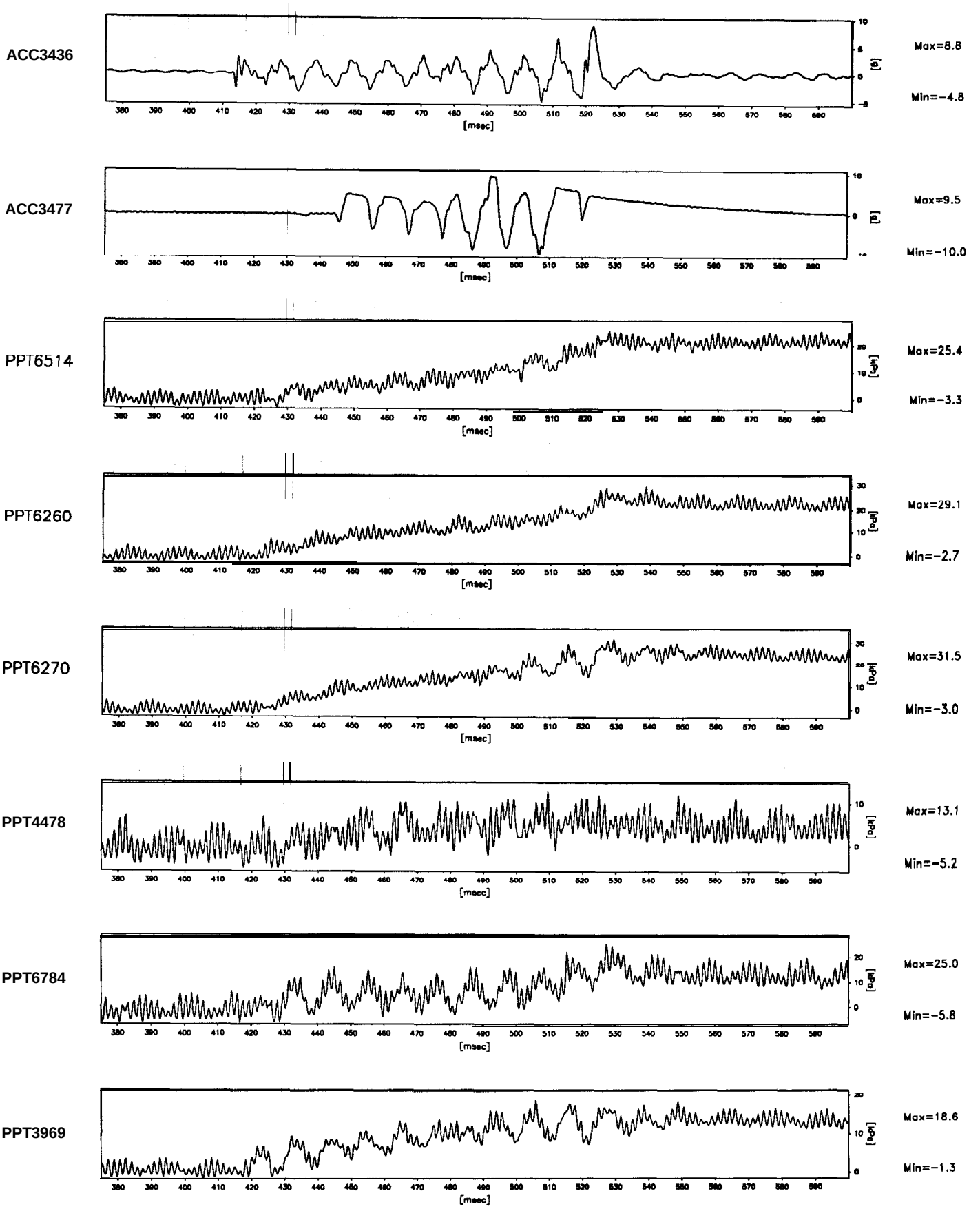

Scales : Prototype

TEST MG-4 MODEL SAT FLIGHT -1	EQ-2	SHORT TERM TIME RECORDS	G Level 50	FIG.NO. 14

1267 data paints plotted per complete transducer record

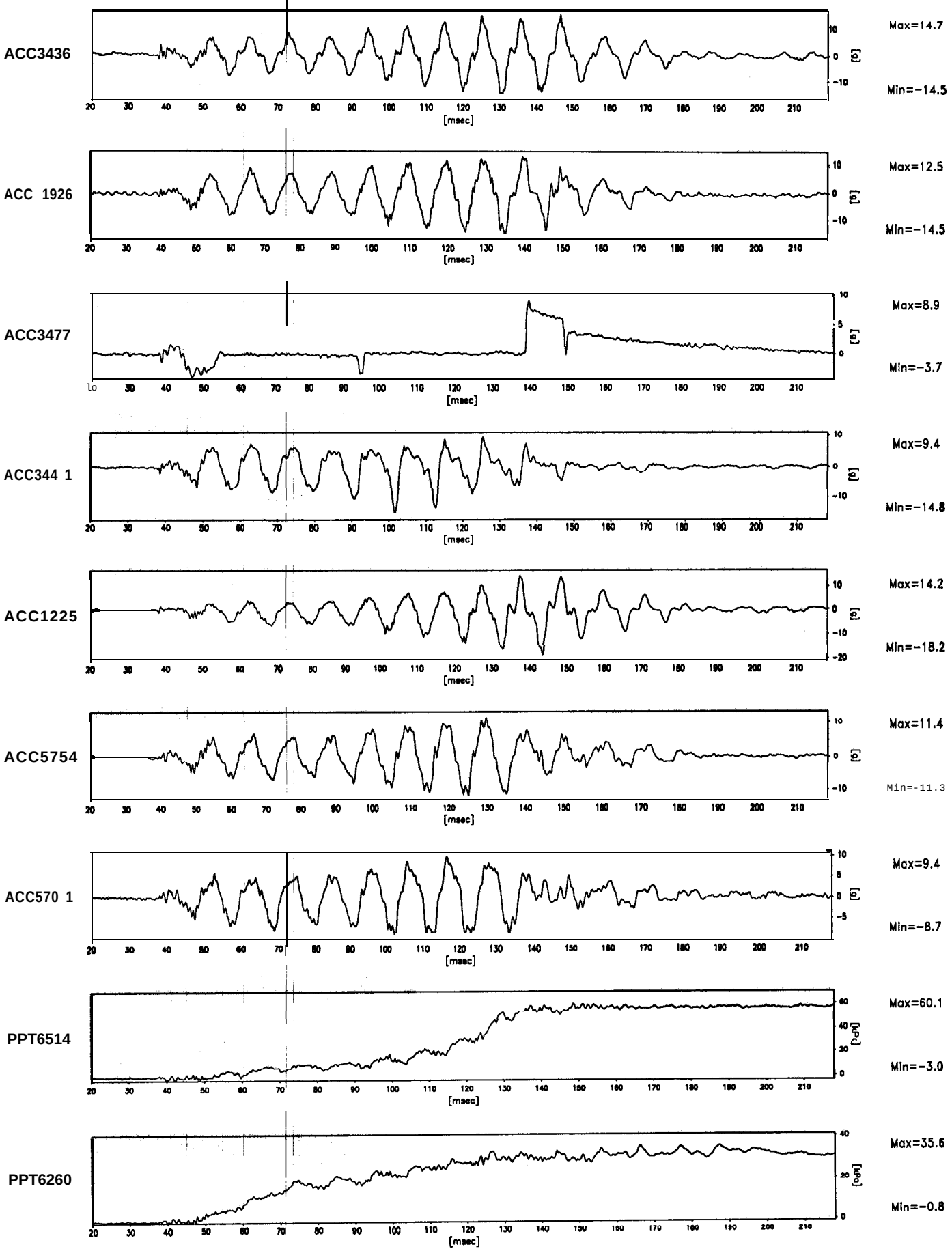

Scales : Model

TEST MG-4 MODEL SAT FLIGHT -1	EQ-3	SHORT TERM TIME RECORDS	G Level 5 0	FIG.NO. 15

1267 da ɑ points plotted per complete transducer record

ACC3436

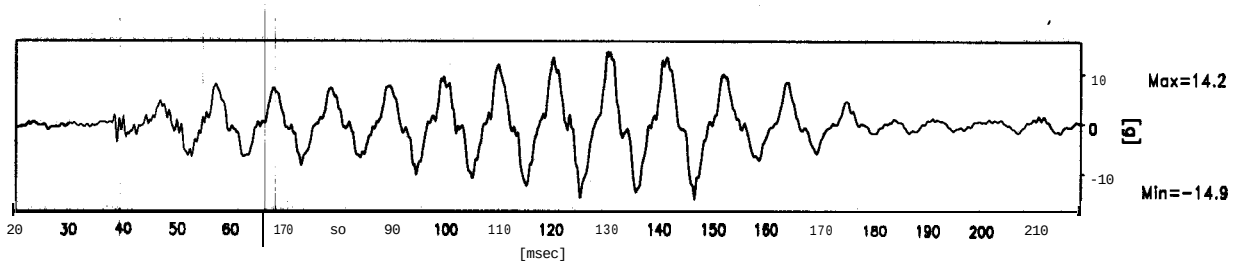

PPT6270

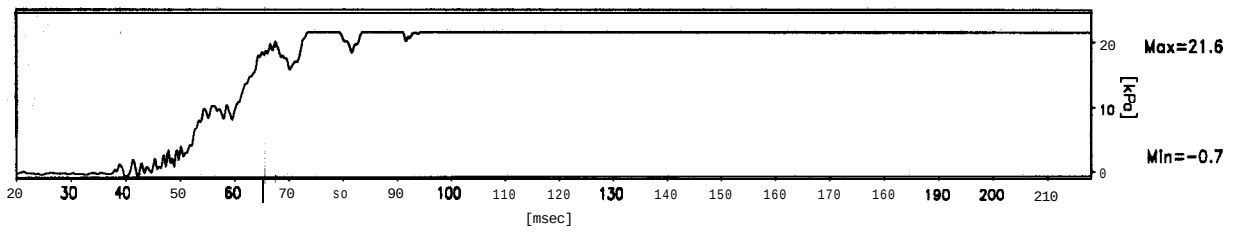

PPT3007

PPT2976

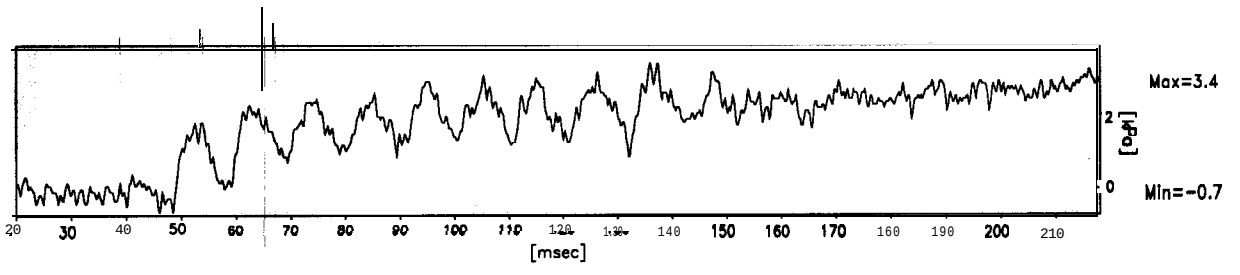

PPT6803

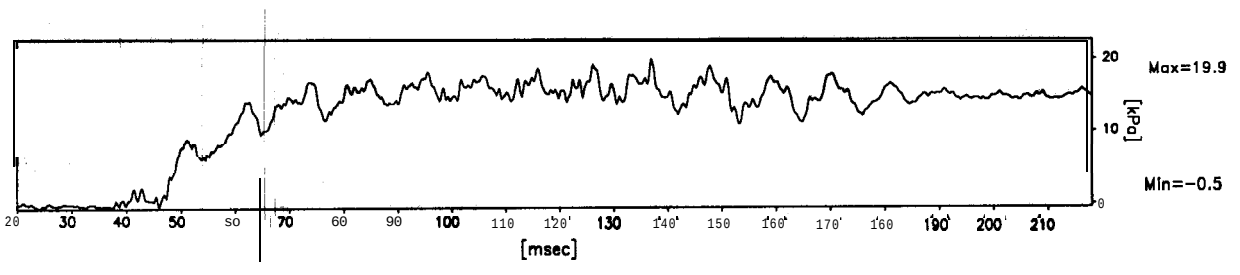

PPT4478

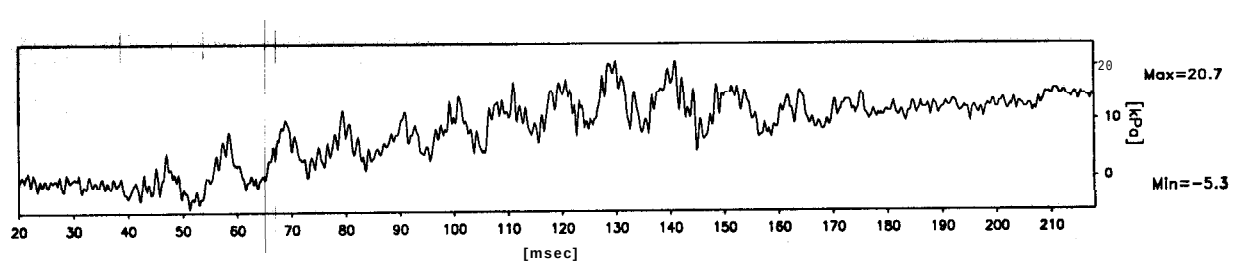

Scales : **Model**

TEST MG-4 MODEL SAT FLIGHT -1	**EQ-3**	**SHORT TERM TIME RECORDS**	**G Level 50**	FIG.NO. 16

901 data points plotted per complete transducer record

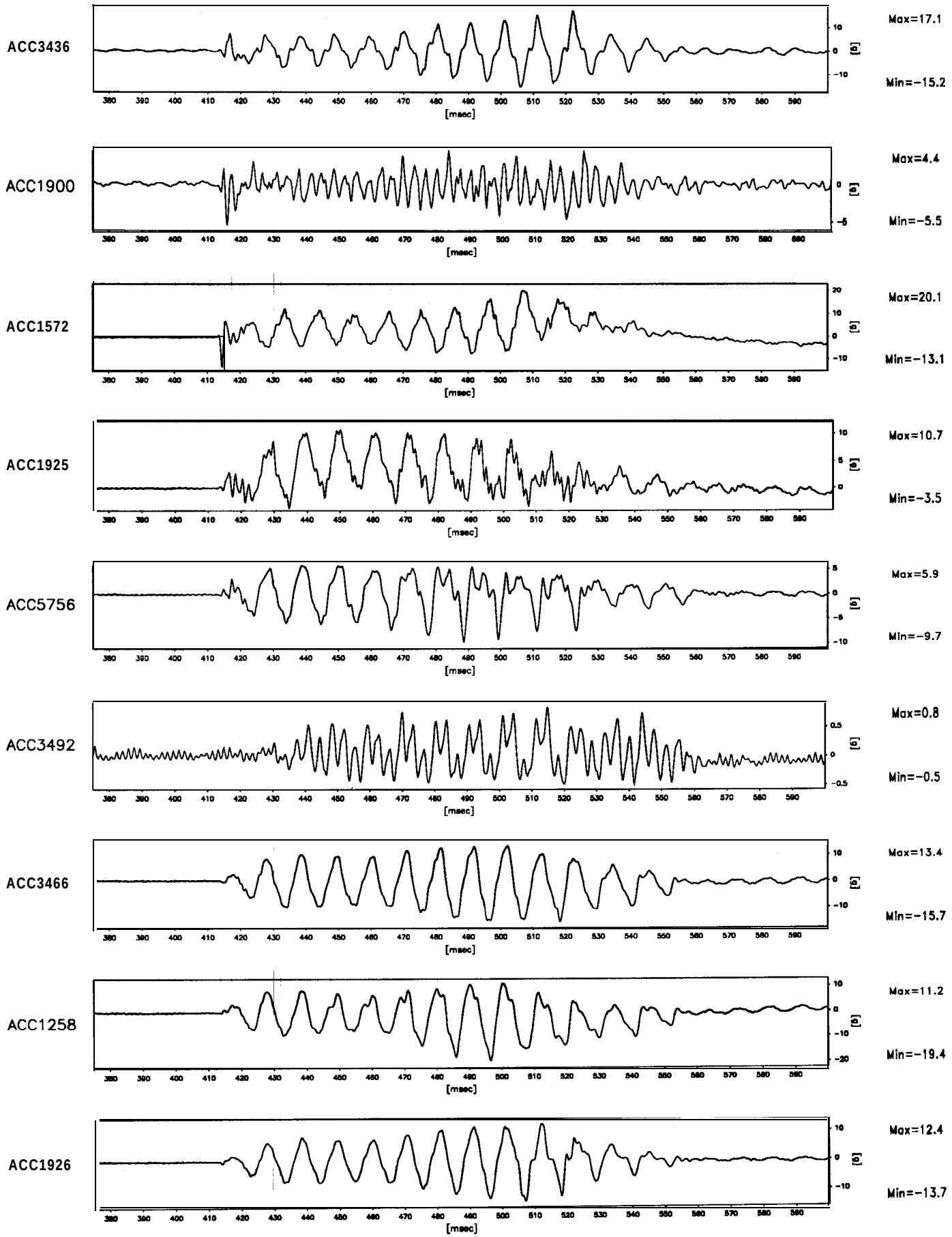

Scales : Prototype

TEST MG-4 MODEL SAT FLIGHT -1	EQ-3 ,	SHORT TERM TIME RECORDS	G Level 50	FIG.NO. 17

901 data points plotted per complete transducer record

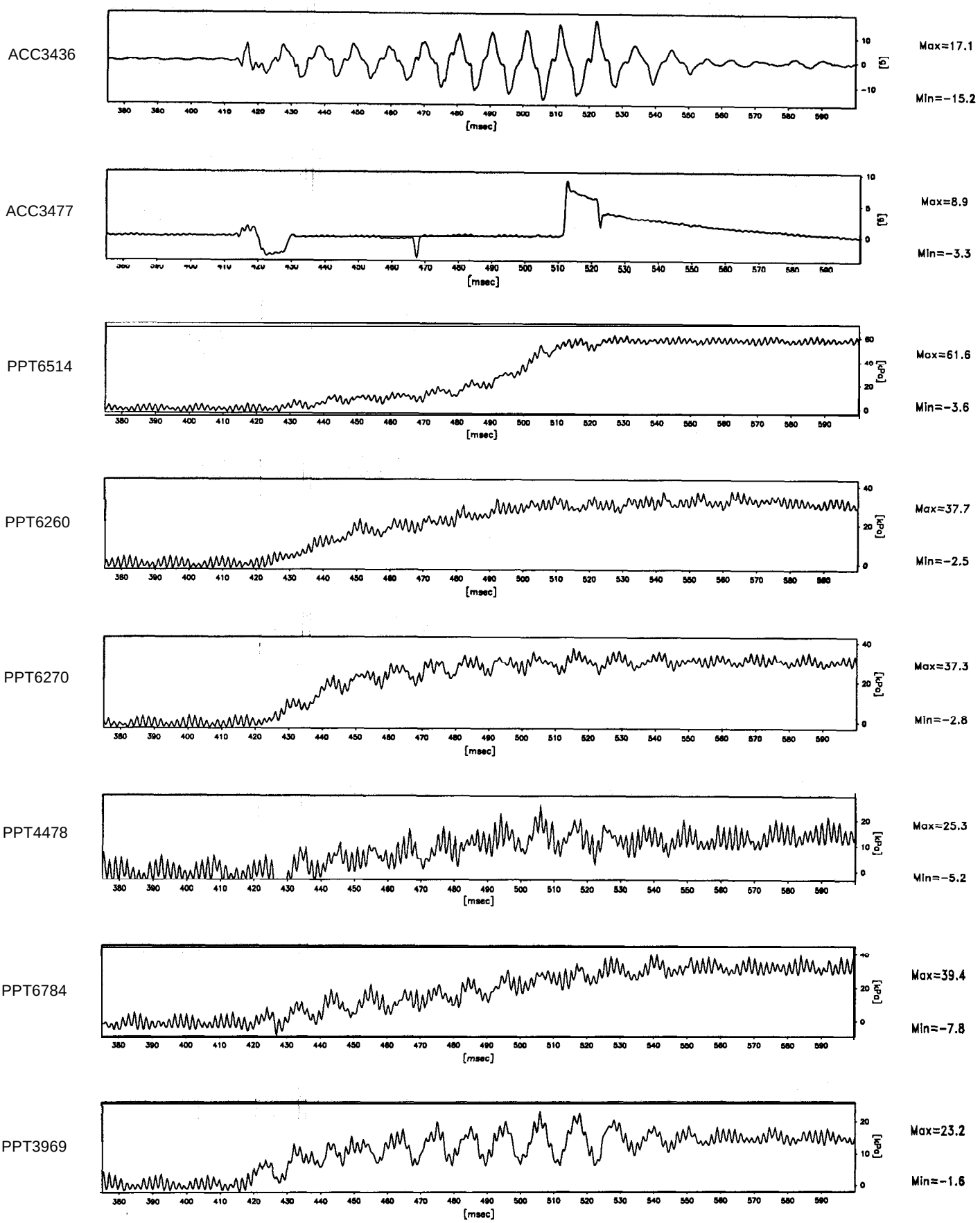

Scales : Model

TEST MG-4 MODEL SAT FLIGHT -1	EQ-3,	SHORT TERM TIME RECORDS	G Level 50	FIG.NO. 18

1267 data points plotted per complete transducer record

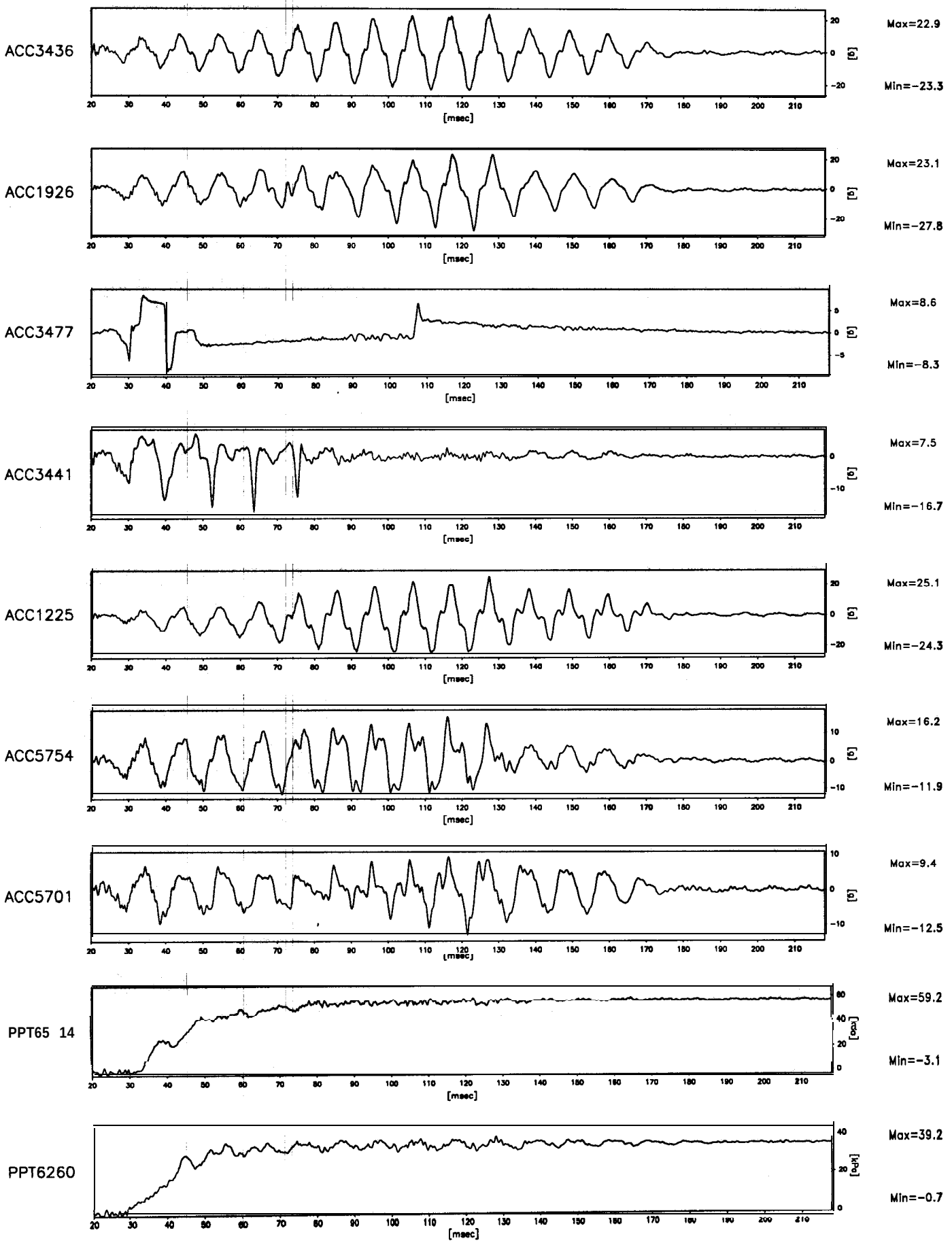

Scales : Model

TEST MG-4 MODEL SAT **FLIGHT – 1**	EQ–4	**SHORT TERM** **TIME RECORDS**	**G Level** **50**	FIG.NO. 19

1267 data points plotted per complete transducer record

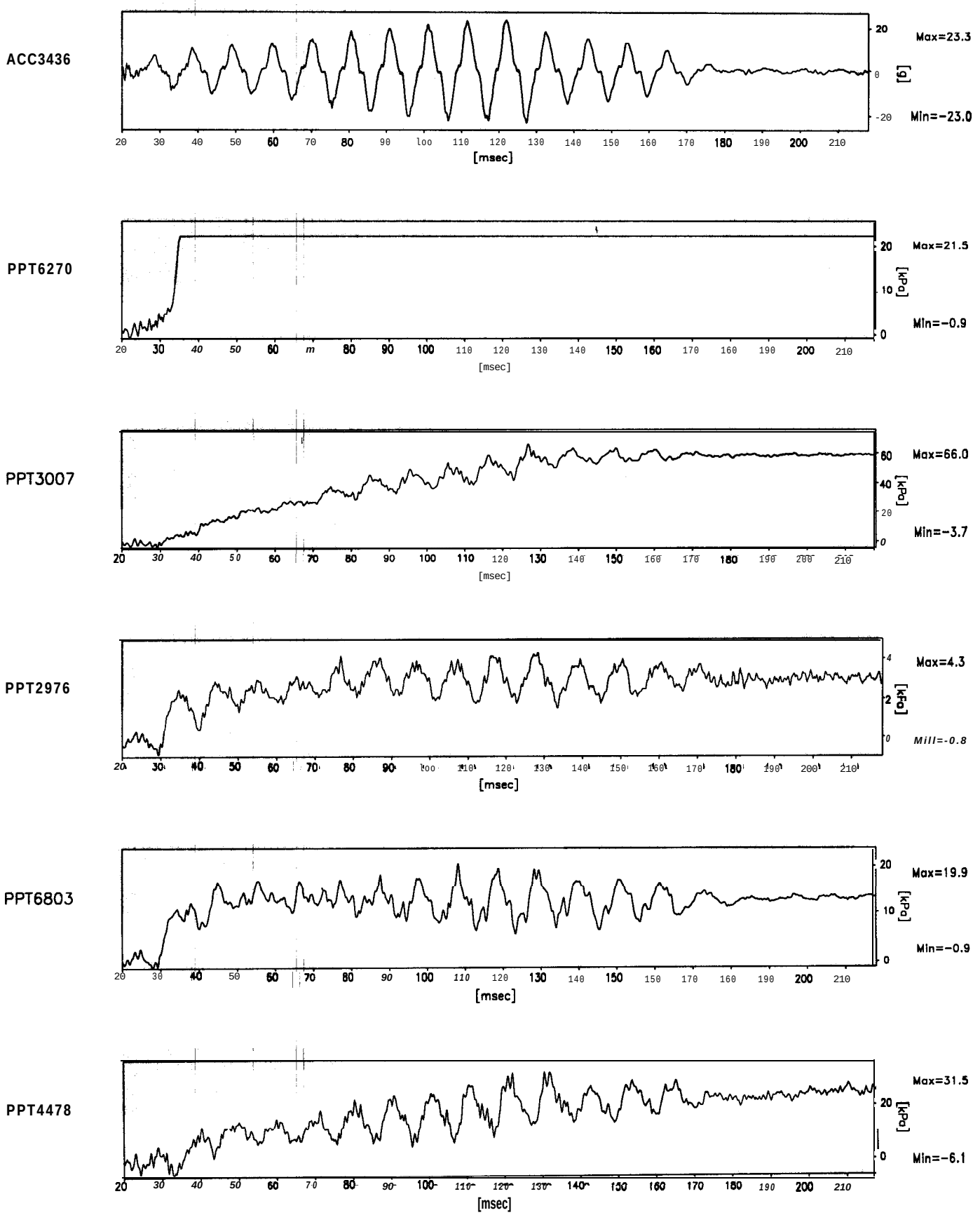

Scales : Model

TEST MG-4 MODEL SAT FLIGHT -1	EQ-4	SHORT TERM TIME RECORDS	G Level 50	FIG.NO. **20**

901 data points plotted per complete transducer record

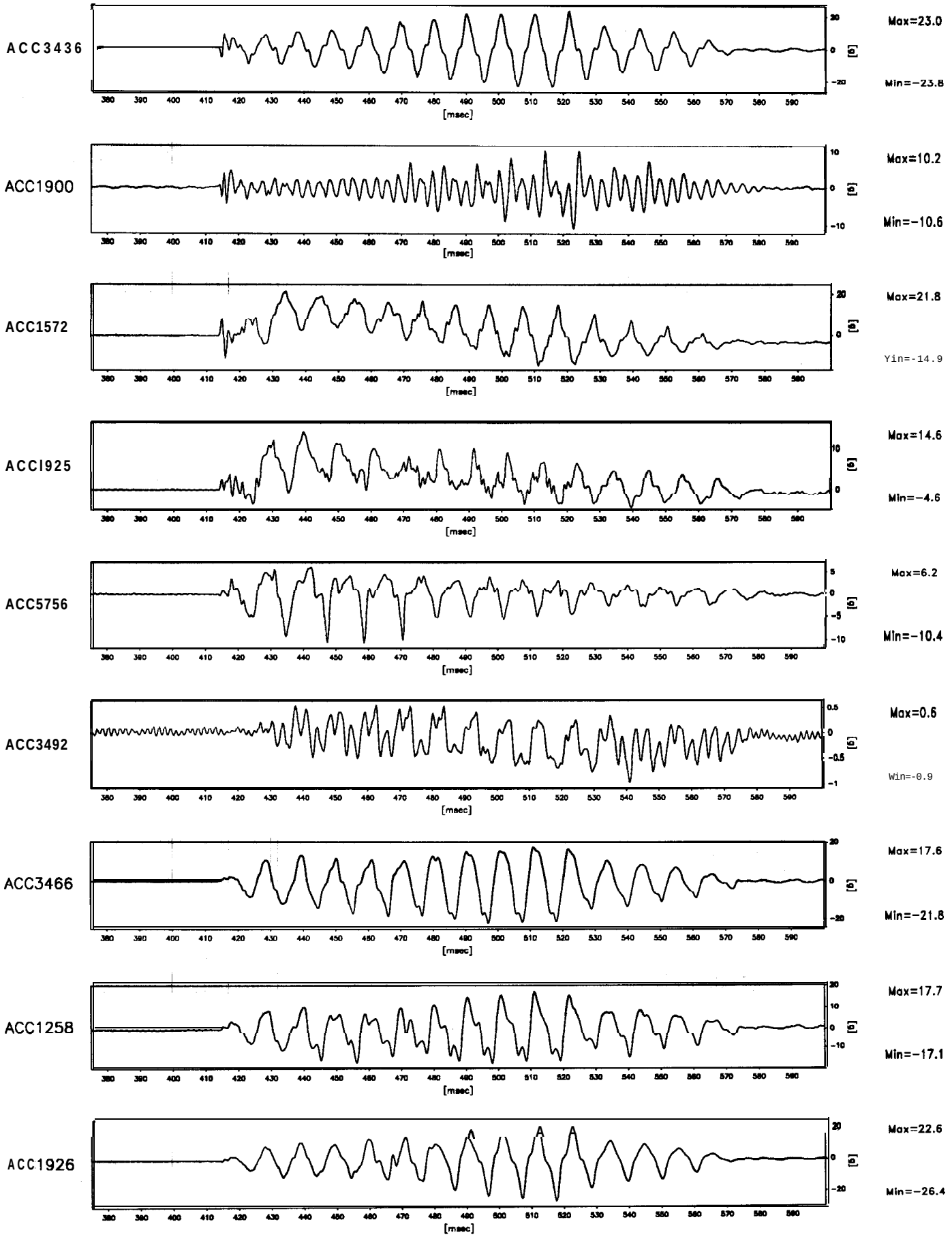

Scales : Prototype

TEST MG-4 MODEL SAT FLIGHT -1	EQ-4	SHORT TERM TIME RECORDS	G Level 50	FIG.NO. **21**

901 data points plotted per complete transducer record

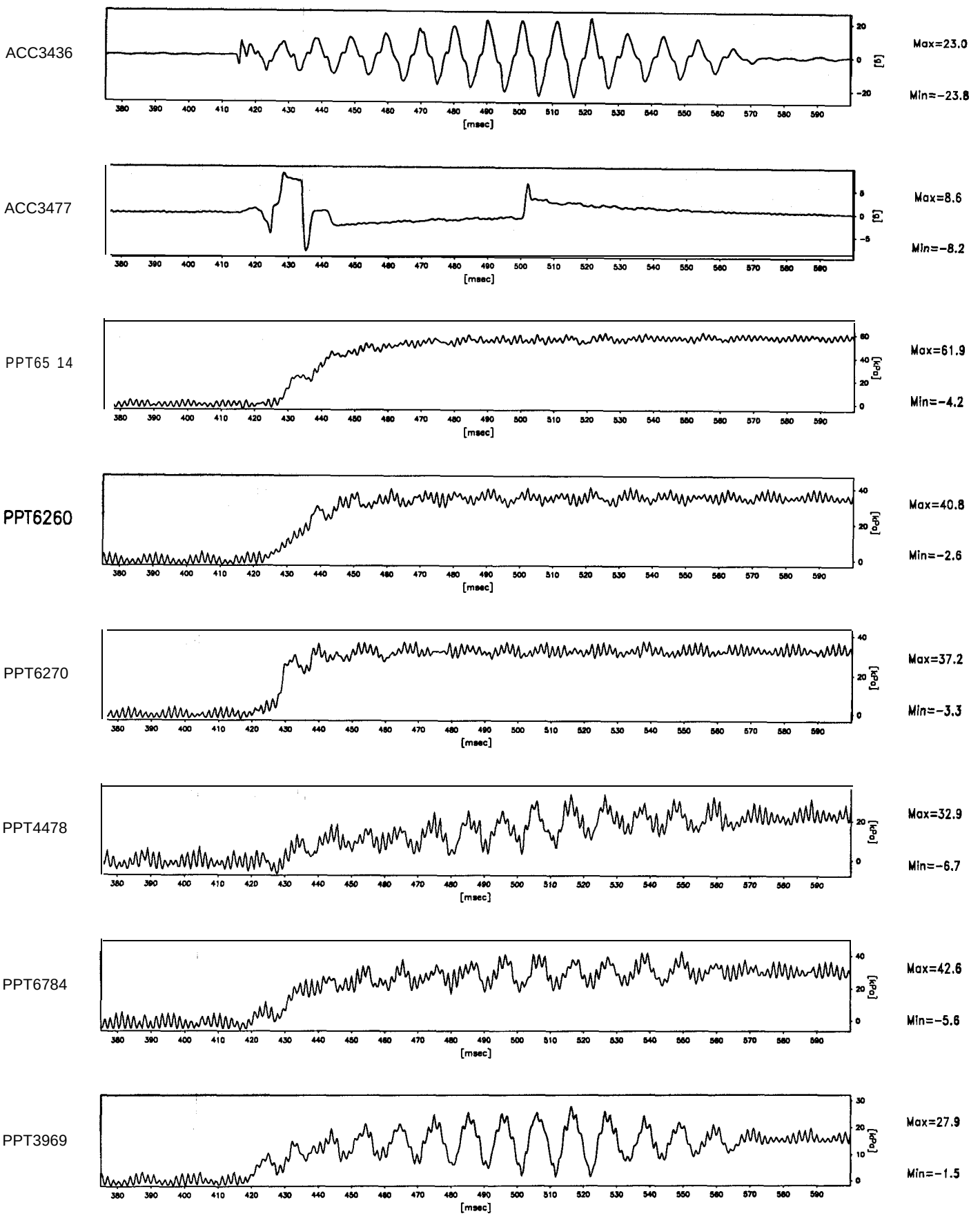

Scales : Model

TEST MG-4 MODEL SAT FLIGHT -1	EQ-4	SHORT TERM TIME RECORDS	G Level 50	FIG.NO. 22

1267 data points plotted per complete transducer record

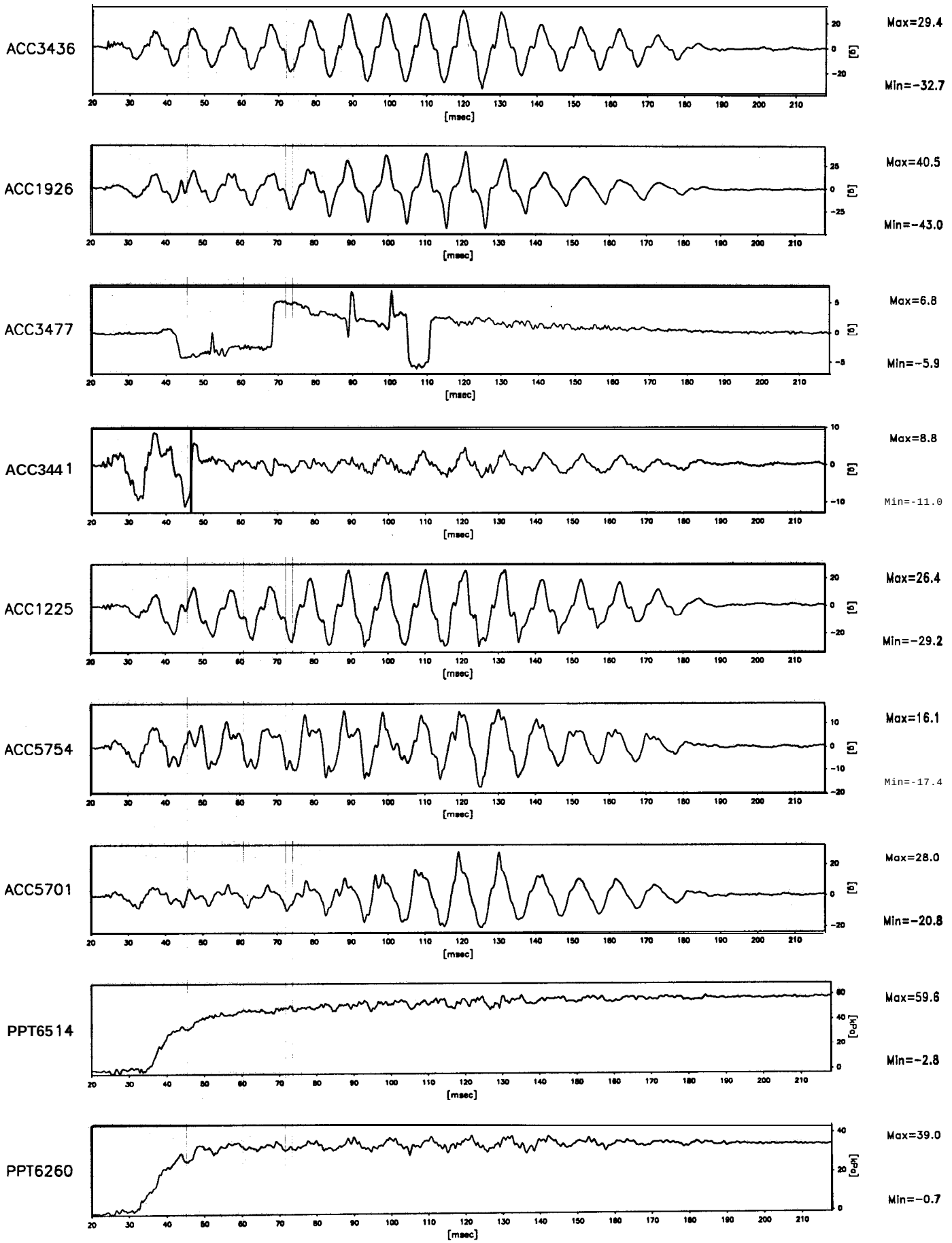

Scales : Model

TEST MG-4 MODEL SAT FLIGHT -1	EQ-5	SHORT TERM TIME RECORDS	G Level 50	FIG.NO. 23

1267 data' points plotted per complete transducer record

ACC3436

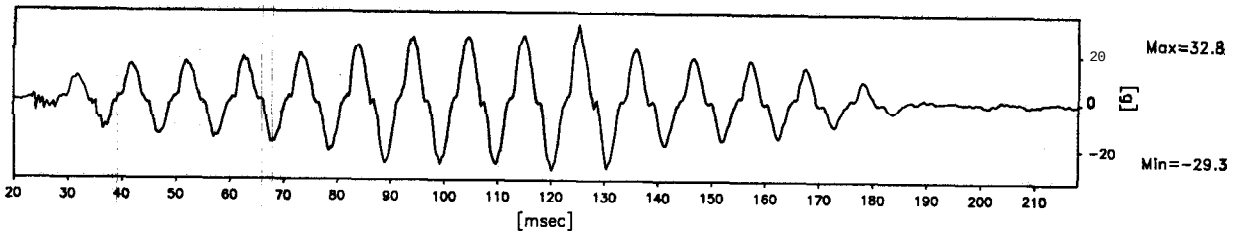

PPT6270

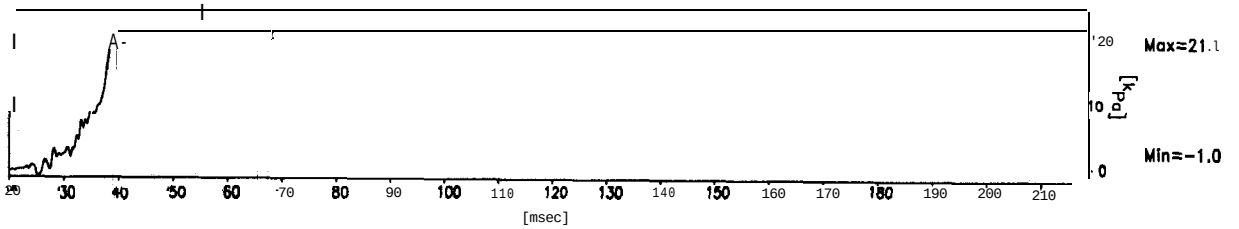

PPT3007

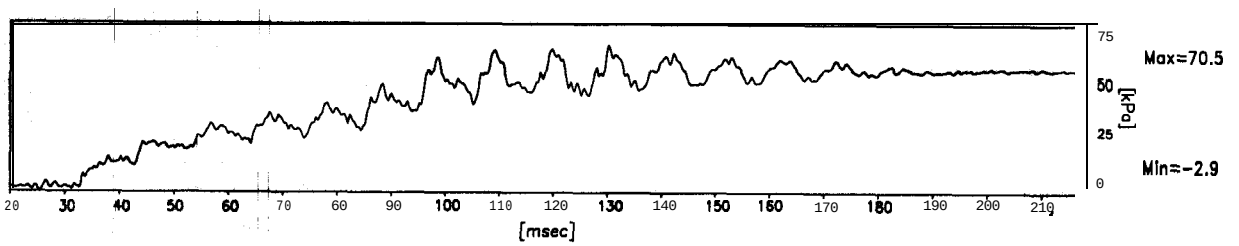

PPT2976

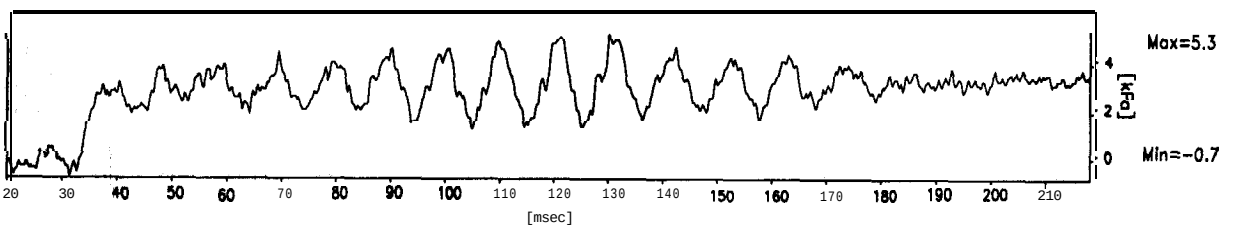

PPT6803

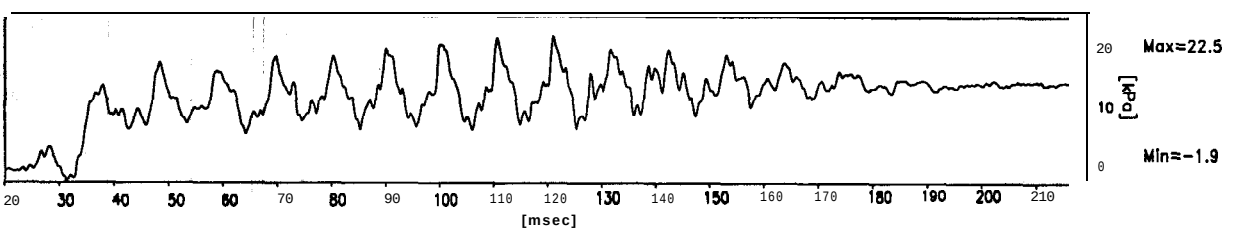

PPT4478

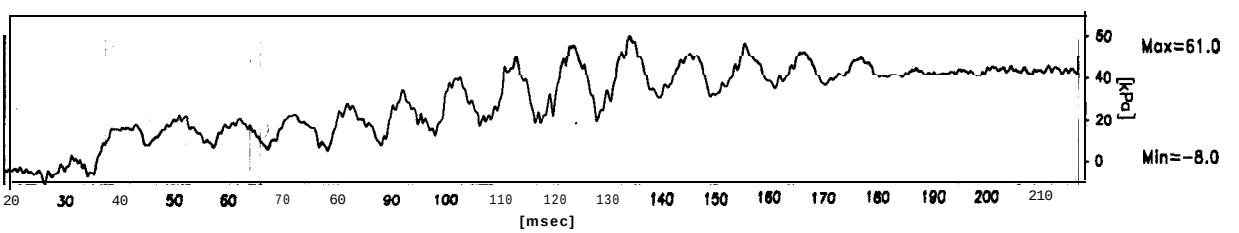

Scales : Model

TEST MG-4 MODEL SAT FLIGHT -1	EQ-5	**SHORT TERM TIME RECORDS**	**G Level 50**	FIG.NO. **24**

901 data points plotted per complete transducer record

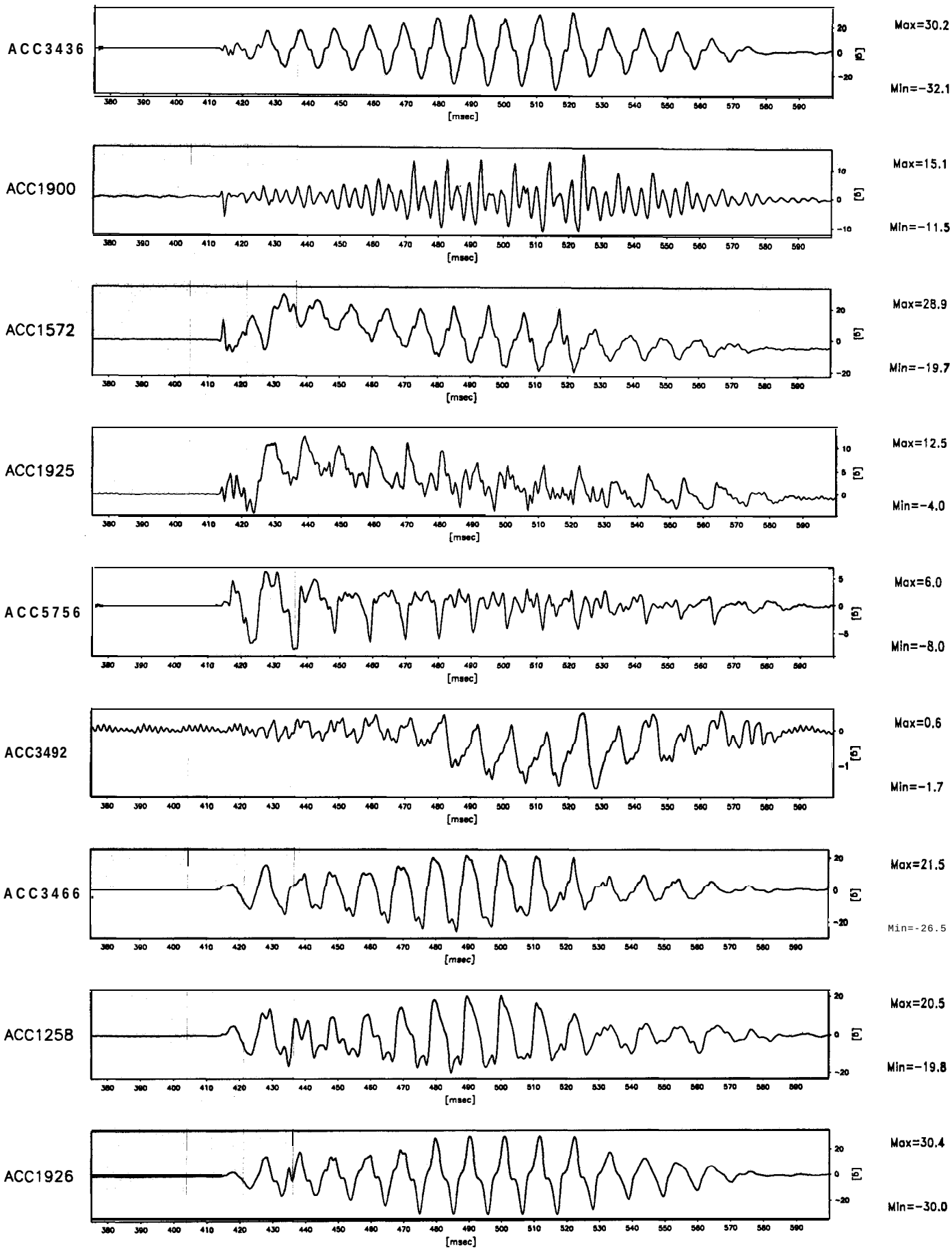

Scales : Model

TEST MG-4 MODEL SAT FLIGHT -1	EQ-5	SHORT TERM TIME RECORDS	G Level 50	FIG.NO. 25

901 data points plotted per complete transducer record

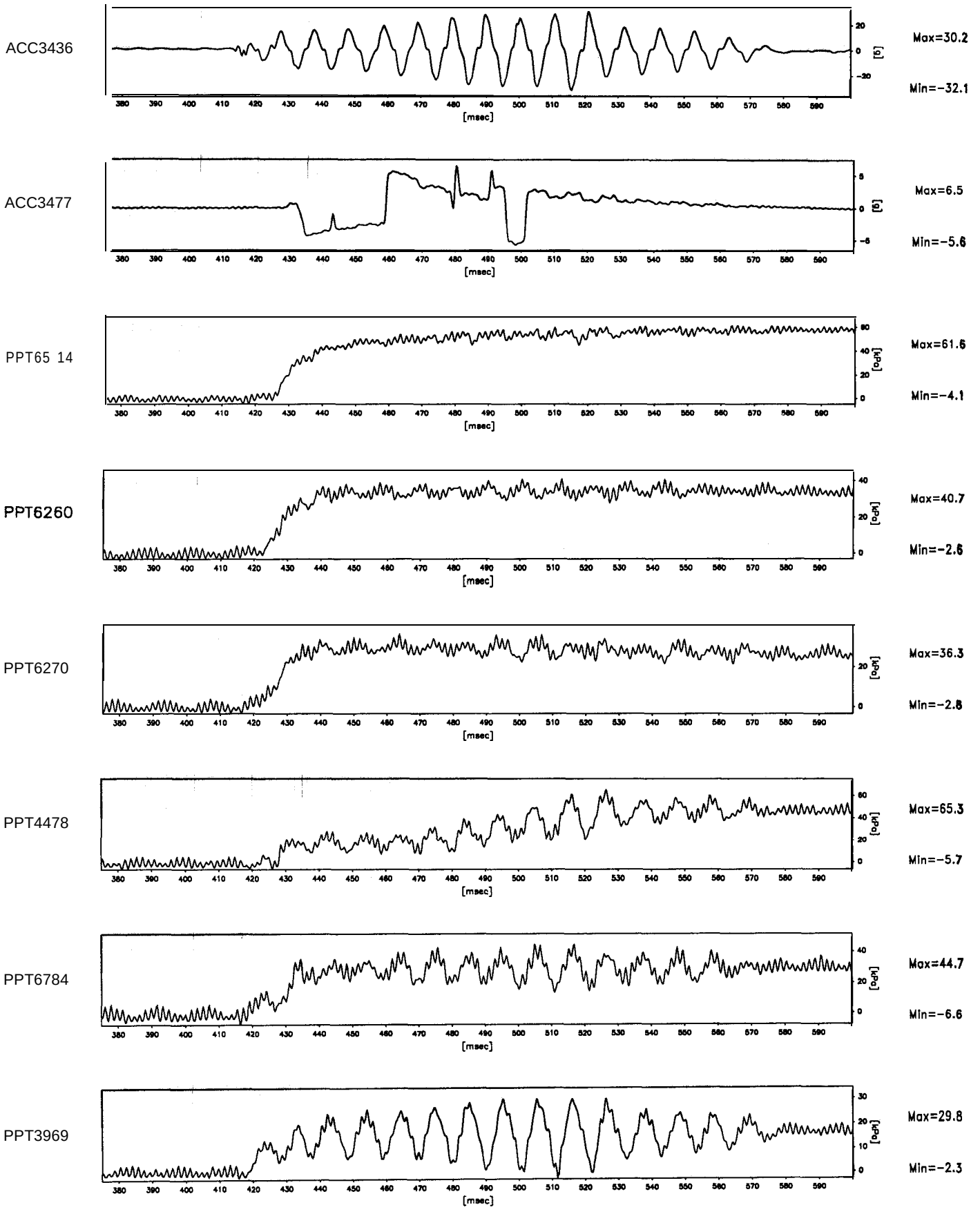

Scales : Model

TEST MG-4 MODEL SAT FLIGHT – 1	EQ-5	SHORT TERM TIME RECORDS	G Level 50	FIG.NO. 26

13.0 Analysis of data from centrifuge test MG-4

The saturated sand bed in centrifuge model MG-4 had a height of 155 mm, The first earthquake was a strong earthquake with a peak acceleration of about 25 %. A smaller strength earthquake of 9.1 % was fired next. After this the strength of the earthquakes was gradually increased in the subsequent events. The hydrostatic pore pressures during the swing up and while increasing the centrifugal acceleration to '50g' are presented in Table 2. Note that during an earthquake event excess pore pressures are generated over and above these hydrostatic pore pressures.

In Fig.27 the near surface accelerations recorded by ACC 3441 in all the earthquakes are presented on the left hand side. During earthquake 1 the input acceleration was strong and the surface accelerations attenuate significantly after first two cycles and following the generation of excess pore pressures within the sand bed. The frequency analysis of this trace is presented on the right hand side in Fig.27. From the frequency analysis of this trace we can see that most of the energy is concentrated at about 100 Hz. A separate peak close to the 95 Hz frequency which is the driving frequency of the earthquake is also seen in this figure. The peak excess pore pressures produced during each earthquake near the base of the sand bed, at mid depth and near the surface are plotted in Fig.28. Earthquake 2 was a small strength earthquake and magnitude of excess pore pressures was small as seen in Fig.28. As a result all the cycles of base shaking are present near the surface of the sand bed as well. Further the frequency analysis of this trace shows that all the energy is now present at the driving frequency of the earthquake which is 95 Hz (see the right hand side in Fig.27). A slightly stronger earthquake was fired next. The excess pore pressures generated were almost equal to those generated during earthquake 1. The near surface accelerations show attenuation compared to the base motion (see Table 3). All the cycles of base motion are present in this trace. However the accelerations on the negative side have a larger amplitude compared to the positive side. Further the frequency analysis of the near surface accelerations during this earthquake as seen on the right hand side of Fig.27 indicate

that there are significant high frequency components in this trace. Earthquake 4 had a similar strength to that of earthquake 1. After $4^1/_2$ cycles the near surface accelerations are significantly attenuated. The frequency analysis of this trace indicate the presence of high frequency components (see the right hand side in Fig.27). Also the near surface accelerations have larger peak accelerations on the negative side compared to the positive side. During the last earthquake the attenuation of near surface accelerations sets in after first $1^1/_2$ cycles itself. However the accelerations appear to recover towards the end of the earthquake as noted in the previous section. The frequency analysis of this trace indicate that most of the energy is present at the driving frequency of the earthquake with some energy at the higher frequencies.

The column of accelerometers (see Fig.6) placed in the middle of the saturated sand bed experienced attenuation of peak accelerations following the generation of excess pore pressures in each earthquake. In table 3 the peak accelerations recorded by the above column of accelerometers which are normalised by the acceleration at the base of the sand column during each earthquake are presented. In Fig.28 the excess pore pressures generated in each earthquake are plotted against the strength of the earthquake. From this figure it is clearly seen that the smaller strength earthquake 2 resulted in smaller excess pore pressures. On the converse larger strength earthquakes all resulted in large excess pore pressures. The larger excess pore pressures also mean lower effective stresses in the soil and hence degradation in soil stiffness. The smaller excess pore pressures during earthquake 2 meant that there was smaller attenuation of the base motion as it propagates towards the soil surface during this earthquake. In sections 3, 4 and 5 of this report the procedure to estimate the natural frequency of the saturated sand bed by using the shear modulus of the soil which is corrected for the shear strain amplitude induced during the earthquake loading and by using effective stresses corrected for excess pore pressures induced during an earthquake is presented. For an earthquake of given strength it is possible to relate the variation of natural frequency with the generation of excess pore pressure. In Fig.29 the variation of

natural frequency of the saturated sand bed used in the centrifuge model MG-4 with the generation of excess pore pressures is presented for earthquakes of varying strengths from 2 % to 20 %. The soil parameters of this centrifuge model were substituted in equations 1 to 12 and the results are plotted in Fig.29. From this figure it is clear that for an earthquake of a particular strength the natural frequency drops with the increase in excess pore pressure. Also stronger earthquakes results in lower natural frequencies as larger shear strains are realised.

In Fig.30 the normalised acceleration in table 3 is plotted against the strength of the earthquakes fired during this centrifuge test. The near surface acceleration is normalised using the acceleration at the base of the sand bed and this normalised acceleration is plotted along the ordinate. From this figure earthquake 2 which had the smallest strength (9.1 %) and produced relatively small excess pore pressures (see Fig.28) results in largest normalised acceleration. In other words earthquake 2 gave rise to the smallest attenuation of base motion as it travelled towards the sand bed. As the strength of the earthquake is increased the normalised acceleration is reduced as seen in Fig.30.

This result can be explained using the theoretical variation shown in Fig.29. Earthquake 2 had resulted in an acceleration of 9.4 % at the base of the soil column considered in above discussion. This earthquake also resulted in the generation of excess pore pressures of the magnitude of about 30 kPa. From Fig.29 we can obtain the natural frequency of the saturated sand bed under these conditions as about 115 Hz. This is close to the driving frequency of the earthquake which is 96 Hz and hence results in relatively low attenuation. From Fig.29 we can see that when the strength of the earthquakes is larger and large excess pore pressures are generated the natural frequency of the sand bed falls to very small values. In other words, under those conditions there will be much larger attenuation of the base shaking as it travels

towards the sand surface. This is confirmed in Fig.30 which shows that stronger earthquakes have indeed led to larger attenuations.

In Fig.31 the pore pressures recorded at the base of the sand column by the pore pressure transducer 6514 (also see Fig.6) during each of the earthquake event is presented. The rate of the excess pore pressure build up clearly appears to be a function of the strength of the earthquake. During the first earthquake which had a strength of 25.3 % the build up was rapid as seen in Fig.31. During the smaller second earthquake not only the magnitude of the excess pore pressure generated is smaller but the rate of build up is much more slower compared to earthquake 1. During earthquake 3 the rate of build up is slightly faster especially towards the end of the earthquake. The rate of pore pressure build up increases further during earthquake 4 and 5 and is comparable to that in the very first earthquake.

data points plotted per complete transducer record

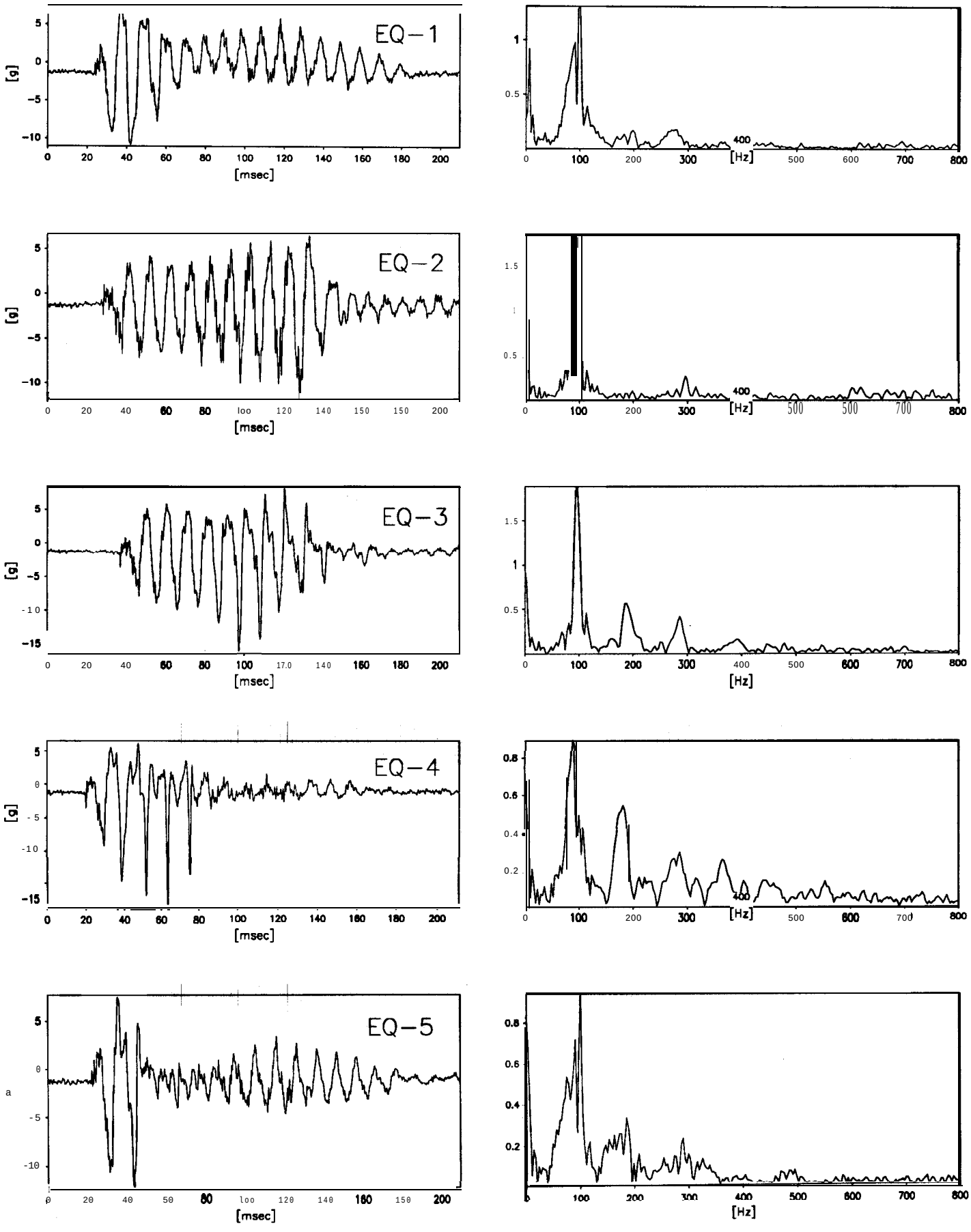

Scales : Prototype

TEST MG-4 MODEL SAT FLIGHT -1		Near Surface Accelerations and Frequency Analyses	FIG.NO. 27

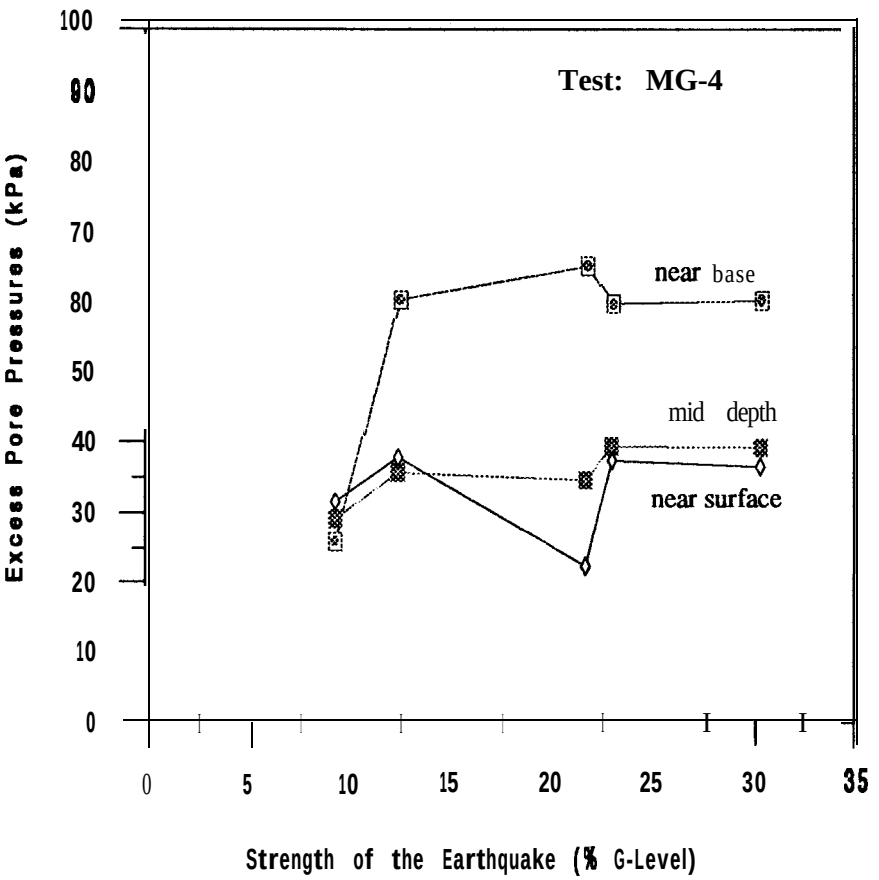

Fig.28 Generation of excess pore pressures during the earthquakes in centrifuge test MG-4

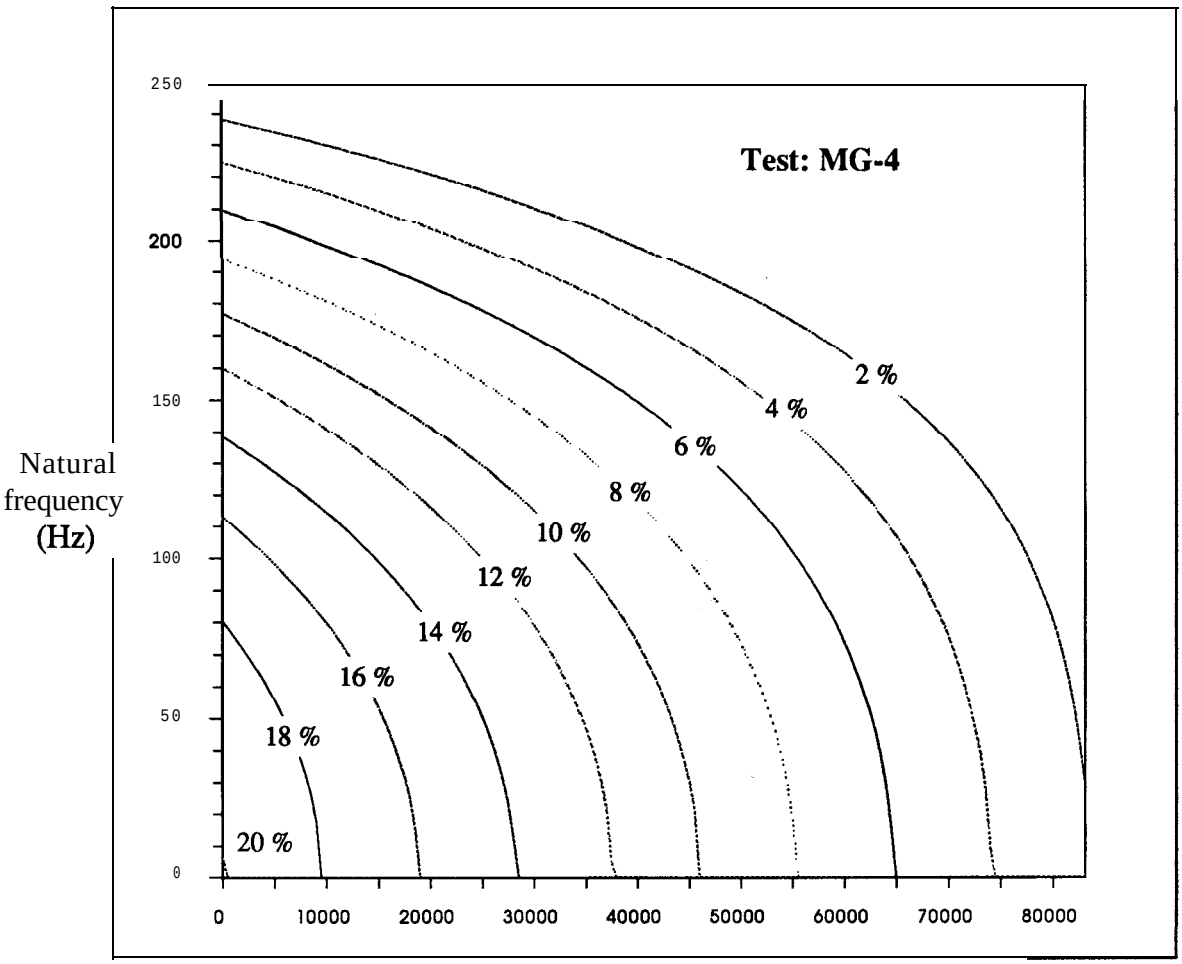

Fig.29 Theoretical relationship between excess pore pressures and the natural frequency

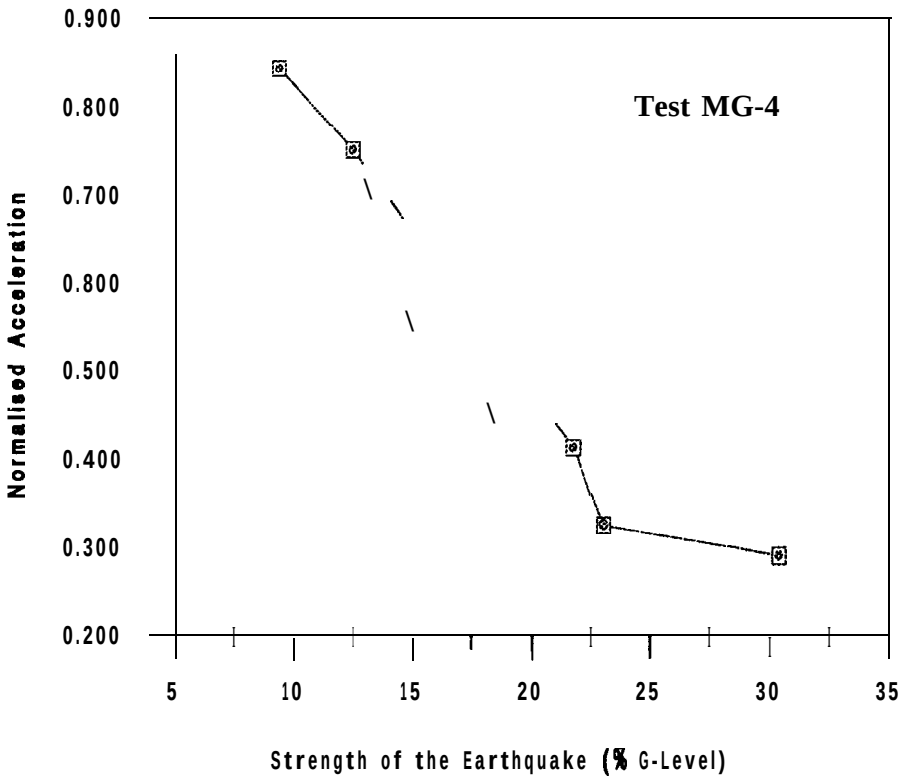

Fig. 30 Variation of normalised acceleration with the strength of the earthquake

data points plotted per complete transducer record

EQ–1

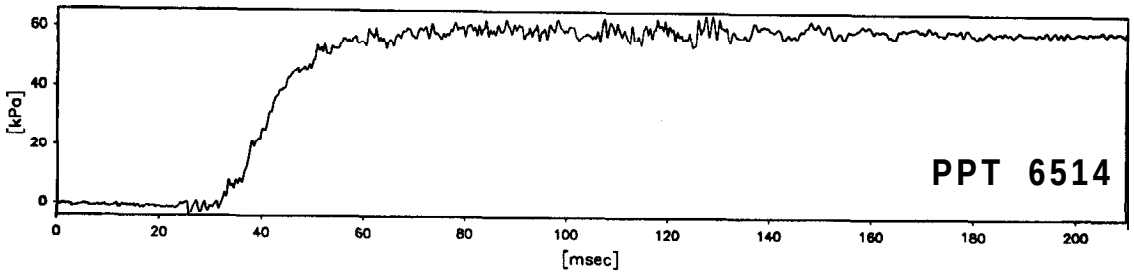

EQ–2

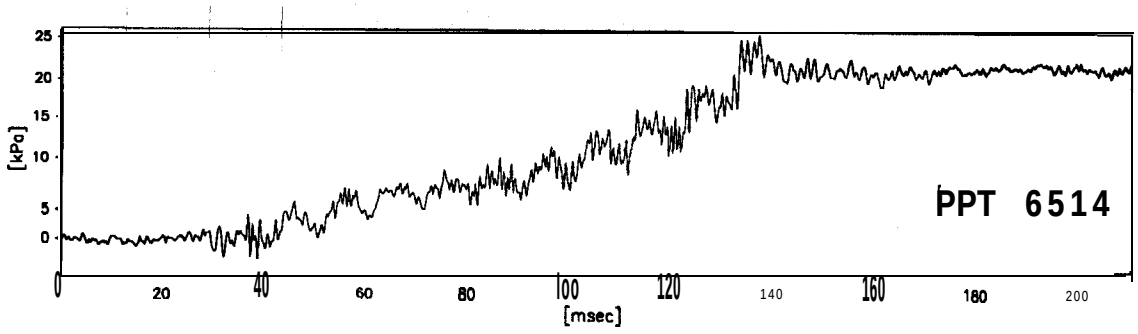

EQ - 3

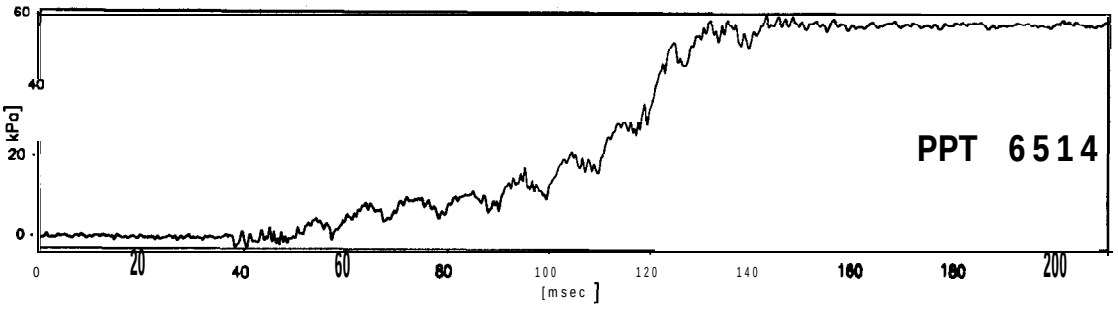

EQ–4

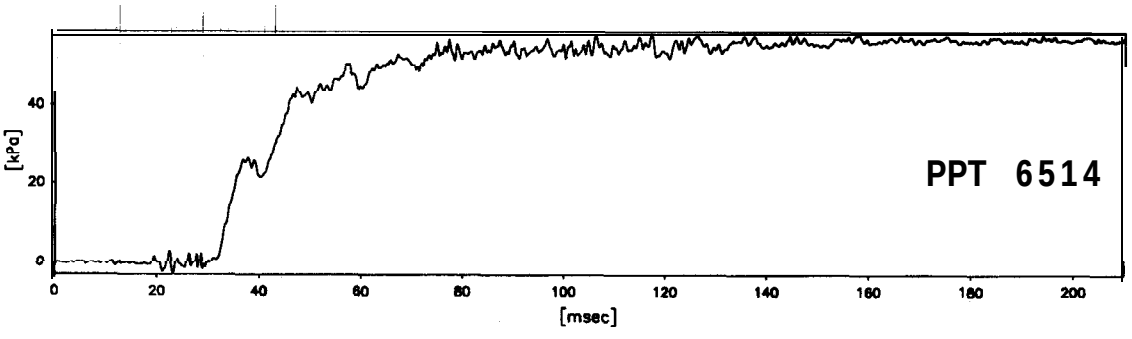

EQ–5

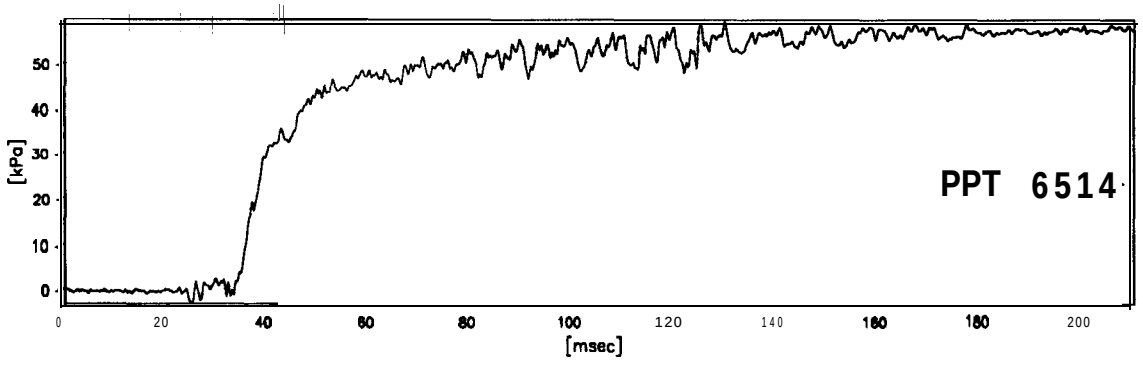

Scales : Prototype

TEST MG-4 MODEL SAT FLIGHT -1		Base Pore Pressure TIME RECORDS		FIG.NO. 31

14.0 Centrifuge test MG-5

As explained in Sec.6 the depth of the sand bed for this centrifuge test was 100.0 mm. The construction of the centrifuge model was in three stages and at the end each stage the void ratio and dry density of sand bed were estimated. The natural frequency of the soil was computed using Eqs. 1 to 12. The final depth of sand bed required so that its natural frequency is close to the driving frequency of the model earthquake was determined after each stage. The schematic diagram showing the section of the centrifuge model and placement of the instruments during this centrifuge test is presented in Fig.32. In table 4 the exact location of each transducer during this experiment is presented. A total of six earthquakes were fired on this centrifuge model at 50g. The data from these earthquakes is presented in Figs.33 to 56. The salient features of the data are presented here while a detailed analysis of the data is presented in next section.

As in the previous centrifuge test two data acquisition systems were used during this centrifuge test. These systems were explained in section 11. Important transducers were logged on both these systems so that reliable measurements can be made. In this centrifuge test all the earthquakes were fired such that the peak acceleration induced in each was greater than the previous earthquake. Earthquake 1 had a strength of about 12.8 %. In Figs.33 and 34 the data from all the instruments acquired using the Racal tape recorder are presented. In Figs.35 and 36 the data obtained directly using Global Lab data acquisition system are presented. Considering the three accelerometers 1926, 3466 and 3477 (see Fig.32) which are placed along the vertical column in the middle of the sand bed we can see that there is significant attenuation of peak acceleration from 12.8 % at the base of the sand column to about 6.2 % at the surface of the sand bed. Traces recorded by ACC 3477 and 3441 in Fig.33 show a clear attenuation of peak accelerations after first few cycles. In fact the second half of the base shaking recorded by ACC 3436 and 1926 is not at all registered by the accelerometers 3466 and 3477. These events coincides with the rise of excess pore pressures indicated by PPT's 6260

and 6270 as seen in Figs.33 and 34. The vertical accelerometers 1572, 1925 and 5756 in Fig.35 are clearly picking up the vertical accelerations unlike in the previous centrifuge test. ACC 1572 however registers some movement of the transducer in the vertical direction. As in the previous test, both the accelerometers and pore pressure transducers placed along the same horizontal plane in general recorded very similar accelerations and excess pore pressures confirming the uniformity of the centrifuge model. PPT 3969 did not function during this earthquake.

An earthquake which produced a peak acceleration of 15.4 % was fired next. The data from this earthquake are presented in Figs.37 to 40. The magnitude of the excess pore pressures generated during this earthquake was almost the same as those generated during earthquake 1. This can be observed by comparing PPT's 6514, 6260 and 6270 in Figs.37 and 38 with corresponding traces obtained during earthquake 1. The accelerometers 1926, 3466 and 3477 along the vertical column in the middle of the sand bed show significant attenuation of peak acceleration. In particular ACC 3477 near the surface of the sand bed registers only five cycles of base motion similar to earthquake 1. This is consistent with the excess pore pressures generated during this earthquake. PPT 3969 did not function during this earthquake or any other subsequent earthquake. The vertical accelerometers 1572, 1925 and 5756 all show different response compared to the vertical acceleration recorded by ACC 1900 on the box (see Figs.32 and 39). It appears that the vertical accelerometers are picking up a component of the horizontal acceleration.

Earthquake 3 had a strength of 22.5 %. The data from this earthquake are presented in Figs. 41 to 44. It is interesting to note that the magnitude of excess pore pressures generated during this earthquake are almost equal to those generated during earthquakes 1 and 2. Also, the accelerometer 3441 near the sand surface registers only the first three cycles of base motion (see Fig.41).

Earthquake 4 had a strength of 25.2 %. The data from this earthquake are presented in Figs. 45 to 48. The excess pore pressures during this earthquake were almost the same as in the previous earthquakes as seen in Figs. 45 and 46. It is interesting to see the acceleration time history recorded by ACC 3477 near the soil surface in Fig.45. After the first $2^1/_2$ cycles the accelerometer registers very small accelerations suggesting that the sand in this region has liquefied.

An even stronger earthquake which produced a peak acceleration of about 27.6 % was fired next. The data from this earthquake are presented in Figs.49 to 52. The magnitude of excess pore pressures generated during this earthquake was almost the same as in the previous earthquakes. However accelerometer 3477 registers signs of liquefaction of the soil surrounding it after first $1^1/_2$ cycles. It does not recover till the end of the earthquake unlike in the previous centrifuge test.

An even stronger earthquake which produced a peak acceleration of about 29.7 % was fired as the last earthquake. The data from this earthquake are presented in Figs.53 to 56. The magnitude of excess pore pressures generated during this earthquake was almost the same as in the previous earthquakes. However accelerometer 3477 registers signs of liquefaction of the soil surrounding it after first $1^1/_4$ cycles. It does not recover till the end of the earthquake unlike in the previous centrifuge test. From the data obtained during this strong earthquake it was felt that by increasing the strength of the earthquake further no useful information can be obtained.

In the next section a more detailed analysis of the data from this centrifuge test is presented.

Fig. 32: Schematic diagram showing the placement of transducers in Centrifuge Test MG-5

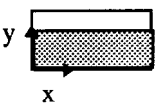

Table 4 Placement of transducers in centrifuge test MG-5

Transducer	x (mm)	Y (mm)
ACC 1225	25	5
ACC 1926	280	5
ACC 1572	320	5
ACC 5701	490	5
ACC 3441	30	42
ACC 3466	250	40
ACC 1925	295	44
ACC 5754	495	41
ACC 3457	20	67
ACC 3477	275	72
ACC 5756	350	72
ACC 1258	490	73
ACC 3436	fixed to the container	
ACC 1900	fixed to the container	
PPT 65 14	265	3
PPT 6803	30	3
PPT 4478	440.5	3
PPT 3969	62	42
PPT 6270	300	37
PPT4481	460	40
PPT 3007	65	72
PPT 6260	315	68
PPT 6784	475	74

Table 5 Hydrostatic pore pressures in centrifuge test MG-5

PPTNO.	10G	20G	40G	50G
PPT6514	5.31	13.56	31.58	41.26
PPT4478	7.65	16.38	35.17	45.57
PPT6803	7.78	16.92	35.77	45.95
PPT6270	5.37	11.55	24.26	31.19
PPT3969	0.52	1.11	2.33	3.00
PPT4481	5.83	12.43	25.97	33.17
PPT6260	1.67	5.47	13.37	17.24
PPT3007	2.62	7.52	17.67	22.68
PPT6784	5.13	11.10	23.37	29.85

Table 6 Normalised accelerations in the sand column in centrifuge test MG-5

Location	Normalised Acceleration
EQ: 1	
At base of the sand column	1
At the mid depth	0.9324
Near the surface of sand bed	0.8378
EQ: 2	
At base of the sand column	1
At the mid depth	1.0349
Near the surface of sand bed	1.1047
EQ: 3	
At base of the sand column	1
At the mid depth	0.6743
Near the surface of sand bed	0.57 14
EQ: 4	
At base of the sand column	1
At the mid depth	0.5357
Near the surface of sand bed	0.4286
EQ: 5	
At base of the sand column	1
At the mid depth	0.3384
Near the surface of sand bed	0.25
EQ: 6	
At base of the sand column	1
At the mid depth	0.4086
Near the surface of sand bed	0.2857

120 data points plotted per complete transducer record

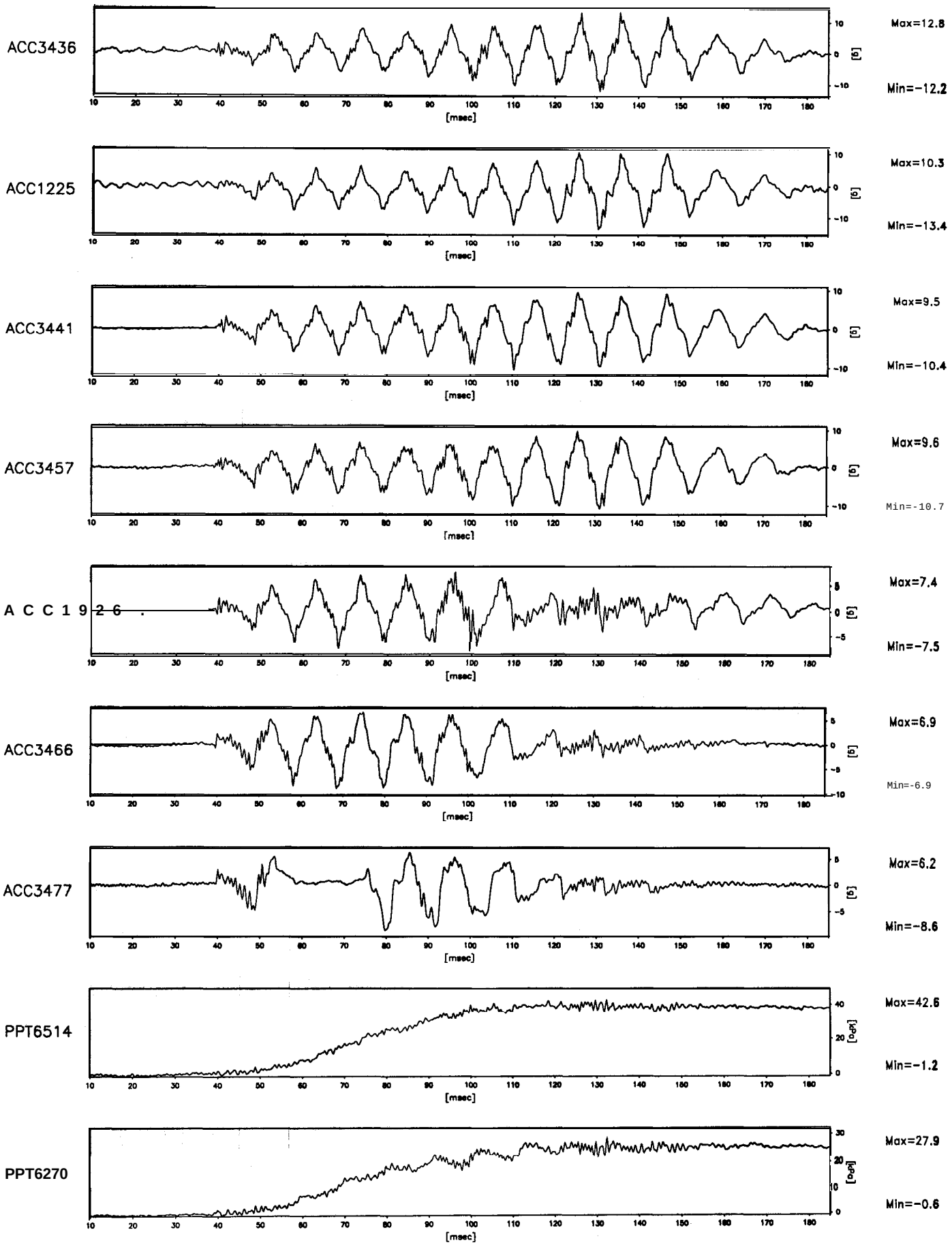

Scales : Model

TEST MG-5 MODEL SAT FLIGHT -1	EQ-1	SHORT TERM TIME RECORDS	G Level 50	FIG.NO. 33

1120 data points plotted per complete transducer record

ACC3436

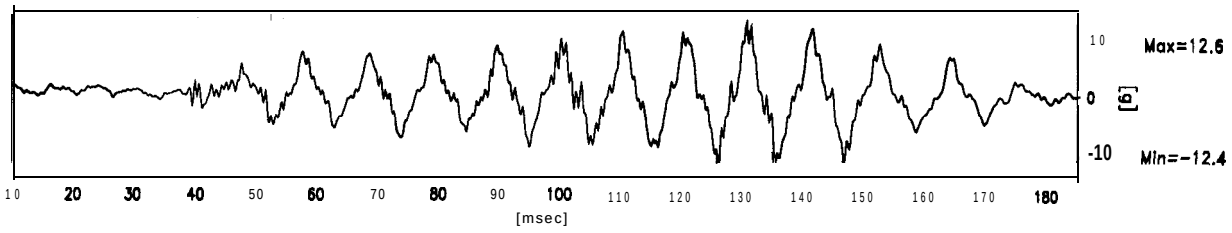

PPT6260

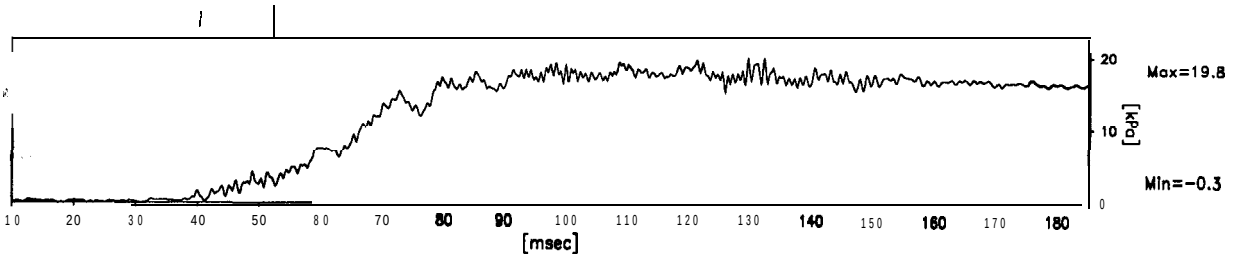

PPT6803

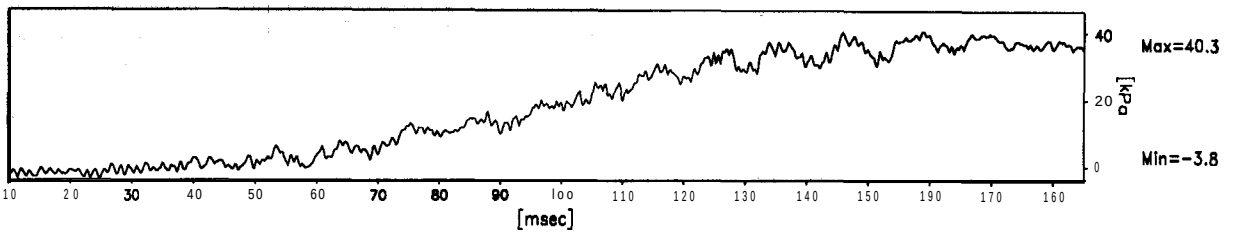

PPT3969

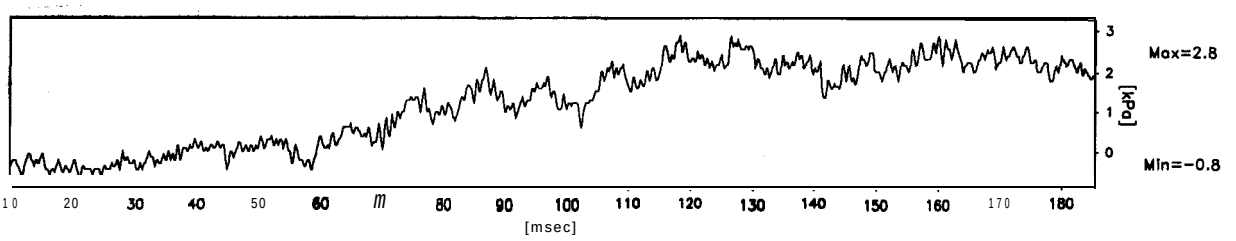

PPT3007

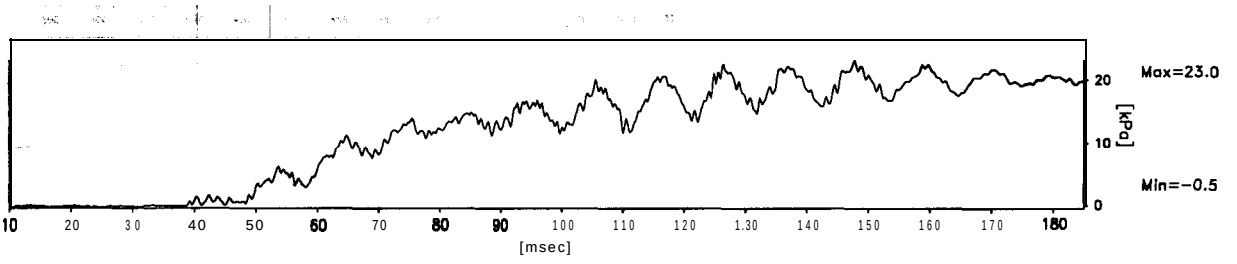

PPT4476

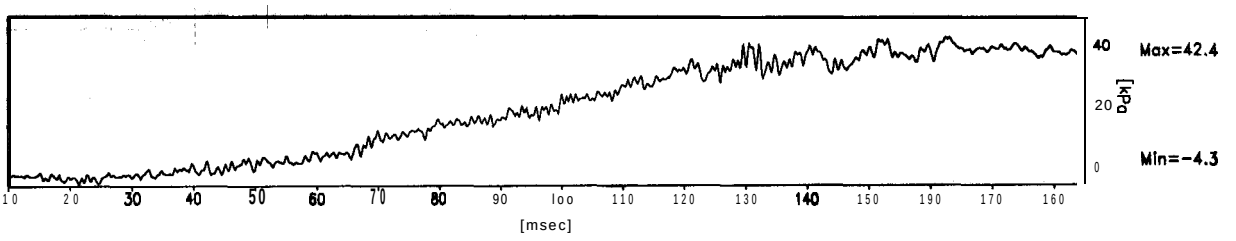

Scales : Model

TEST MG-5 MODEL SAT FLIGHT -1	**EQ- 1**	**SHORT TERM TIME RECORDS**	G Level 50	FIG.NO. **34**

901 data points plotted per complete transducer record

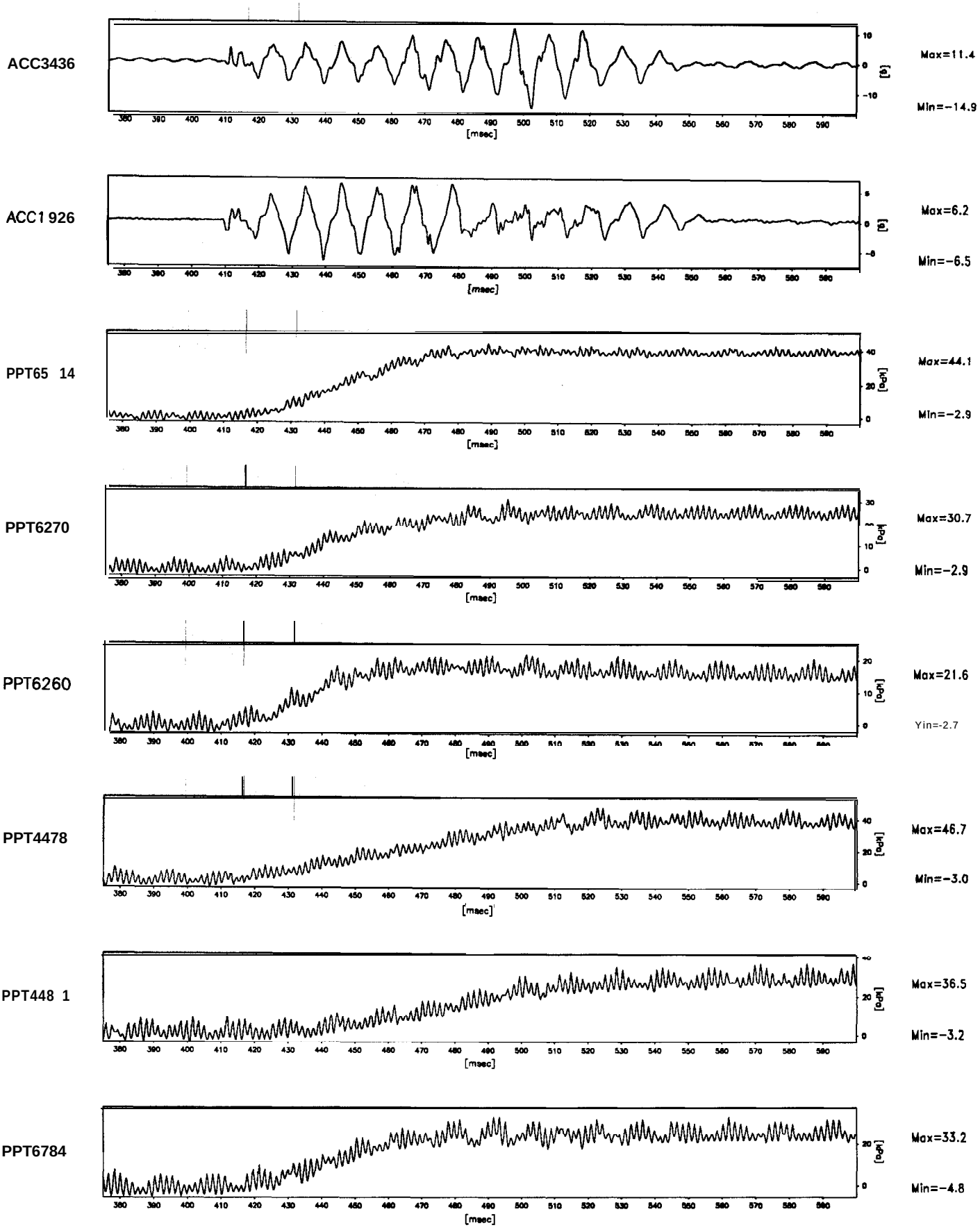

Scales : Prototype

TEST MG-5 MODEL SAT FLIGHT -1	EQ-1	SHORT TERM TIME RECORDS	G Level 50	FIG.NO. 36

1120 data points plotted per complete transducer record

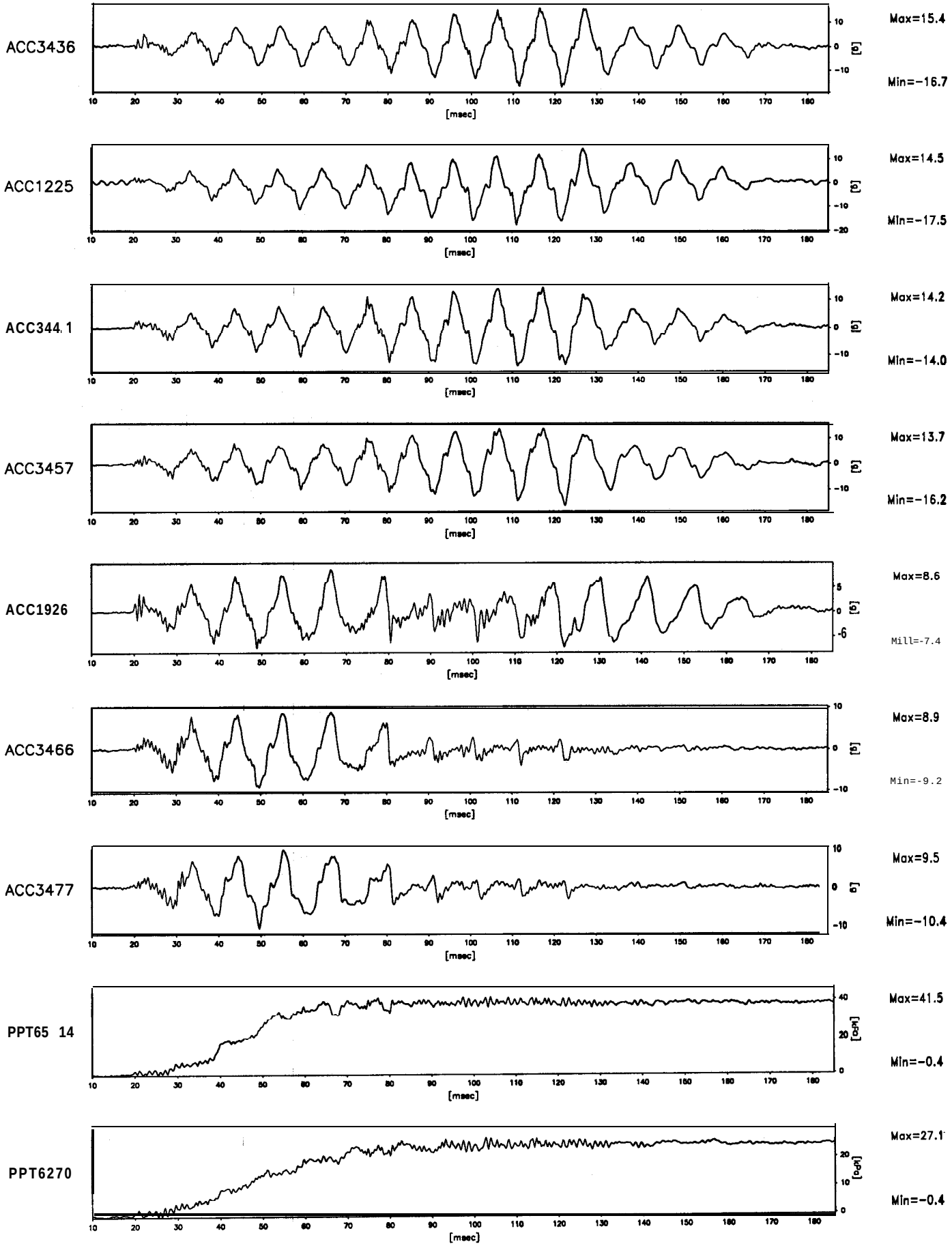

Scales : Model

TEST MG-5 MODEL SAT FLIGHT -1	EQ-2	SHORT TERM TIME RECORDS	G Level 50	FIG.NO. 37

1120 data paints plotted per complete transducer record

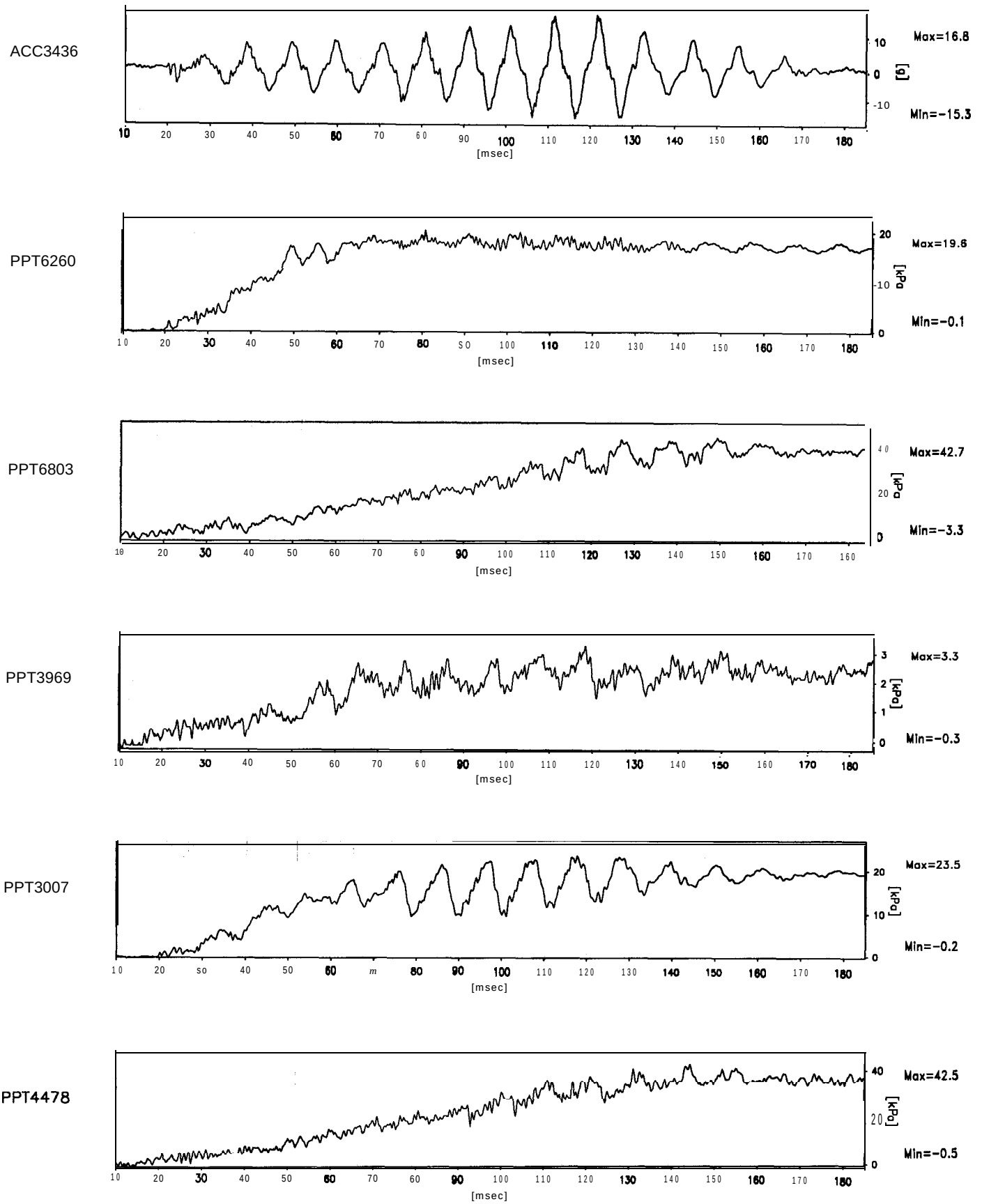

Scales : Model

TEST MG-5 MODEL SAT FLIGHT – 1	EQ-2	SHORT TERM TIME RECORDS	G Level 50	FIG.NO. 38

901 data points plotted per complete transducer record

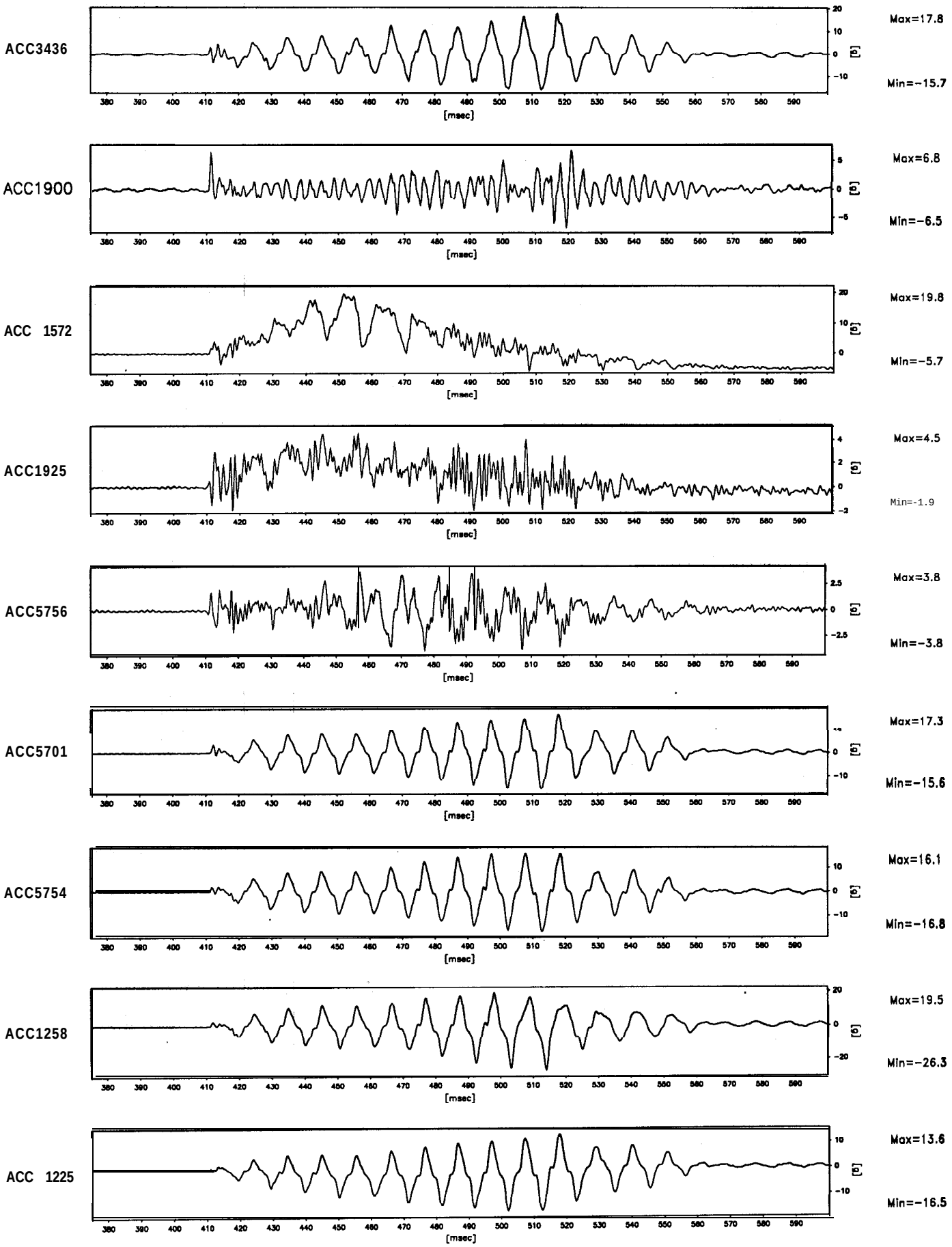

Scales : Model

TEST MG-5 MODEL SAT FLIGHT -1	EQ-2	SHORT TERM TIME RECORDS	G Level 50	FIG.NO. **39**

901 data points plotted per complete transducer record

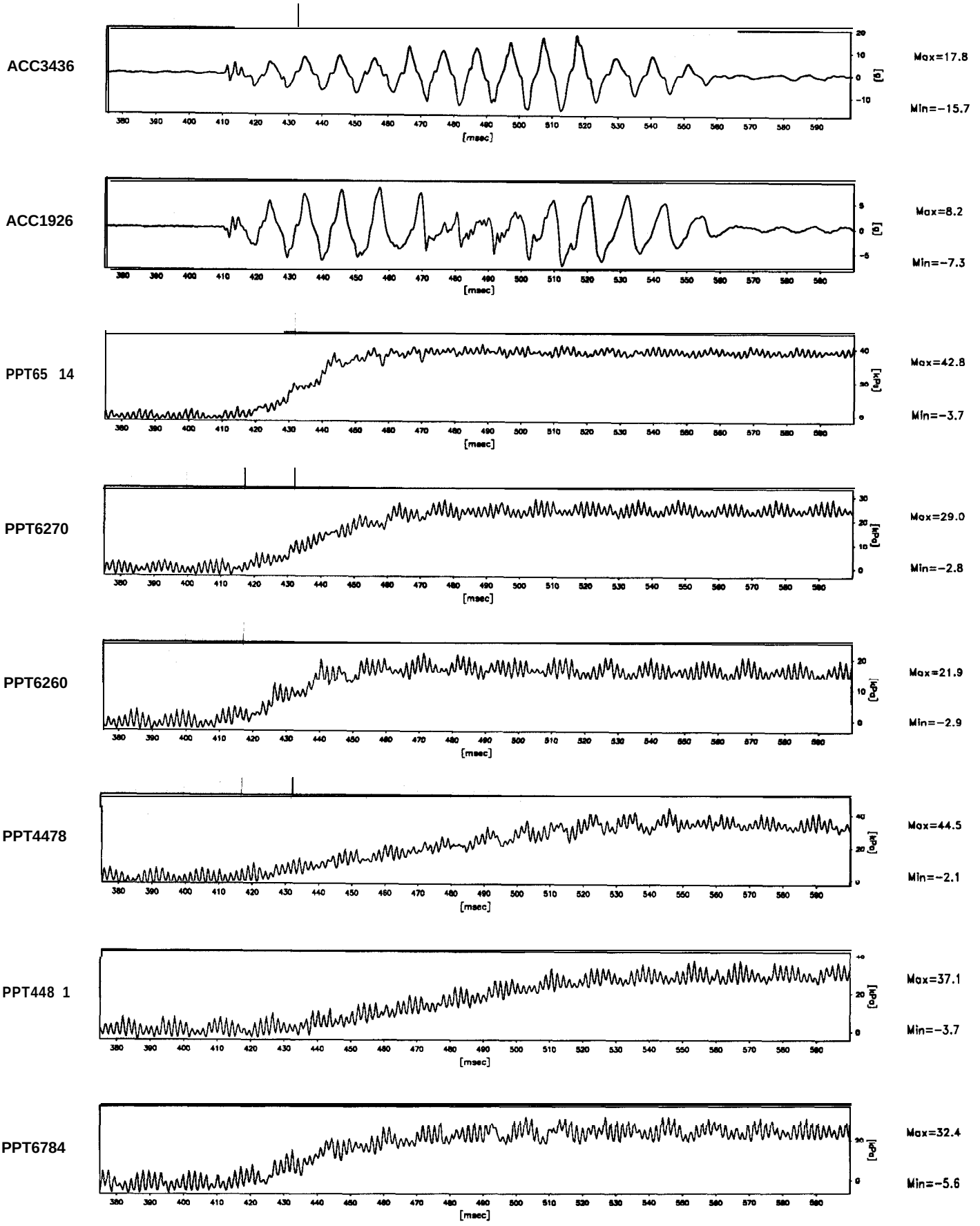

Scales : Prototype

TEST MG-5 MODEL SAT FLIGHT -1	EQ-2	SHORT TERM TIME RECORDS	G Level 50	FIG.NO. 40

1120 data paints platted per complete transducer record

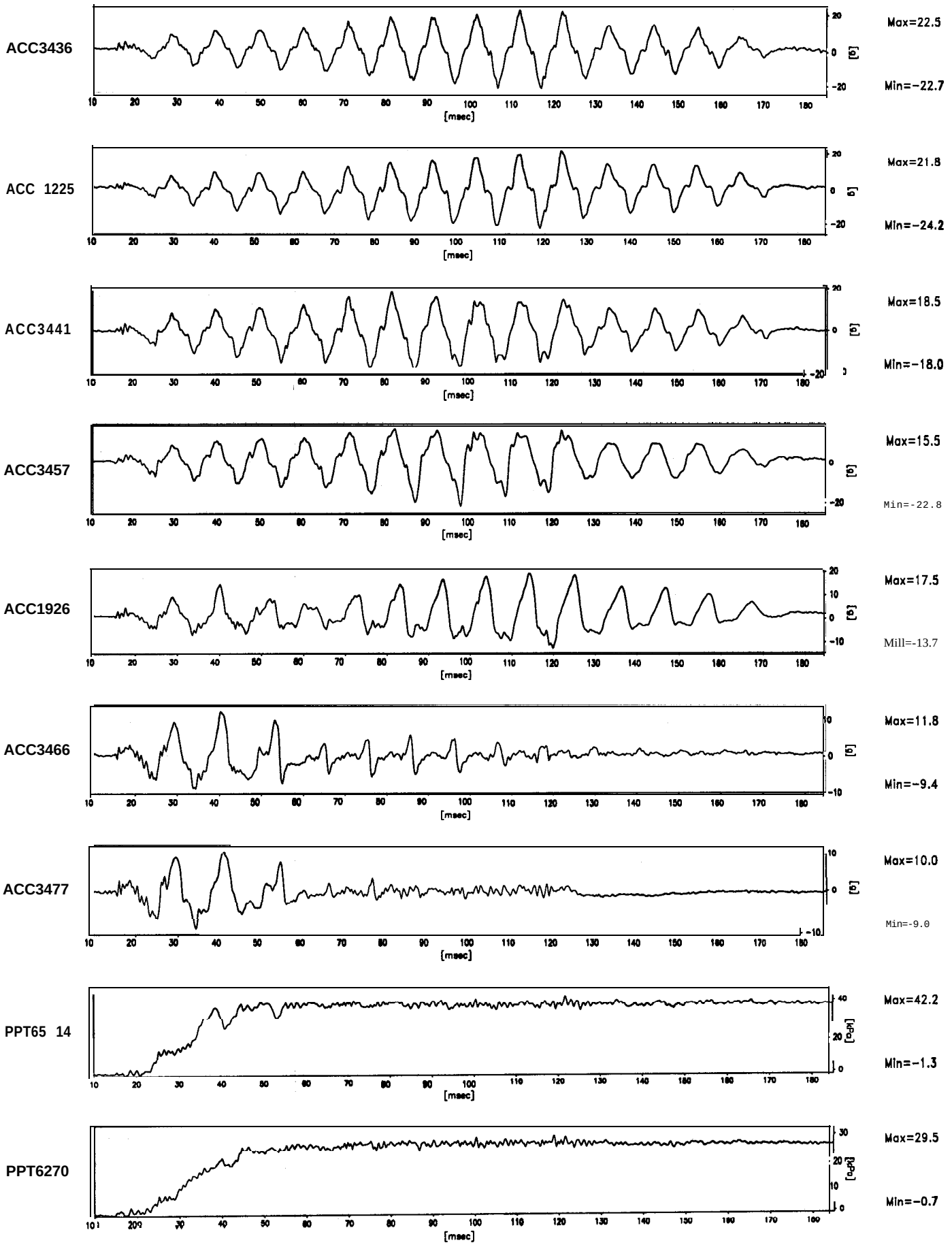

Scales : Model

TEST MG-5 MODEL SAT FLIGHT -1	EQ-3	SHORT TERM TIME RECORDS	G Level 50	FIG.NO. 41

1120 data paints plotted per complete transducer record

ACC3436

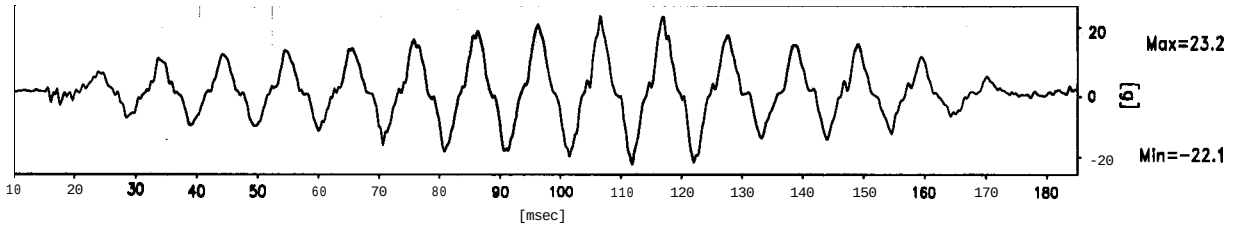

PPT6260

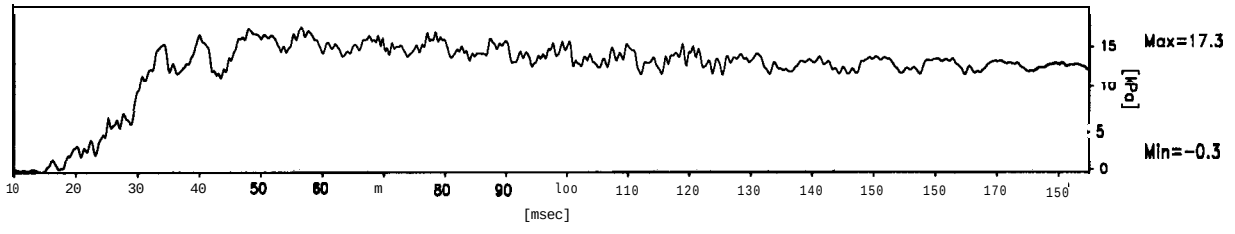

PPT6803

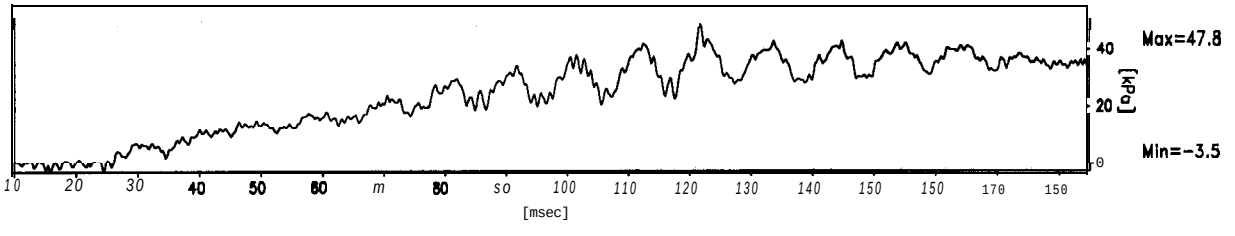

PPT3969

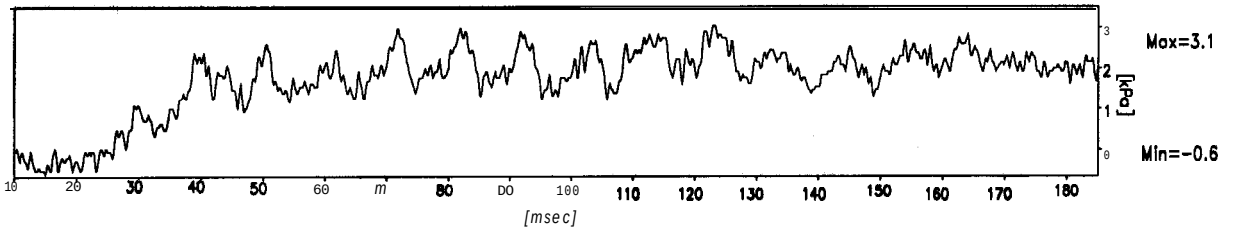

PPT3007

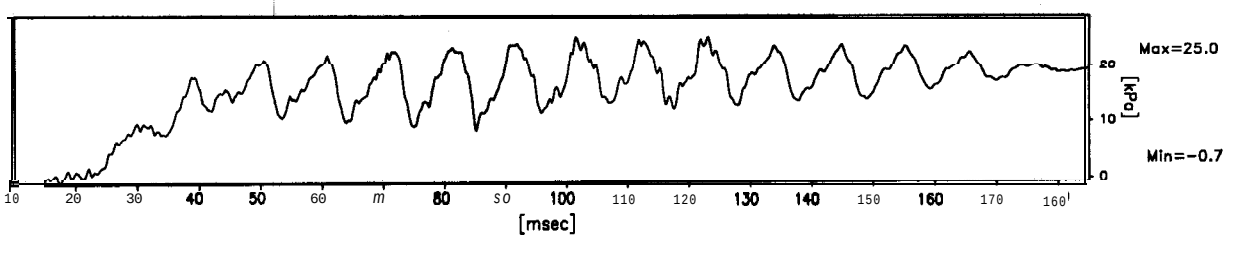

PPT4478

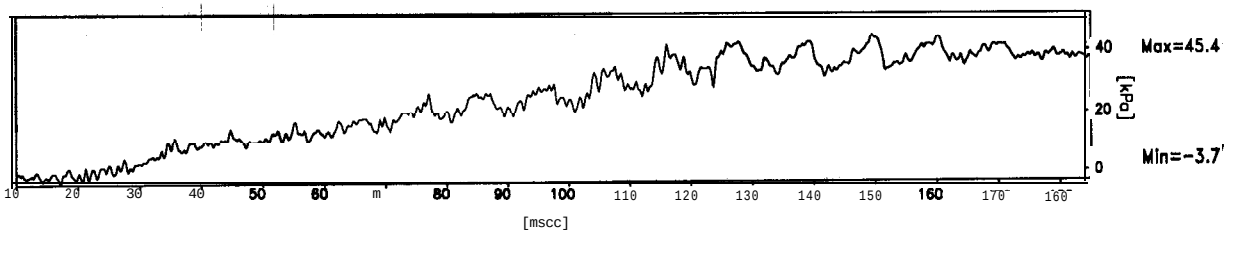

Scales : Model

TEST MG-5 MODEL SAT FLIGHT -1	EQ-3	SHORT TERM TIME RECORDS	**G Level** 50	FIG.NO. **42**

901 data points plotted per complete transducer record

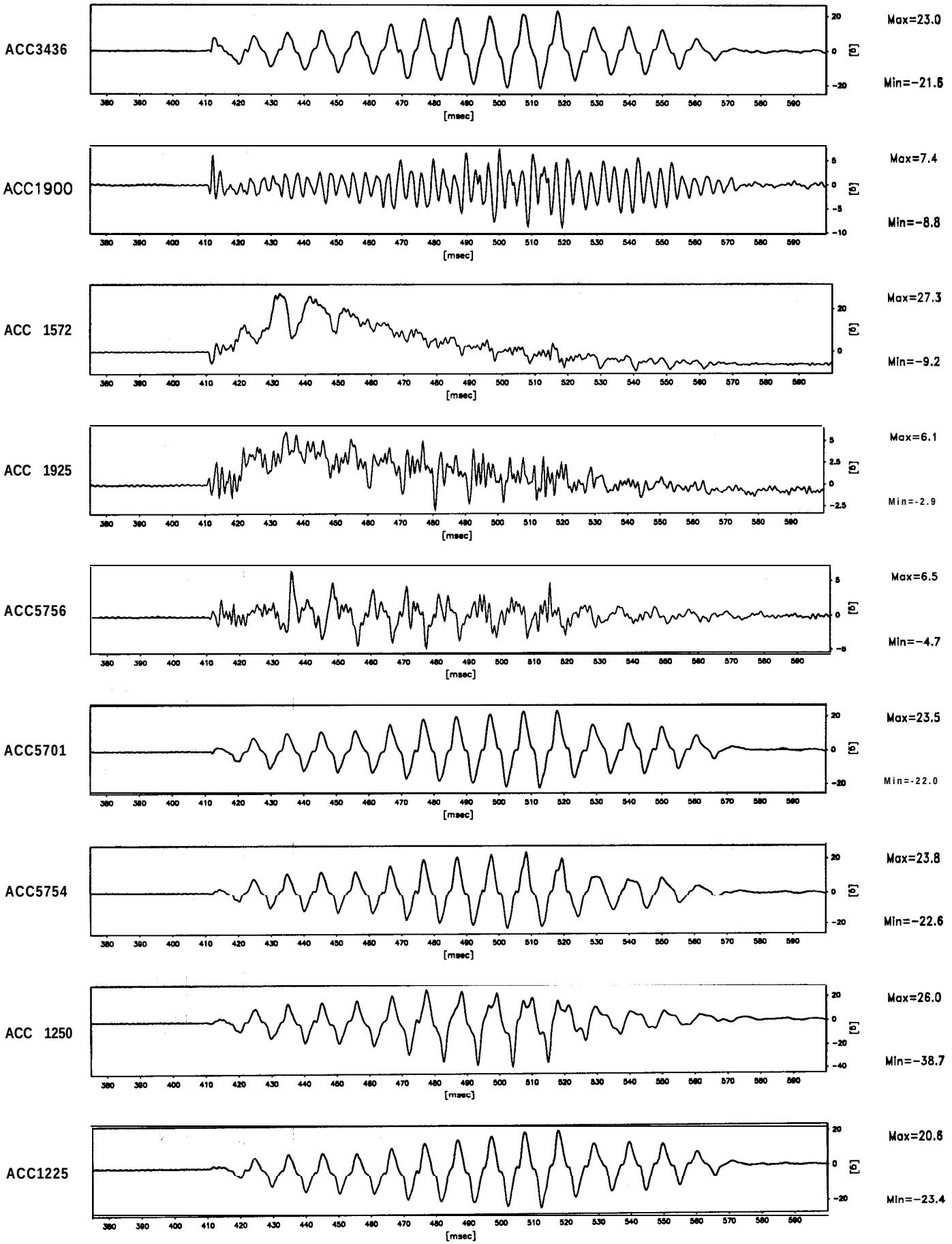

Scales : Model

TEST MG-5 **MODEL SAT FLIGHT -1**	**EQ-3**	SHORT TERM TIME **RECORDS**	G Level **50**	FIG.NO. 43

901 data points plotted per complete transducer record

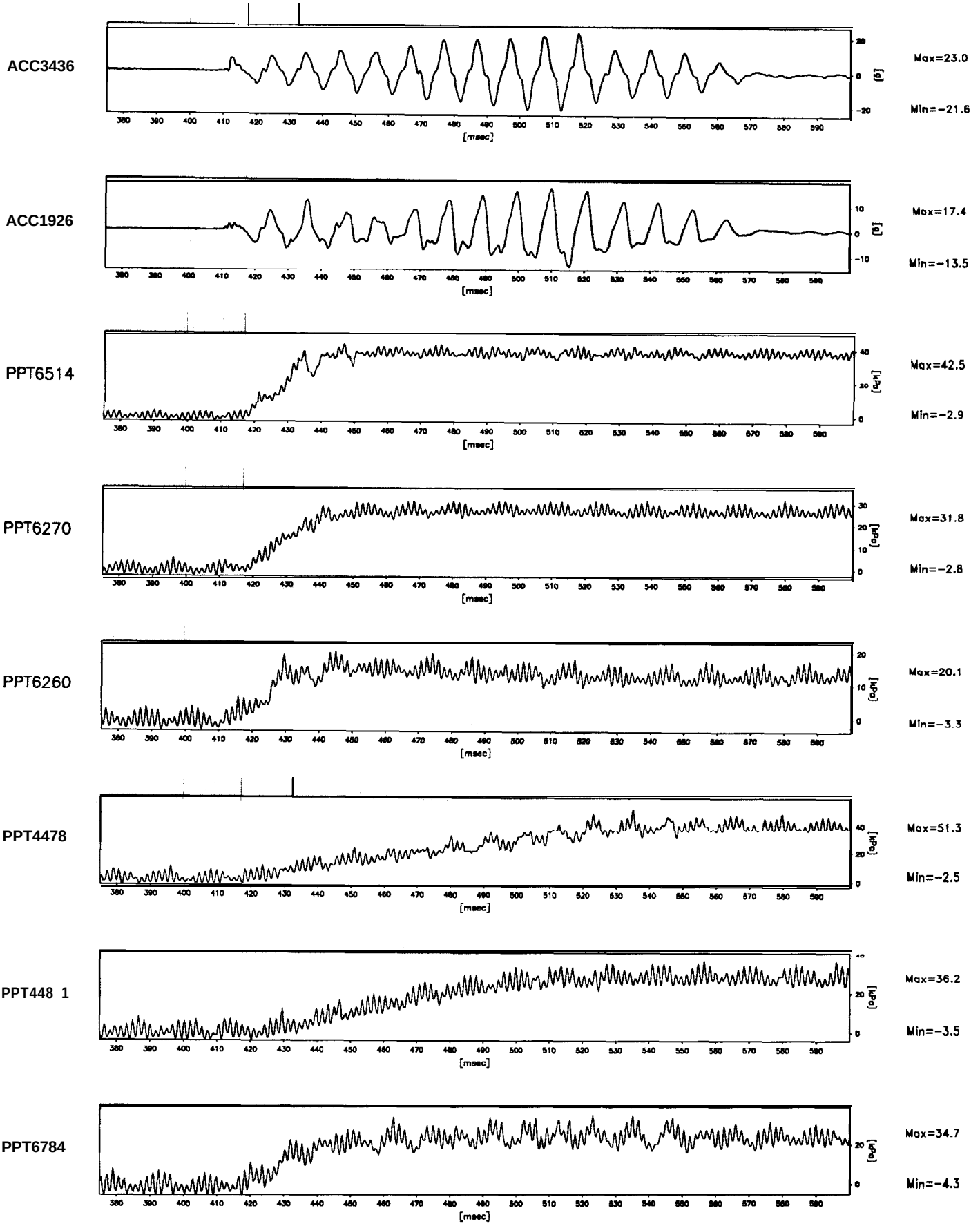

Scales : Prototype

TEST MG-5 MODEL SAT FLIGHT -1	EQ-3	SHORT TERM TIME RECORDS	G Level 50	FIG.NO. 44

1120 data paints plotted per complete transducer record

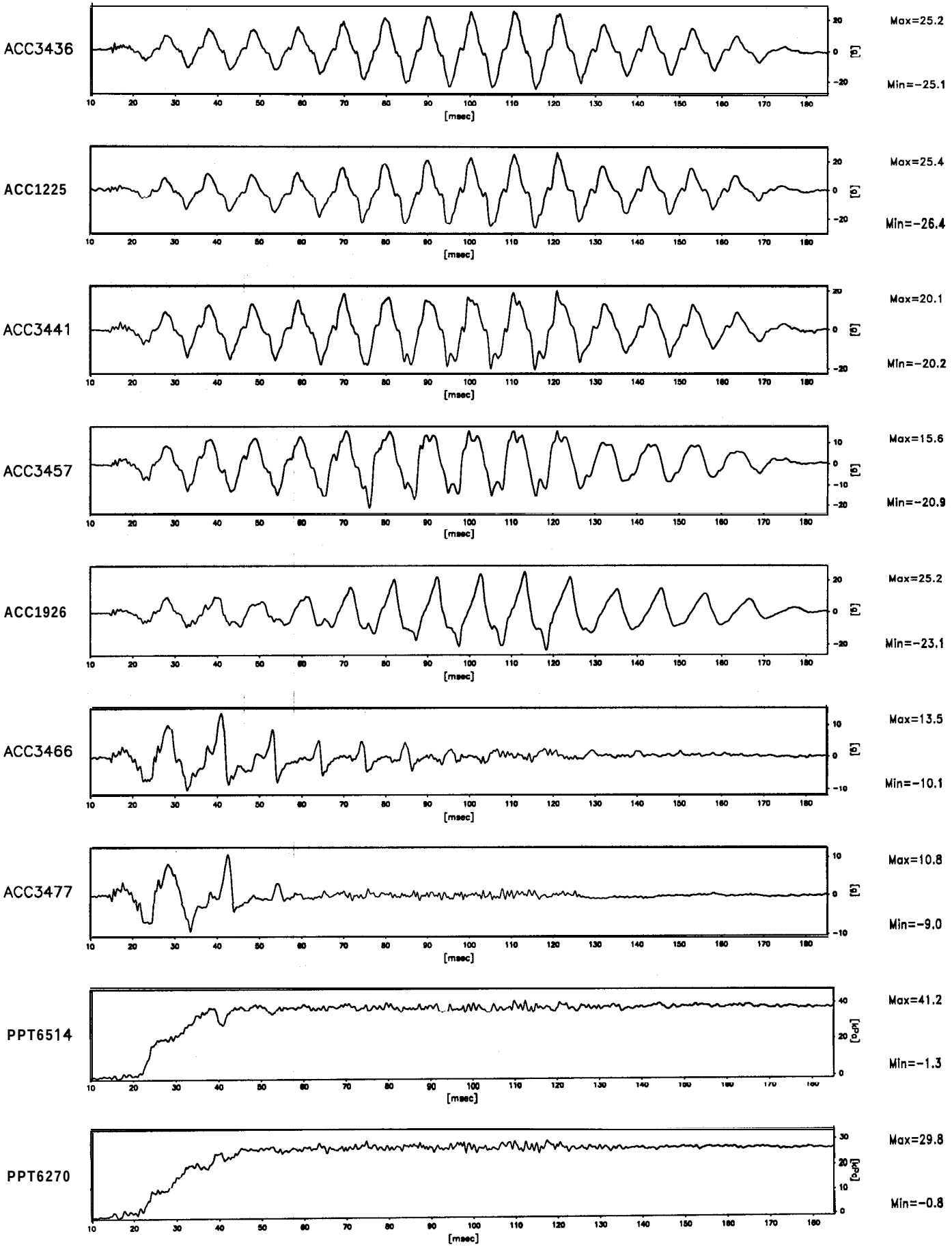

Scales : Model

TEST MG-5 MODEL SAT FLIGHT -1	E Q - 4	SHORT TERM TIME RECORDS	G Level 50	FIG.NO. 45

1 120 data points plotted per complete transducer record

ACC3436

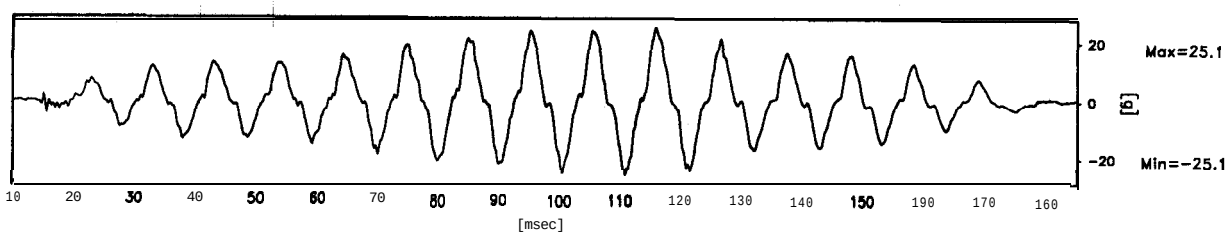

PPT6260

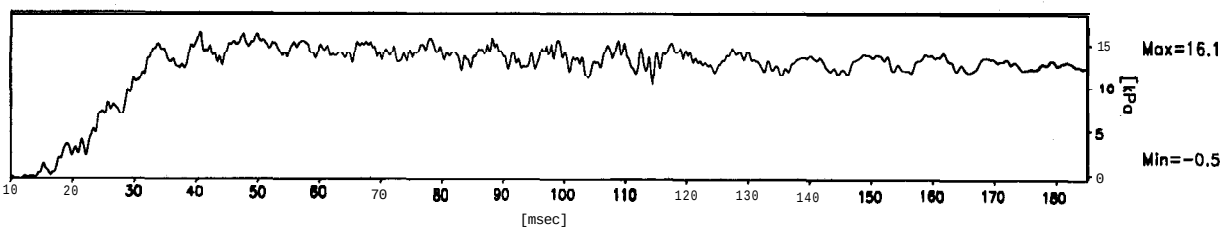

PPT6803

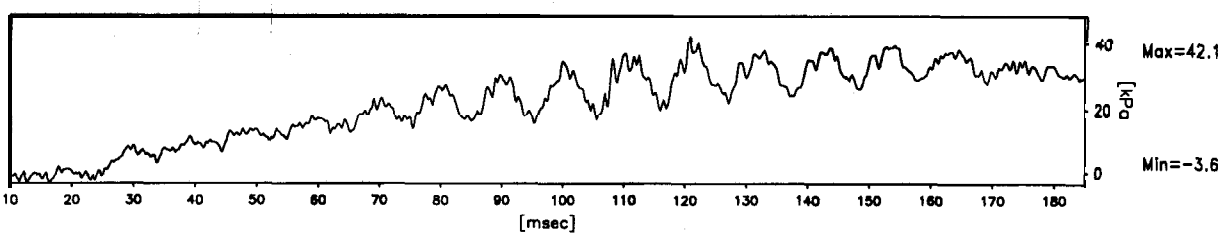

PPT3969

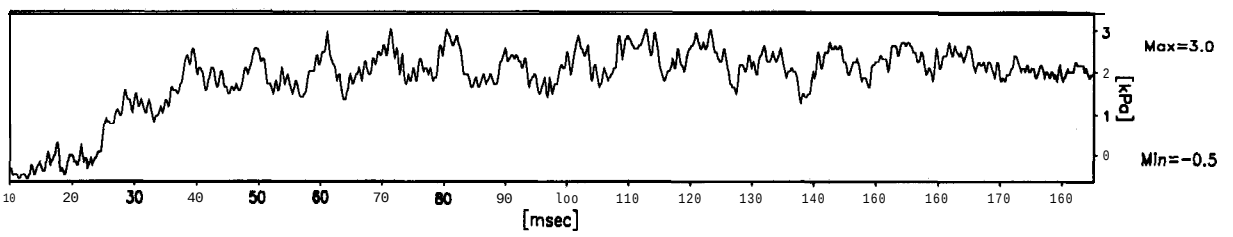

PPT3007

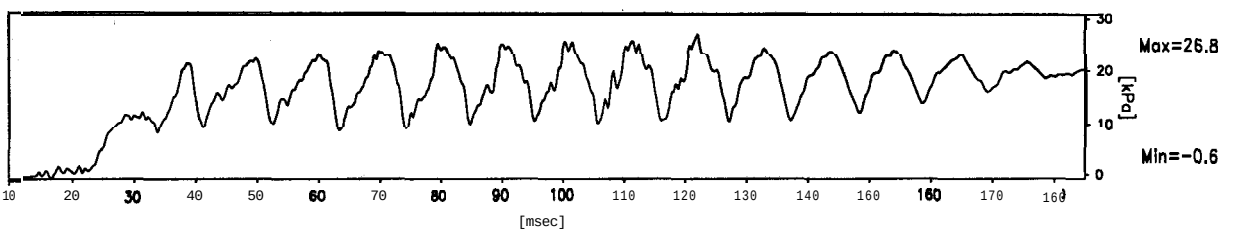

PPT4478

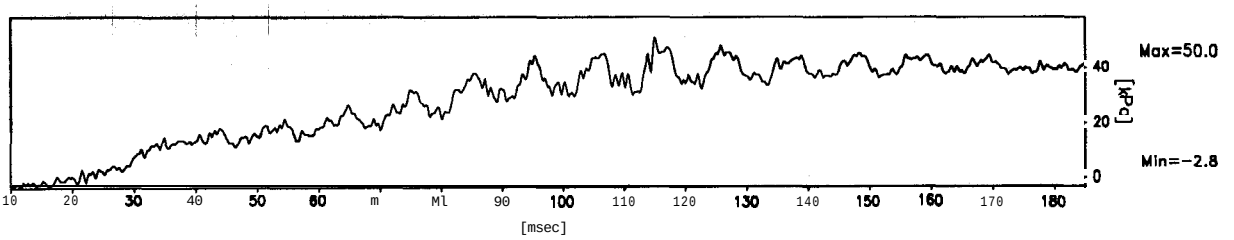

Scales : Model,

TEST MG-5 MODEL SAT F L I G H T - 1	E Q - 4	SHORT TERM TIME RECORDS	G Level 5 0	FIG.NO. **46**

901 data points plotted per complete transducer record

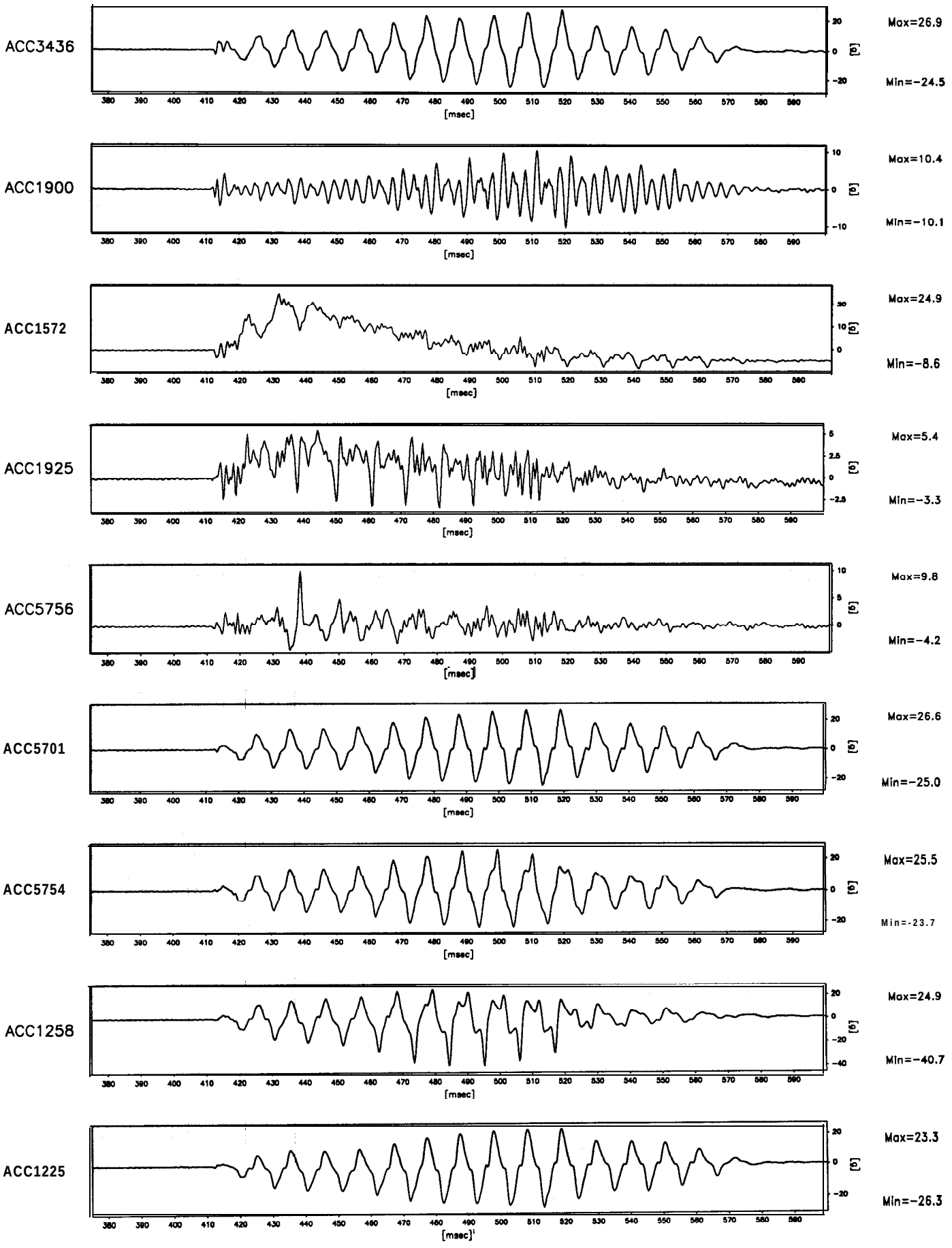

Scales : Model

'TEST MG-5 MODEL SAT FLIGHT -1	EQ-4	SHORT TERM TIME RECORDS	G Level 50	FIG.NO. 47

901 data points plotted per complete transducer record

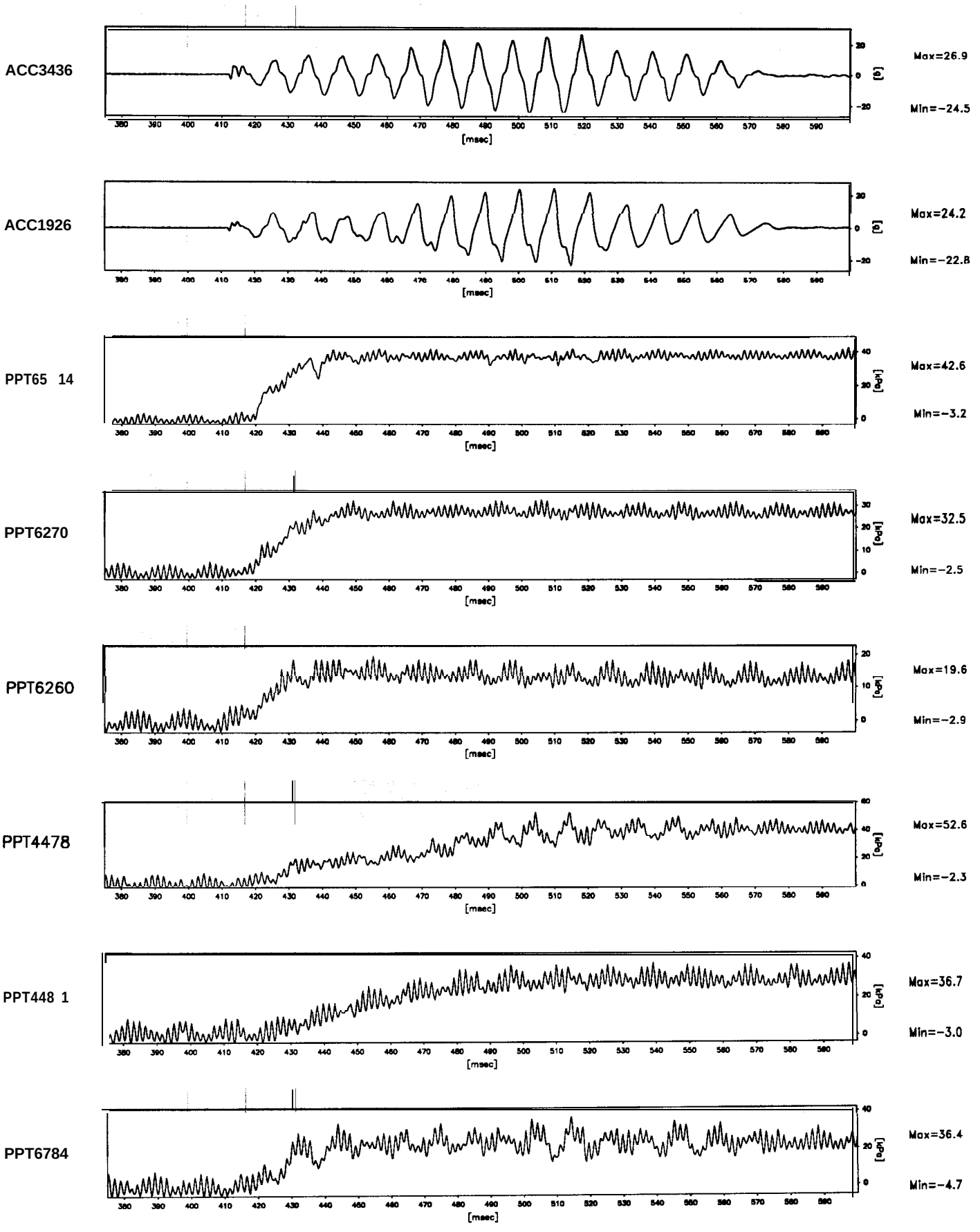

Scales : Prototype

TEST MG-5 MODEL SAT FLIGHT -1	EQ-4	SHORT TERM TIME RECORDS	G Level 50	FIG.NO. 48

1120 data paints plotted per complete transducer record

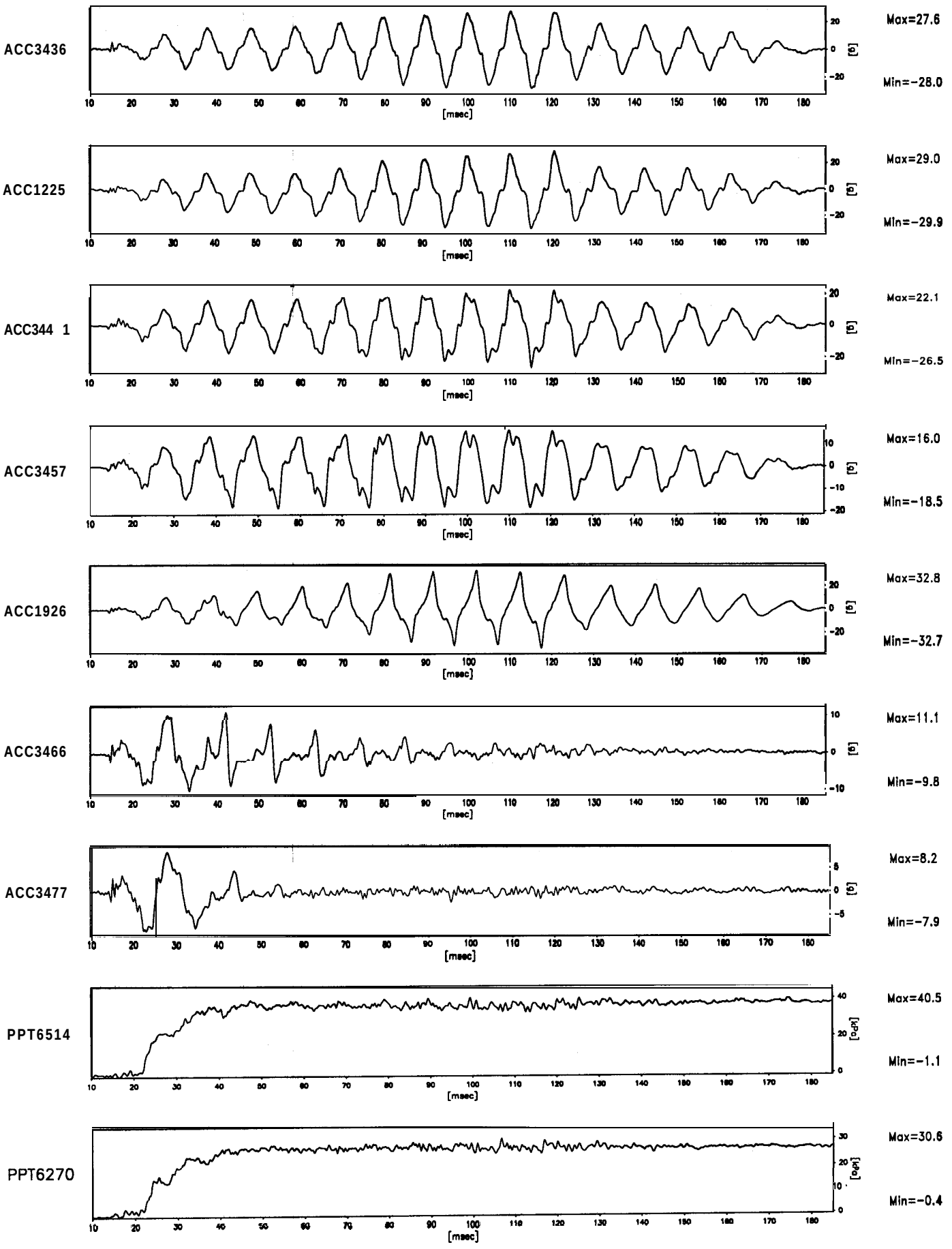

Scales : Model

TEST MG-5 MODEL SAT FLIGHT -1	EQ-5	SHORT TERM TIME RECORDS	G Level 50	FIG.NO. 49

1120 data points plotted per complete transducer record

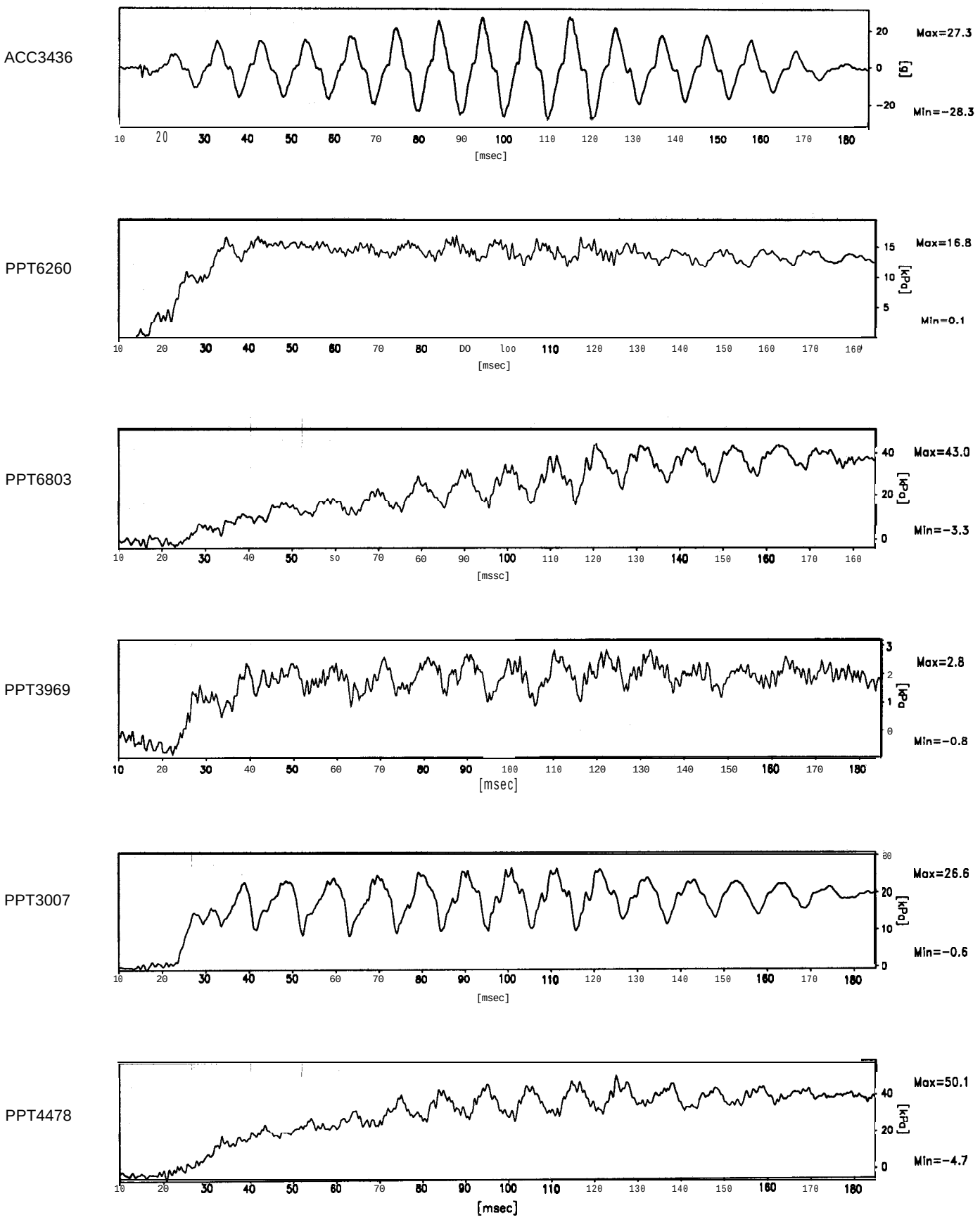

Scales : Model

TEST MG-5 MODEL SAT FLIGHT -1	EQ-5	SHORT TERM TIME RECORDS	G Level 50	FIG.NO. 50

901 dato points plotted per complete transducer record

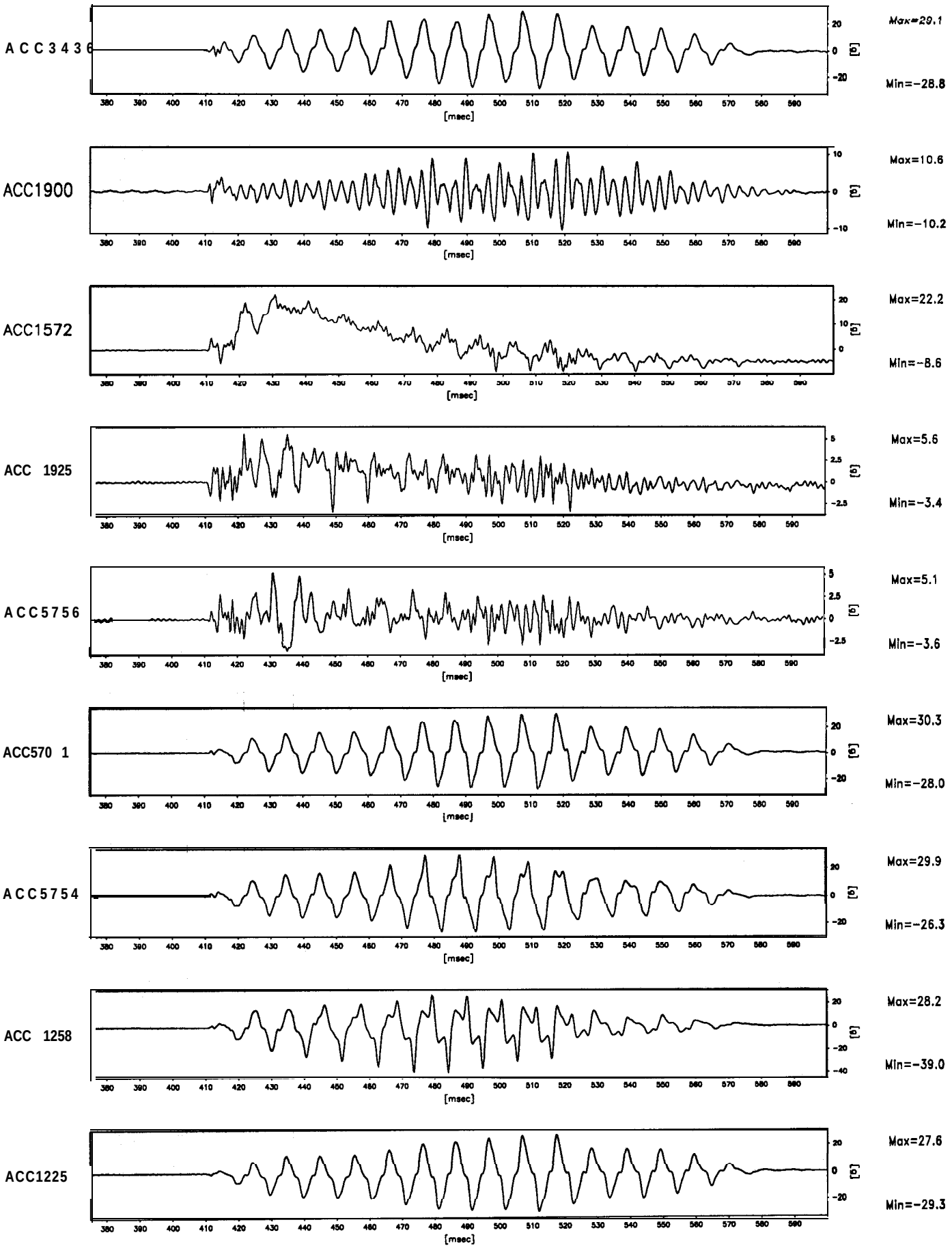

Scales : Model

TEST MG-5 MODEL SAT FLIGHT -1	EQ-5	SHORT TERM TIME RECORDS	G Level 50	FIG.NO. 51

901 data points plotted per complete transducer record

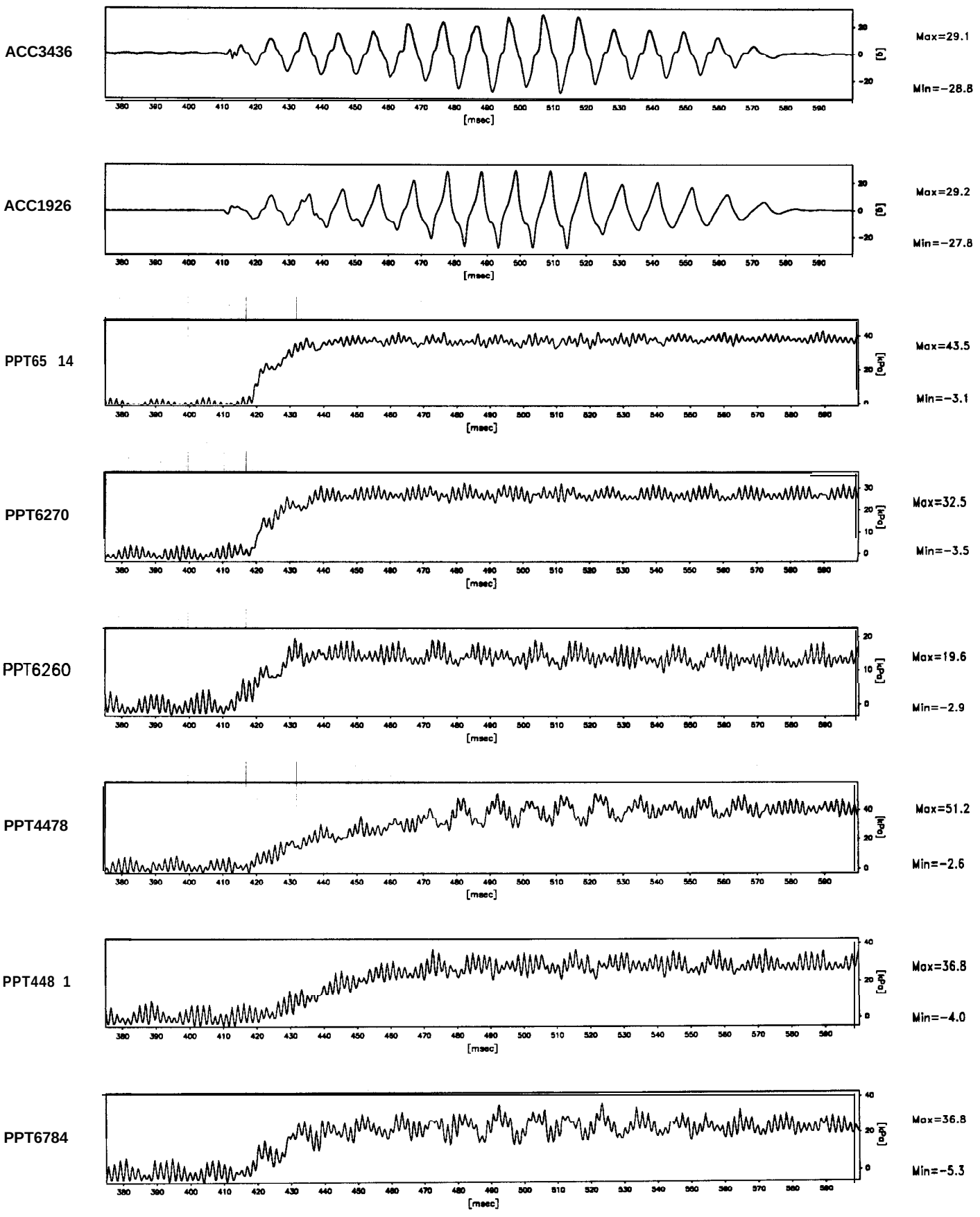

Scales : Prototype

TEST MG-5 MODEL SAT FLIGHT -1	EQ-5	SHORT TERM TIME RECORDS	G Level 50	FIG.NO. 52

1120 data points plotted per complete transducer record

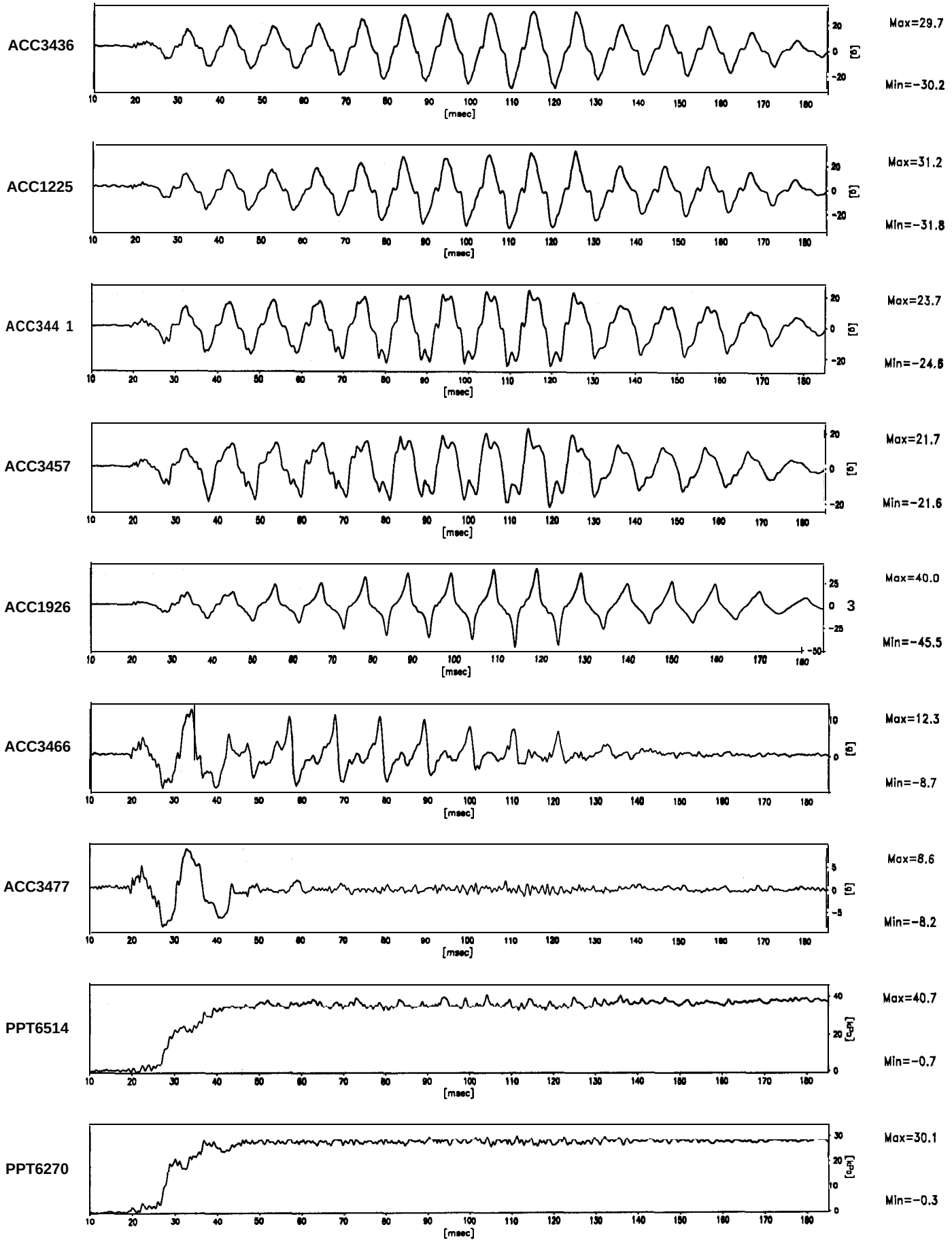

Scales : Model

TEST MG-5 MODEL SAT FLIGHT –1	EQ-6 ,	SHORT TERM TIME RECORDS	G Level 50	FIG.NO. 53

1120 data paints platted per complete transducer record

ACC3436

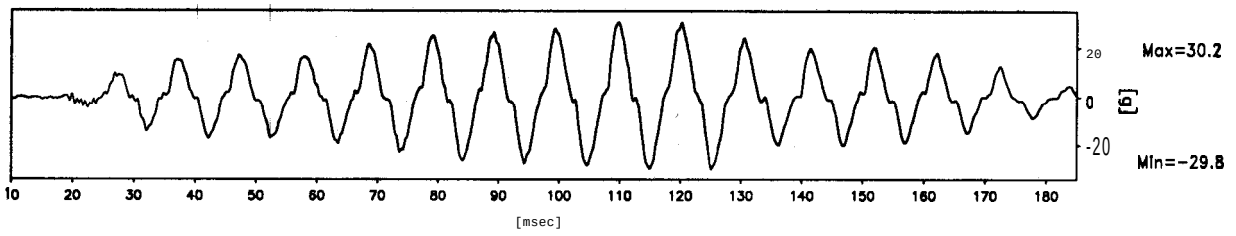

PPT6260

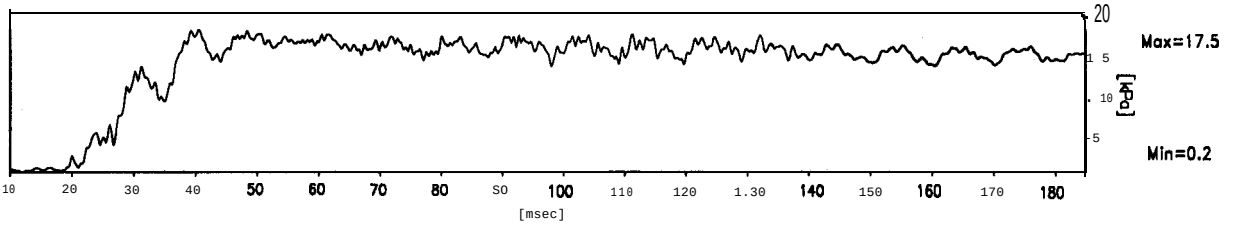

PPT6803

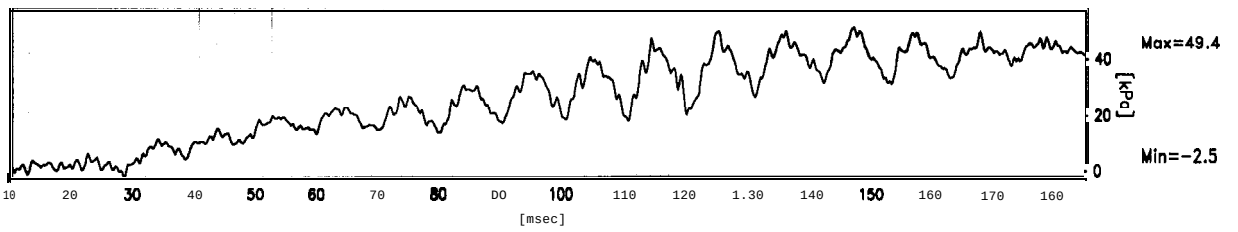

PPT3969

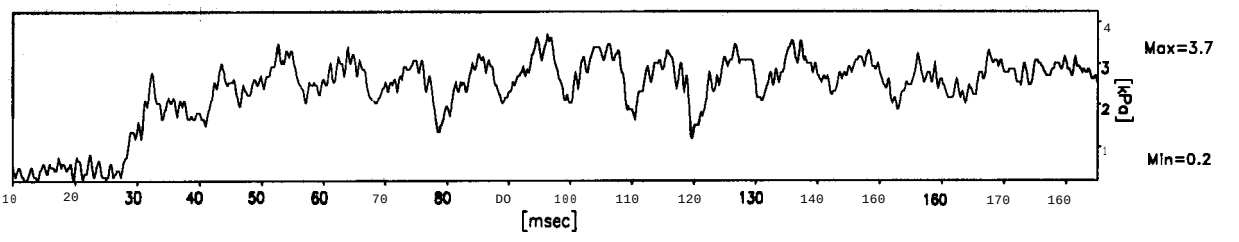

PPT3007

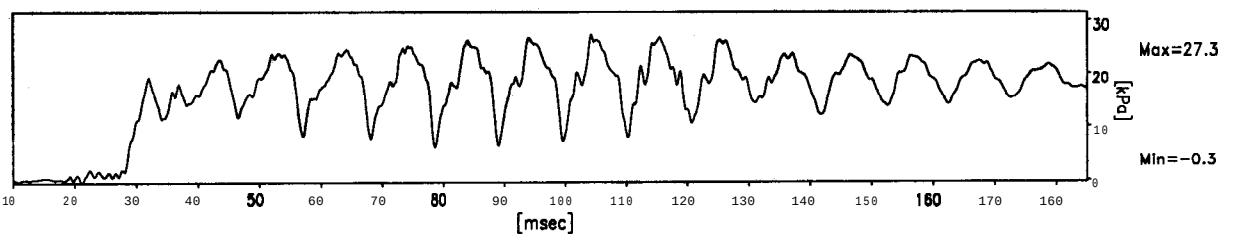

PPT4478

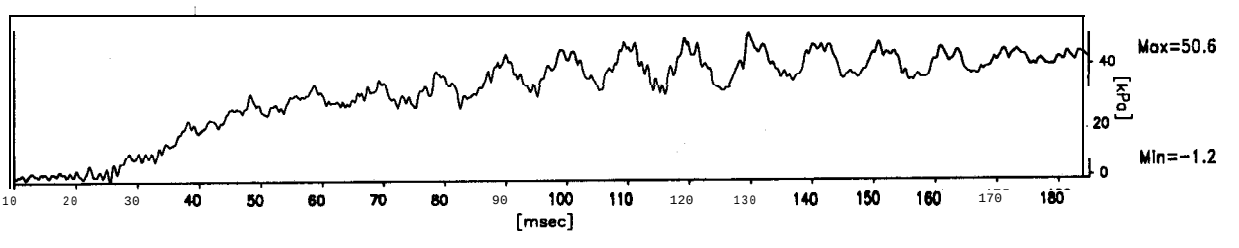

Scales : Model

TEST MG-5 MODEL SAT FLIGHT -1	**EQ-6**	**SHORT TERM TIME RECORDS**	**G Level 50**	FIG.NO. **54**

901 data points plotted per complete transducer record

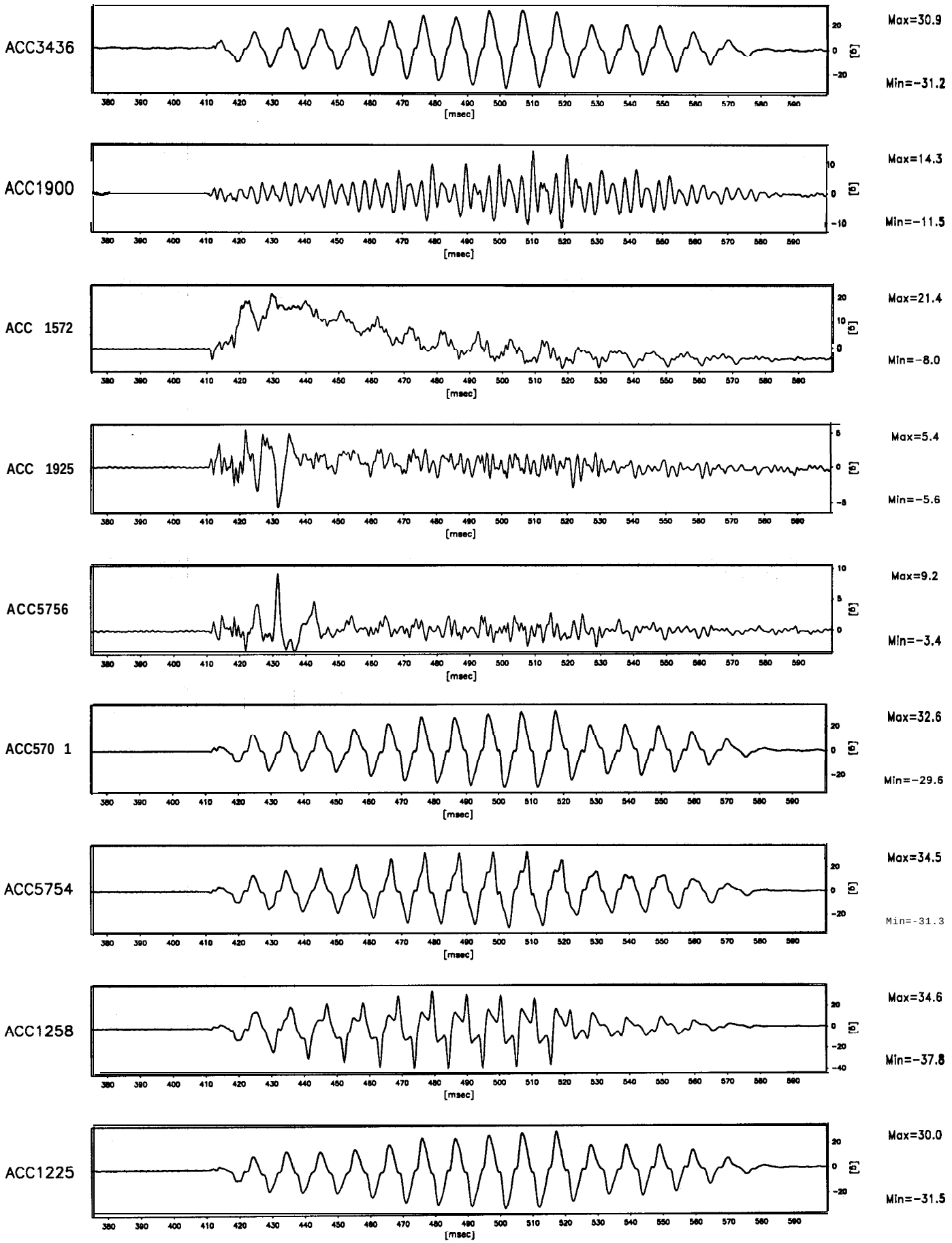

Scales : Model

TEST MG-5 MODEL SAT FLIGHT -1	EQ-6	SHORT TERM TIME RECORDS	G Level 50	FIG.NO. 55

901 data points plotted per complete transducer record

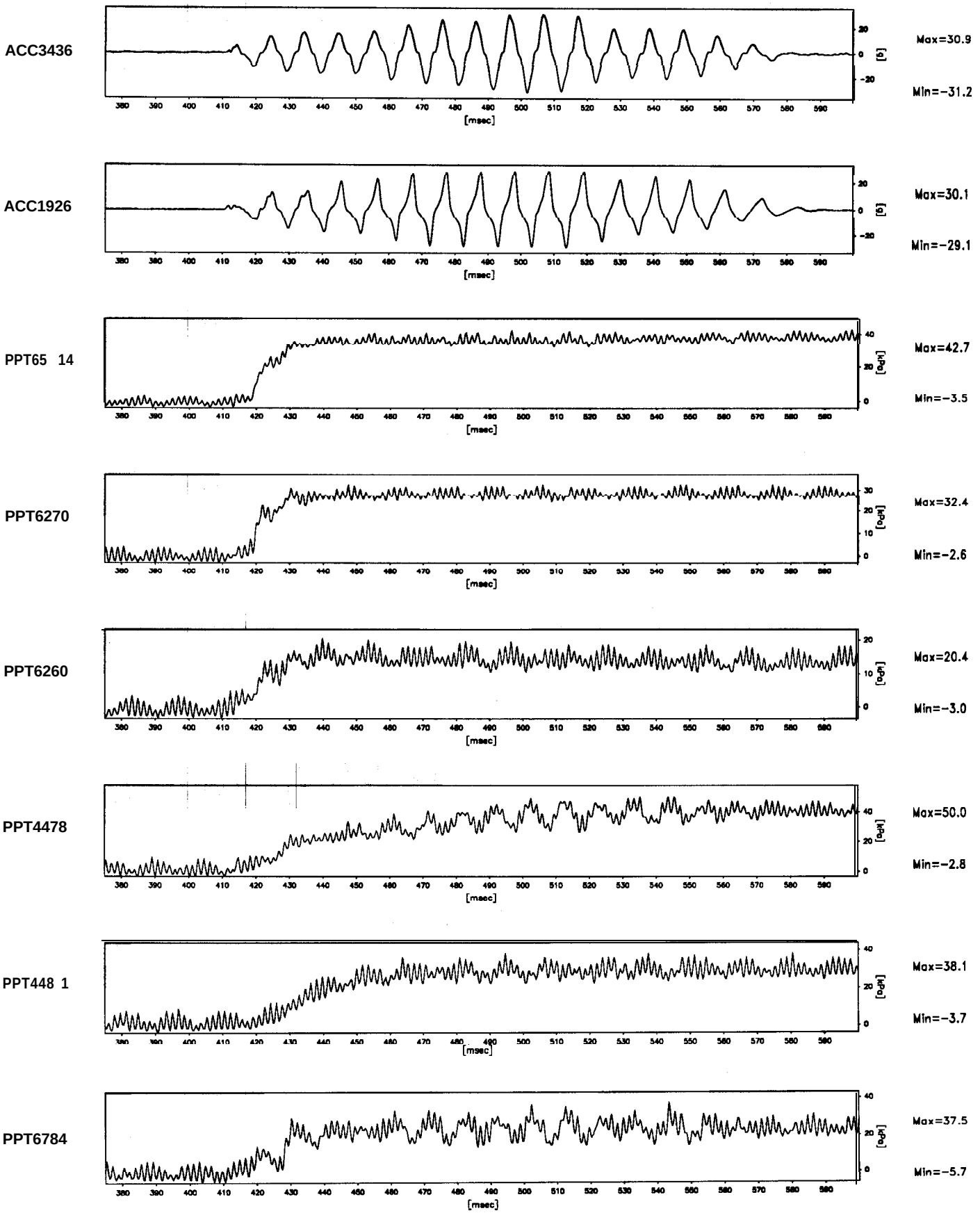

Scales : Prototype

TEST MG-5 MODEL SAT FLIGHT -1	EQ-6	SHORT TERM TIME RECORDS	G Level 50	FIG.NO. 56

15.0 Analysis of data from centrifuge test MG-5

The saturated sand bed in centrifuge model MG-5 had a height of 100 mm. The first earthquake was a strong earthquake with a peak acceleration of about 12.8 %. A slightly stronger earthquake which produced a peak acceleration of 15.4 % was fired next. After this the strength of the earthquakes was gradually increased in the subsequent events. The hydrostatic pore pressures during the swing up and while increasing the centrifugal acceleration to '50g' are presented in Table 5. Note that, as in the previous centrifuge test, during an earthquake event excess pore pressures are generated over and above these hydrostatic pore pressures.

In Fig.57 the near surface accelerations recorded by ACC 3477 in all the six earthquakes are presented on the left hand side. During earthquake 1 the input acceleration was about 12.8 % and the surface accelerations attenuated significantly after first cycle following the generation of excess pore pressures within the sand bed. However the surface accelerations recover after the first cycle but are again attenuated towards the strong base shaking felt towards the end of the earthquake. The frequency analysis of this trace is presented on the right hand side in Fig.57. From the frequency analysis of this trace we can see that most of the energy is concentrated at about 100 Hz. The peak excess pore pressures produced during each earthquake near the base of the sand bed, at mid depth and near the surface are plotted in Fig.58. Earthquake 2 was a slightly stronger earthquake and magnitude of excess pore pressures was the same as in earthquake 1 and as seen in Fig.58. The first five cycles of base shaking are present near the surface of the sand bed during this earthquake. Further the frequency analysis of this trace shows that all the energy is present at the driving frequency of the earthquake which is 95 Hz (see the right hand side in Fig.57). A slightly stronger earthquake was fired next. The excess pore pressures generated were almost equal to those generated during earthquakes 1 and 2. The near surface accelerations show attenuation compared to the base motion (see Table 6). The first three cycles of base motion are present in this trace. However the accelerations on the negative side have a

slightly larger amplitude compared to the positive side. Further the frequency analysis of the near surface accelerations during this earthquake as seen on the right hand side of Fig.57 indicate that there are significant high frequency components in this trace. Earthquake 4 had resulted in peak accelerations of 25.2 %. After $1^3/_4$ cycles the near surface accelerations are significantly attenuated. The frequency analysis of this trace indicate the presence of high frequency components (see the right hand side in Fig.57). Also the near surface accelerations have slightly larger peak accelerations on the negative side compared to the positive side. During the fifth earthquake the attenuation of near surface accelerations sets in after first $1^1/_2$ cycles itself. The frequency analysis of this trace indicate that most of the energy is present at the driving frequency of the earthquake with some energy at the higher frequencies. Earthquake 6 was even stronger and the peak acceleration induced by this earthquake was about 29.7 % at the base of the soil column. The near surface accelerations were attenuated after the first $1^1/_4$ cycles. The frequency analysis of this trace is presented on the right hand side of Fig.57. By comparing the frequency analysis of all the near surface accelerations traces in Fig.57 from earthquake 1 to earthquake 6 we can see that there is a gradual dispersion of the energy about the driving frequency of the earthquake (which is 96 Hz) as the strength of the earthquake is increased from 12.8% to 29.7 %.

The **column** of accelerometers (see Fig.32) placed in the middle of the saturated sand bed experienced attenuation of peak accelerations following the generation of excess pore pressures in each earthquake. In table 6 the peak accelerations recorded by the above column of accelerometers which are normalised by the acceleration at the base of the sand column during each earthquake are presented. In Fig.58 the excess pore pressures generated in each earthquake are plotted against the strength of the earthquake. From this figure it is clearly seen that all the six earthquakes resulted in more or less the same magnitude of excess pore pressures. This contrasts strongly with the smaller excess pore pressures generated during earthquake 2 in the previous centrifuge test MG-4. In sections 3, 4 and 5 of this report the procedure to estimate

the natural frequency of the saturated sand bed by using the shear modulus of the soil which is corrected for the shear strain amplitude induced during the earthquake loading and by using effective stresses corrected for excess pore pressures induced during an earthquake is presented. For an earthquake of given strength it is possible to relate the variation of natural frequency with the generation of excess pore pressure. In Fig.59 the variation of natural frequency of the saturated sand bed used in the centrifuge model MG-5 with the generation of excess pore pressures is presented for earthquakes of varying strengths from 2 % to 20 %. The soil parameters of this centrifuge model were substituted in equations 1 to 12 and the results are plotted in Fig.59. The small strain natural frequency of the sand bed in this centrifuge model was about 430 Hz when there is no excess pore pressure generated. Also, from this figure it is clear that for an earthquake of a particular strength the natural frequency drops with the increase in excess pore pressure. Also stronger earthquakes results in lower natural frequencies as larger shear strains are realised.

In Fig.60 the normalised acceleration in table 6 is plotted against the strength of the earthquakes fired during this centrifuge test. The near surface acceleration is normalised using the acceleration at the base of the sand bed and this normalised acceleration is plotted along the ordinate. From this figure earthquake 2 which produced a peak acceleration of 8.6 % at the base of the sand column resulted in the largest normalised acceleration. In other words earthquake 2 gave rise to the smallest attenuation of base motion as it travelled towards the sand bed. As the strength of the earthquake is increased the normalised acceleration is reduced as seen in Fig.60.

This result can be explained using the theoretical variation shown in Fig.59. During earthquake 1 the peak acceleration observed at the base of the sand column is 7.4 % (see Fig.33) and the excess pore pressure generated at the base of the sand column during this earthquake was 40 kPa. From Fig.59 we can get the natural frequency under these conditions of the saturated sand bed in this centrifuge model as 205 Hz.

This frequency if far from the driving frequency of the earthquake which is at 96 Hz. Hence there will be attenuation of base shaking as it travels to the surface of the sand during this earthquake. Earthquake 2 had resulted in an acceleration of 8.6 % at the base of the soil column considered in above discussion. This earthquake also resulted in the generation of excess pore pressures of the magnitude of about 40 kPa at the base of the sand column as seen in Fig. 58. From Fig.59 we can obtain the natural frequency of the saturated sand bed under these conditions as about 100 Hz. This is very close to the driving frequency of the earthquake which is 96 Hz and hence results in relative amplification of base shaking as it travels towards the surface of the sand. From Fig.59 we can see that when the strength of the earthquakes is larger and large excess pore pressures are generated the natural frequency of the sand bed falls to very small values. In other words, under those conditions there will be much larger attenuation of the base shaking as it travels towards the sand surface. This is confirmed in Fig.60 which shows that stronger earthquakes have indeed led to larger attenuations.

In Fig.61 the pore pressures recorded at the base of the sand column by the pore pressure transducer 6514 (also see Fig.32) during each of the earthquake event is presented. The rate of the excess pore pressure build up clearly appears to be a function of the strength of the earthquake. During the first earthquake which had a strength of 12.8 % the build up was rapid as seen in Fig.61. During the stronger second earthquake the magnitude of the excess pore pressure generated is same but the rate of build up is much more faster compared to earthquake 1. During earthquake 3 the rate of build up is slightly faster especially towards the end of the earthquake. The rate of pore pressure build up increases further during earthquake 4, 5 and 6. From this figure and the corresponding result in centrifuge test MG-4 we can say that the rate of pore pressure build up increases with the increase in the strength of the earthquake.

data points plotted per complete transducer record

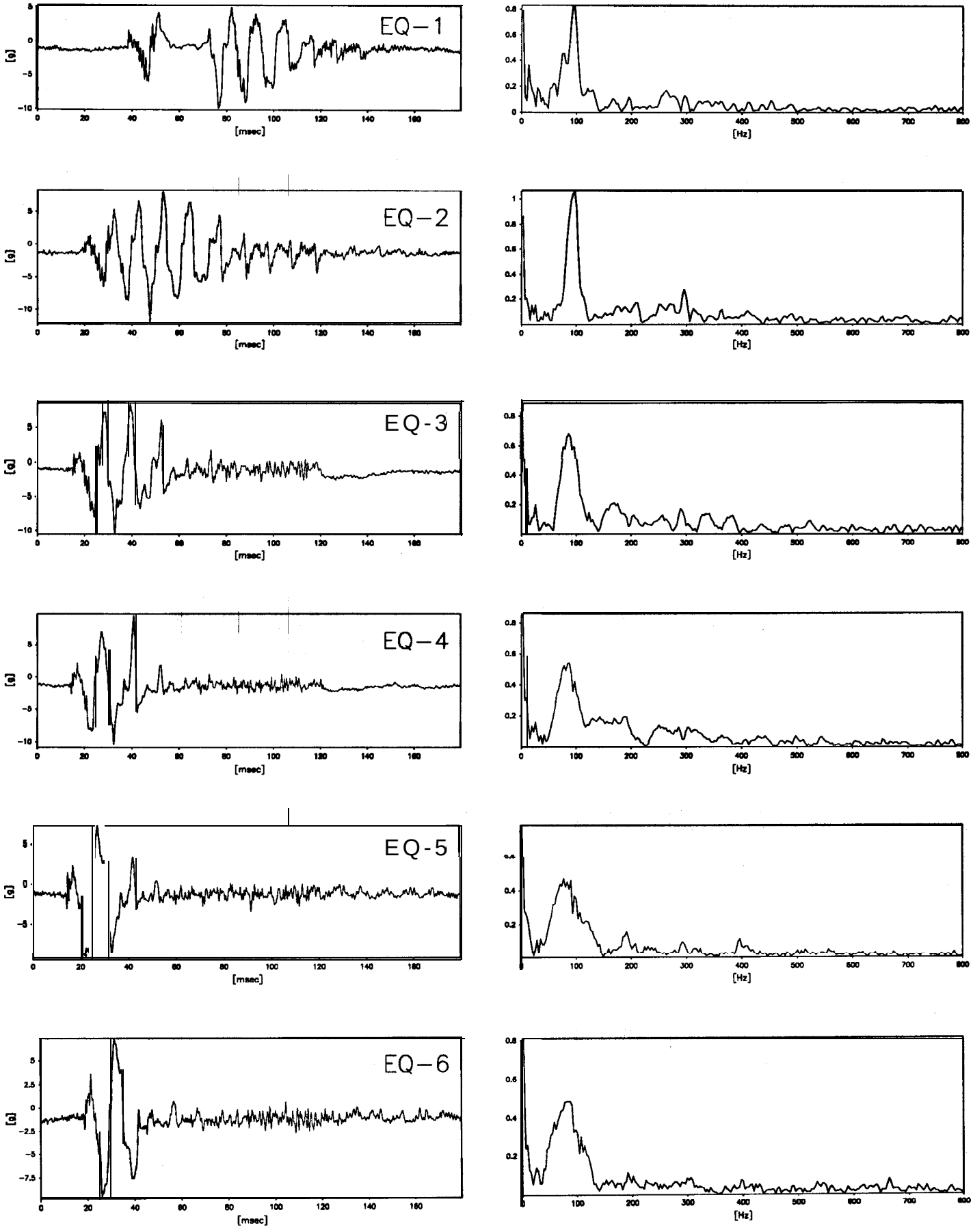

Scales : Prototype

TEST MG-5 MODEL SAT FLIGHT -1		Near Surface Accelerations and Frequency Analyses	FIG.NO. 57

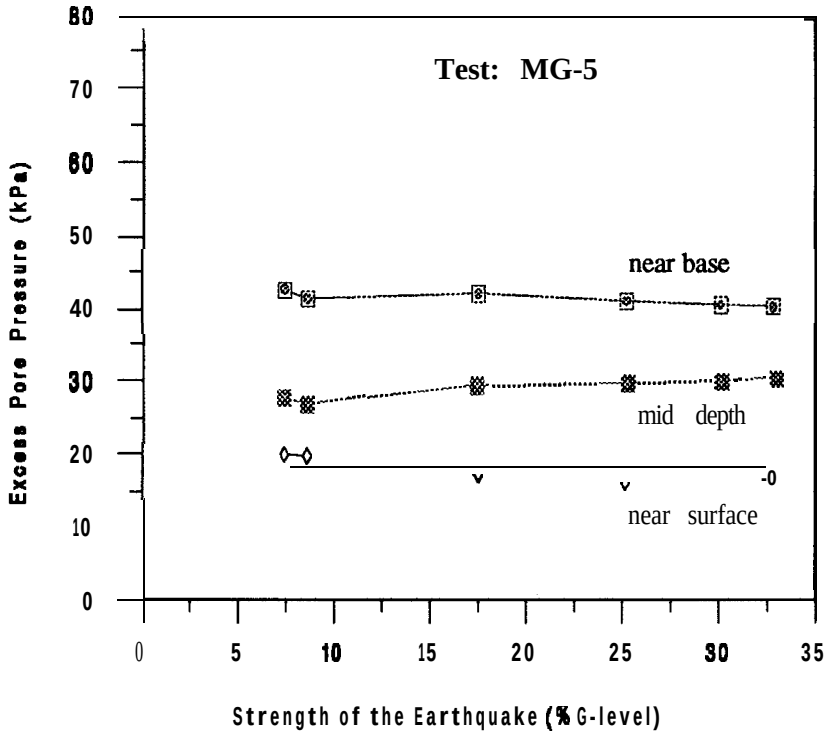

Fig.58 Generation of excess pore pressures during the earthquakes in centrifuge test MG-5

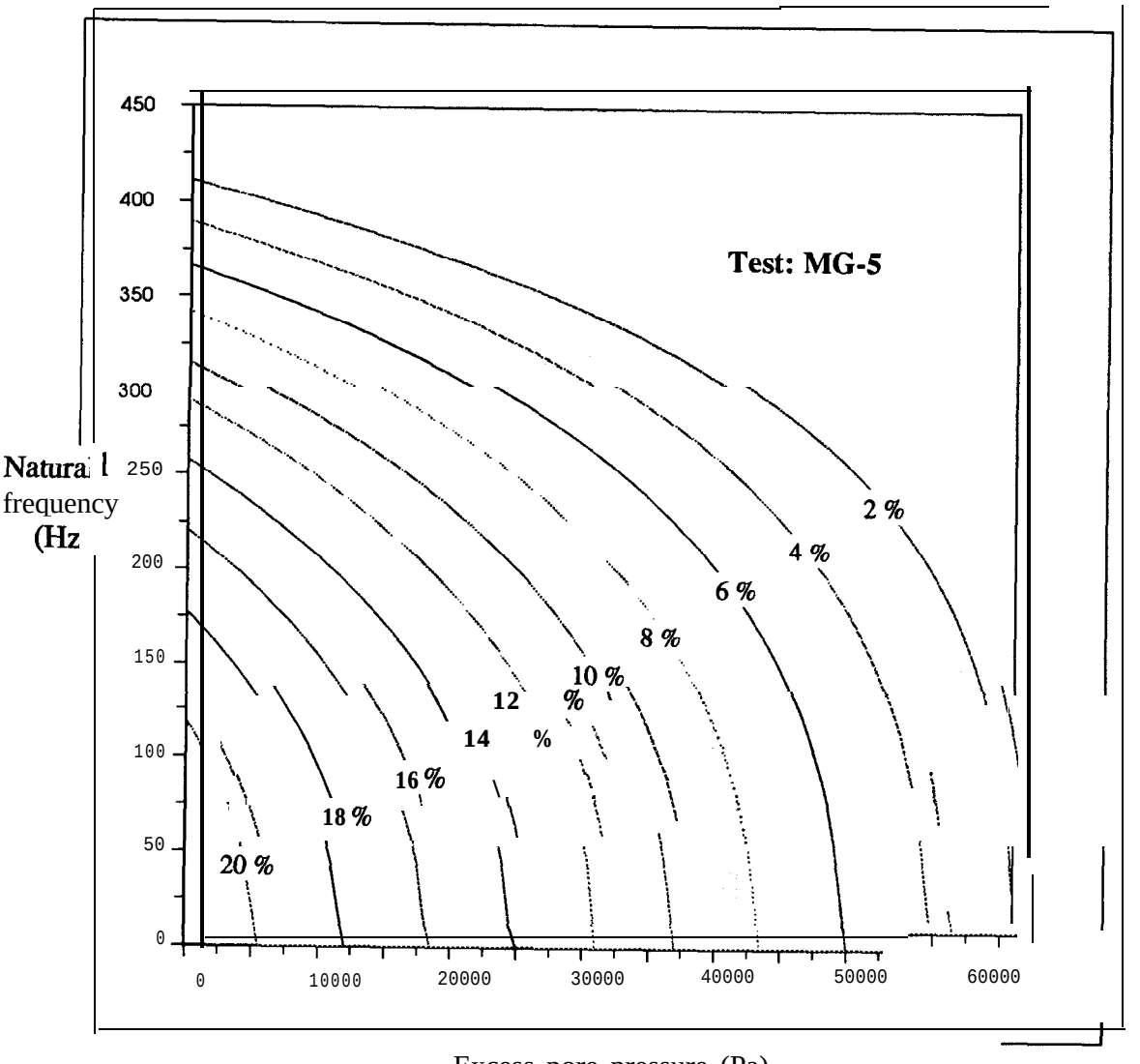

Fig.59 Theoretical relationship between the excess pore pressures and the natural frequency

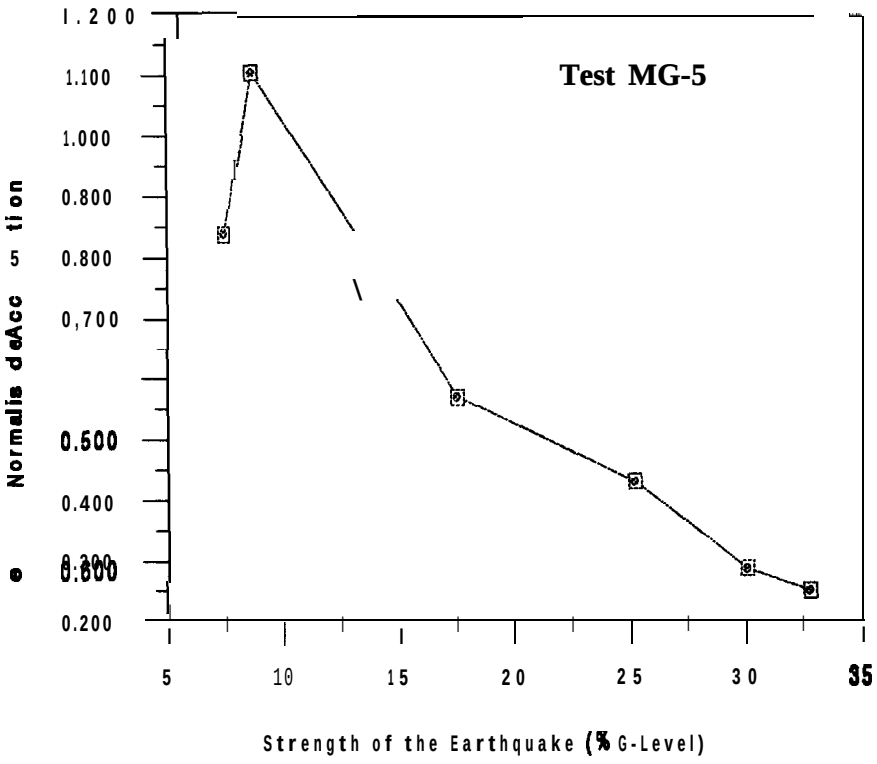

Fig.60 Variation of the normalised acceleration with the strength of the earthquake

239 data points plotted per complete transducer record

EQ−1

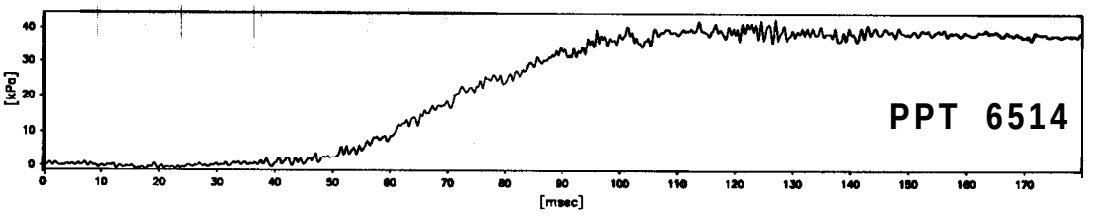

EQ−2

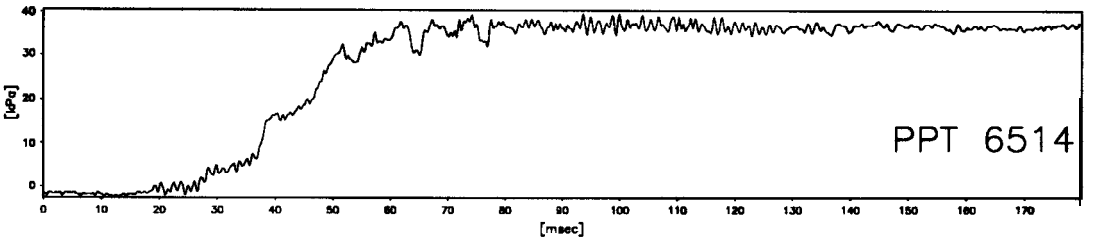

EQ−3

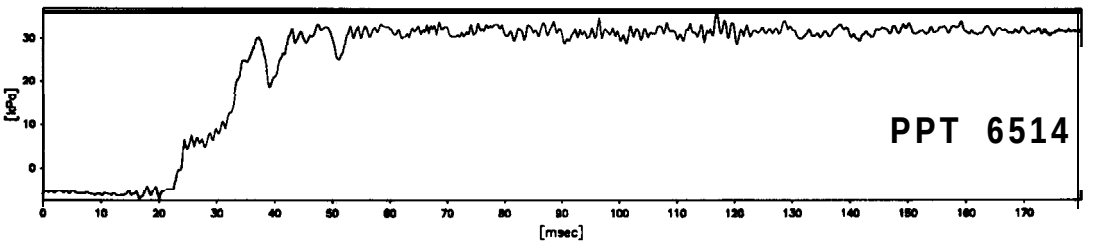

EQ−4

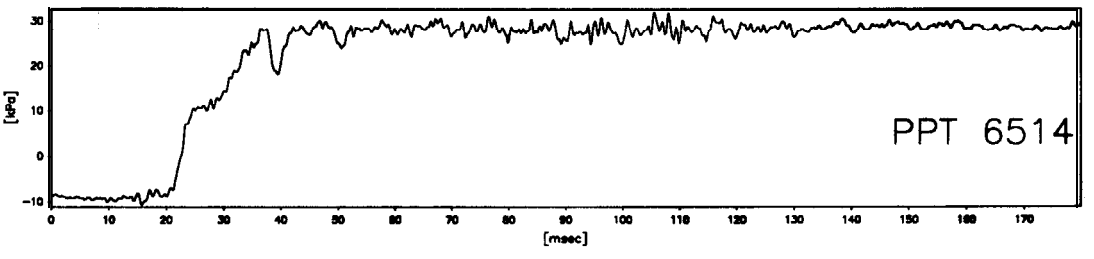

EQ−5

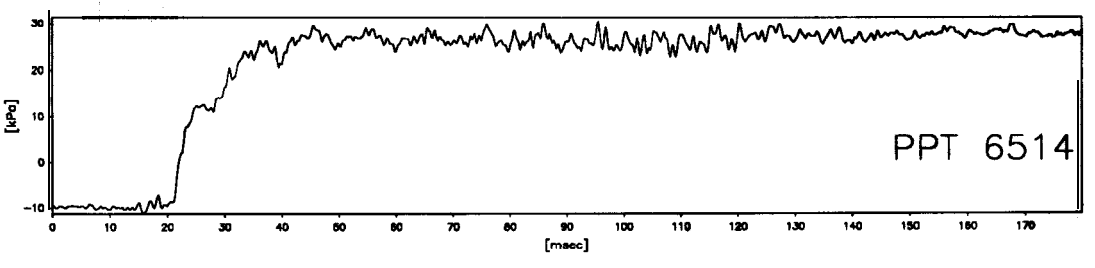

EQ−6

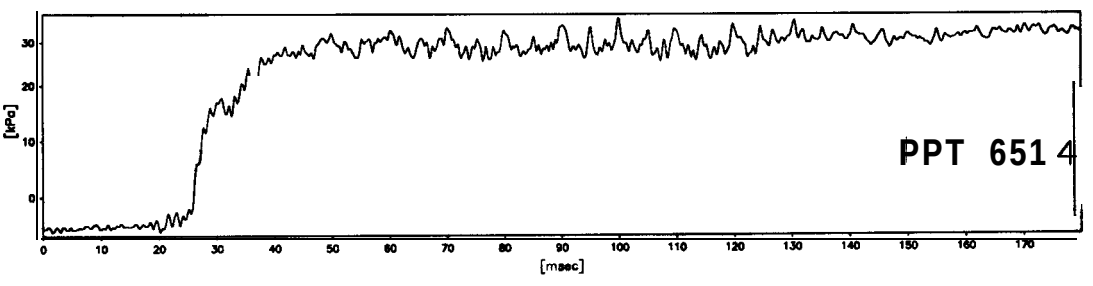

Scales : Prototype

TEST MG-5 MODEL SAT FLIGHT -1		**Base Pore Pressure TIME RECORDS**		FIG.NO. 61

16.0 Conclusions

The dynamic response of a horizontal sand bed was investigated under saturated conditions. Two centrifuge tests MG-4 and MG-5 were conducted on saturated sand beds of different heights. Several earthquakes were fired on the centrifuge models during each experiment. The data from these centrifuge tests is presented in this report. This series of centrifuge tests were carried out in continuation of work done on dry sand beds earlier, Madabhushi (1994).

The depth of the sand bed was arranged so that the small strain natural frequencies were 250 and 450 Hz for the centrifuge models MG-4 and MG-5 respectively. When the shear modulus of the sand bed is corrected for the shear strain amplitude the natural frequency of the sand bed will be lower than the above values. Also when the effective stress in the sand bed is corrected for the excess pore pressures generated during the earthquake loading the natural frequency of the sand bed will be even lowered.

In the first centrifuge test MG-4 a strong earthquake was fired first followed by a smaller second earthquake. The subsequent earthquakes had increasing strengths. The excess pore pressures generated at different heights within the sand bed followed the strength of the earthquakes. Also the maximum amplification was observed during the second earthquake when the excess pore pressures were small. The natural frequency predicted by theoretical approach suggested that during earthquake 2 the natural frequency of the saturated sand bed approaches the driving frequency of the earthquake and hence results in relatively smaller attenuation of base motion as it travels to the surface of the sand bed. During all other earthquakes the attenuation is much larger as the natural frequency of the sand bed falls well below the driving frequency. Also the data suggests that the rate of pore pressure build up is a direct function of the strength of the earthquake.

In the second centrifuge test MG-5 earthquakes were fired in strictly the order of increasing intensity. The magnitude of the excess pore pressures generated at different heights within the sand bed remained more or less the same during all the six earthquakes fired on this centrifuge model. The natural frequency predicted by theoretical approach suggested that during earthquake 1 the natural frequency of the saturated sand bed is far above the driving frequency of the earthquake and hence results in some attenuation of base motion as it travels to the surface of the sand bed. During the second earthquake the natural frequency is almost the same as the driving frequency resulting in the relative amplification of base motion as it travels towards the sand surface. During all other earthquakes the attenuation is much larger as the natural frequency of the sand bed falls well below the driving frequency. Also the data from this centrifuge test suggests that the rate of pore pressure build up is a direct function of the strength of the earthquake.

REFERENCES

Hardin, B.O. and Drnevich, V.P., (1972), Shear modulus and damping in soils: design equations and curves, Jnl. of Soil Mech. and Found. Eng.Div., ASCE, No.SM7, pp.667-692.

Kutter, B.L., (1982), Centrifuge modelling of response of clay embankments to earthquakes, Ph.d thesis, Cambridge University, England.

Madabhushi, S.P.G., (1994), Natural frequency of a Horizontal Soil Layer, Part I: Dry sand bed, Technical Report, CUED/D-SOILS/TR27 1, Cambridge University, England.

Seed, H.B., Lee, K.H. and Idriss, I.M. and Makadisi, F.I (1975), The slides in the San Fernando dams during the earthquake of February 9, 1971, ASCE Jnl. of Geotechnical Engineering Div., GT7, pp 651-688.